

International Journal of Modern Physics E
© World Scientific Publishing Company

**THERMAL AND TRANSPORT PROPERTIES OF A
NON-RELATIVISTIC QUANTUM GAS INTERACTING
THROUGH A DELTA-SHELL POTENTIAL**

SERGEY POSTNIKOV

*Nuclear Theory Center, Indiana University,
Bloomington, Indiana 47405, USA
spostnik@indiana.edu*

MADAPPA PRAKASH

*Department of Physics and Astronomy, Ohio University,
Athens, OH 45701-2979, USA
prakash@harsha.phy.ohiou.edu*

Received (received date)

Revised (revised date)

This work extends the seminal work of Gottfried on the two-body quantum physics of particles interacting through a delta-shell potential to many-body physics by studying a system of non-relativistic particles when the thermal De-Broglie wavelength of a particle is smaller than the range of the potential and the density is such that average distance between particles is smaller than the range. The ability of the delta-shell potential to reproduce some basic properties of the deuteron are examined. Relations for moments of bound states are derived. The virial expansion is used to calculate the first quantum correction to the ideal gas pressure in the form of the second virial coefficient. Additionally, all thermodynamical functions are calculated up to the first order quantum corrections. For small departures from equilibrium, the net flows of mass, energy and momentum, characterized by the coefficients of diffusion, thermal conductivity and shear viscosity, respectively, are calculated. Properties of the gas are examined for various values of physical parameters including the case of infinite scattering length when the unitary limit is achieved.

arXiv:1307.5439v1 [nucl-th] 16 Jul 2013

2 *Contents***Contents**

1	Introduction	4
2	Quantum mechanics of the two-body problem	7
3	Phase shifts for scattering states	8
4	The density of states and the phase shifts	11
5	Energies of bound states	14
6	The scattering length, effective range and the delta-shell model of the deuteron	16
7	Differential equation for S-wave scattering length and effective range	19
8	Momentum-space wave-function and form-factor for the S-wave	21
9	The Feynman-Hellmann theorem applied to the delta-shell model	22
10	Wave function normalization for bound states	25
11	Virial theorem	27
12	Relationship between moments: Kramers-Pasternak-like relation	29
13	The first quantum correction to the ideal-gas law	32
14	Cluster-two integral and the first correction	34
15	Region of validity for the second virial coefficient	36
16	The second virial coefficient in terms of the scattering length and the range parameter	37
17	Gas of nonzero spin particles	39
18	Thermodynamical properties in terms of the second virial coefficient	43
19	Transport coefficients	58
20	Delta-shell gas and resonances	61

Contents 3

21 Asymptotic behavior at low temperatures	63
22 Ratio of shear viscosity to entropy density	66
23 Summary and conclusions	75

4 *Contents***1. Introduction**

Recently, studies of transport properties, particularly viscosities of interacting particles in a many-body system, have attracted much attention as observed phenomena in diverse fields of physics (such as atomic physics and relativistic heavy ions physics) are greatly influenced by their effects¹. In atomic physics, the relaxation of atomic clusters from an ordered state have been observed². In relativistic heavy-ion physics, viscosities influence the observed elliptic and higher order collective flows versus transverse momentum of final state hadrons³. In both of these fields, the challenge of determining the transport properties at varying temperatures and densities has been vigorously pursued¹.

In this work, we study a simple system in which the high temperature thermal and transport properties of a dilute gas are significantly affected by the nature of two-body interactions. The two-body interaction chosen for this study - the delta-shell interaction - allows us to study the roles of long scattering lengths, finite-range corrections, and resonances on the thermal and transport properties of a quantum gas through an extension of the classic work of Gottfried^{4,5} to the many-body context. Our pedagogical study reveals several universal characteristics. Our results stress the need to perform analyses beyond what we offer here, particularly with regard to contributions from higher than two-body interactions.

Gottfried's treatment^{4,5} of the quantum mechanics of two particles interacting through a delta-shell potential

$$V(r) = -v \delta(r - R), \quad (1)$$

where v is the strength and R is the range, forms the basis of this work in which the thermal and transport properties of a dilute gas of non-relativistic particles are calculated for densities n for which the average inter-particle distance $d \sim n^{-1/3} \gg R$. The delta-shell potential is particularly intriguing as the scattering length a_{sl} and the effective range r_0 can be tuned at will, including the interesting case of $a_{sl} \rightarrow \infty$ (the unitary limit) that is accessible in current atomic physics experiments (see, for e.g., Ref.²). The delta-shell potential also allows us to understand the transport characteristics of nuclear systems in which the neutron-proton and neutron-neutron scattering lengths ($a_{sl} \simeq -23.8$ fm and -18.5 fm, respectively⁶) are much longer than the few fm ranges of strong interactions. In addition, the delta-shell potential admits resonances.

The schematic diagram in Fig. 1 illustrates a gas of particles interacting through the delta-shell potential and the relevant length scales.

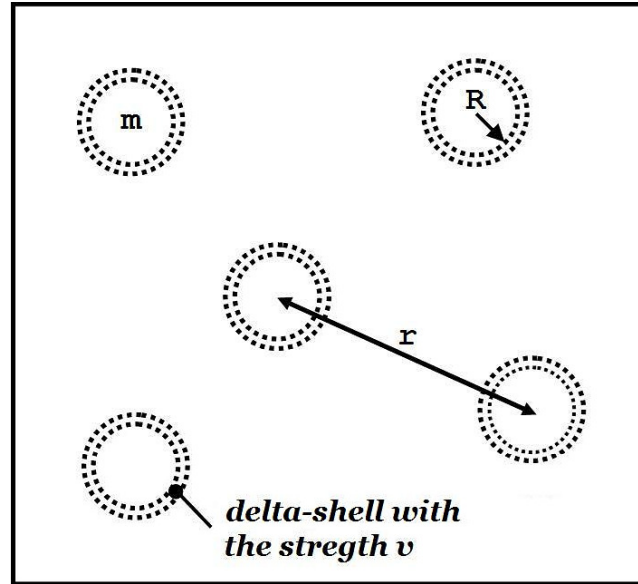


Fig. 1. Illustration of a system of particles interacting through a delta-shell potential $V(r) = -v\delta(r - R)$, where v is the strength and R is the range of the potential. The distance between a pair of particles is denoted by r .

This work consists of three main parts: (i) The quantum mechanics of the 2-body problem (sections 2 through 11), (ii) Thermal and statistical physics of the delta shell gas (sections 13 - 18) and (iii) Transport properties of the delta shell gas (19 - 22).

In part (i), we begin by summarizing the text book results of Ref.^{4,5} and complement them with additional material related to the scattering state and bound state solutions of the Schrödinger equation for two particles interacting through the delta-shell potential (section 2). These solutions are analytical and allow us to calculate phase shifts for all partial waves (section 3), the density of scattering states (section 4), energies of bound states (section 5), the scattering length and the effective range. The conditions for the unitary limit and for resonances to occur are identified. In section 6, the ability of the delta-shell potential to reproduce some basic properties of the loosely bound deuteron (binding energy is -2.23 MeV) is examined. With the exception of the shape parameter (sensitive only to moderately high-energy scattering), the calculated results (e.g., the deuteron root-mean-square radius) agree very well with experiment (and for good reasons). The disagreement with the shape parameter is also understandable. In section 7, a differential equation to determine the S-wave scattering length and the effective range is established. The momentum-space wave function and the form factor for the S-wave are presented in section 8. Next, consequences from the Feynman-Hellman theorem^{7,8} for wave functions with a kink (as is the case for the delta-shell potential) are exam-

6 *Contents*

ined in section 9. The normalization constants for bound states are determined in section 10. Insights gained through an application of the virial theorem, which takes a special form for the delta-shell potential is discussed in section 11. Relations between the various moments of the bound-state wave functions are derived section 12. These relations are analogous to those derived by Kramers⁹ and Pasternak¹⁰ for the hydrogen atom, but for wave functions that exhibit a kink. We show how special care must be taken to derive these relations in the presence of a kink.

In sections 13 and 14 of part (ii), we calculate the first quantum correction to the ideal-gas pressure in the form of the second virial coefficient¹¹. The physical conditions for which the second virial coefficient gives an adequate description is examined in section 15. The case in which the scattering length becomes infinite (the unitary limit) is examined in some detail in sections 16 and 17. In addition, all thermodynamical functions are calculated including corrections from the second virial coefficient (section 18).

The transport properties of a delta-shell gas are calculated in part (iii). Small departures from equilibrium result in net flows of mass, energy and momentum which are characterized by the coefficients of diffusion, thermal conductivity and shear viscosity, respectively. These coefficients are calculated in first and second order of deviations (from the equilibrium distribution function) using the Chapman-Enskog method¹² in section 19. The transport properties are examined in various physical situations, including the case of an infinite scattering length and when resonances occur in sections 20 and 21. In section 22, The ratio of shear viscosity to entropy density is calculated and compared to the recently the proposed universal minimum value of $\simeq 1/(4\pi)$ ^{13,14}.

Section 23 contains a summary with concluding remarks.

2. Quantum mechanics of the two-body problem

We begin by adopting solutions and expressions derived in the book by Gottfried⁴. The Hamiltonian for two particles interacting via the delta-shell potential has the form

$$\hat{H} = -\hbar^2 \frac{\Delta}{2\mu} - v \delta(r - R), \quad (2)$$

where μ denotes the reduced mass,

$$\Delta = \frac{1}{r^2} \frac{\partial}{\partial r} r^2 \frac{\partial}{\partial r} - \frac{\hat{L}^2}{r^2} \quad (3)$$

is the Laplacian in spherical coordinates (\hat{L} is the orbital momentum operator), \hbar is the Plank constant, r is the separation distance, v and R are the strength and range parameters of the potential, respectively. Introducing the dimensionless position variable $\rho = kr$ (k is the wave number), the radial part of the stationary Schrödinger equation

$$\hat{H} \psi(r) Y_{lm}(\theta, \phi) = E \psi(r) Y_{lm}(\theta, \phi) \quad (4)$$

($Y_{lm}(\theta, \phi)$ are the spherical harmonics which are eigenfunctions of the operator \hat{L}^2 with eigenvalues $l(l+1)$) takes the form

$$u''(\rho) + \left(1 - \frac{l(l+1)}{\rho^2}\right) u(\rho) = -\frac{\Lambda}{k} \delta(\rho - kR) u(\rho), \quad (5)$$

where

$$u(\rho) = \frac{\rho}{k} \psi(\rho), \quad \Lambda = v \frac{2\mu}{\hbar^2}, \quad \text{and} \quad E = \frac{\hbar^2 k^2}{2\mu}, \quad (6)$$

and l is the usual orbital quantum number. Above, primes denote appropriate spatial derivatives. The general solution of Eq. (5) is given by a combination of Bessel functions of the first kind, $J_{l+\frac{1}{2}}(\rho)$, and the second kind, $N_{l+\frac{1}{2}}(\rho)$ ¹⁵:

$$u(\rho) = c_1 \sqrt{\rho} J_{l+\frac{1}{2}}(\rho) + c_2 \sqrt{\rho} N_{l+\frac{1}{2}}(\rho), \quad (7)$$

or in terms of the spherical Bessel functions $j_l(\rho)$ and $n_l(\rho)$:

$$\psi(\rho) \equiv \frac{u(\rho)}{\rho} = A_l j_l(\rho) + B_l n_l(\rho). \quad (8)$$

The δ -function part of Eq. (5) requires that at $r = R$,

$$\psi'(kR+0) - \psi'(kR-0) = -\frac{\Lambda}{k} \psi(kR). \quad (9)$$

The physical boundary condition that the radial wave function be continuous at $r = R$ implies that

$$\psi(kR-0) = \psi(kR+0). \quad (10)$$

The condition that the wave function is well behaved at the origin requires

$$u(0) = 0. \quad (11)$$

8 *Contents*

For a bound state, the boundary condition

$$\psi(\rho \rightarrow \infty) \rightarrow 0 \quad (12)$$

assures square integrability.

3. Phase shifts for scattering states

Positive energy ($E > 0$, hence the wave number k is real) solutions correspond to scattering states. As the potential is confined to a finite volume, the calculation of the phase shift δ_l is straightforward. From the asymptotic behavior ($\rho \rightarrow \infty$) of the general solution in Eq. (8), one has

$$\psi(\rho \rightarrow \infty) \rightarrow A_l \frac{\sin(\rho - \frac{\pi l}{2})}{\rho} - B_l \frac{\cos(\rho - \frac{\pi l}{2})}{\rho} = \sqrt{A_l^2 + B_l^2} \frac{\sin(\rho - \frac{\pi l}{2} + \delta_l)}{\rho}, \quad (13)$$

whence

$$\tan(\delta_l) = -\frac{B_l}{A_l}. \quad (14)$$

Utilizing Eq. (8), the ratio on the right-hand side of the above equation is found by satisfying the boundary conditions in Eq. (9), Eq. (10) and Eq. (11). The result is⁴

$$\tan(\delta_l) = \frac{g x j_l^2(x)}{1 + g x j_l(x) n_l(x)}, \quad (15)$$

where

$$g \equiv \Lambda R = \frac{2\mu v}{\hbar^2} R, \quad (16)$$

and

$$x = kR \quad (17)$$

are dimensionless parameters.

In deriving Eq. (15), use of the Wronskian relation

$$j_l(x) n_l'(x) - j_l'(x) n_l(x) = \frac{1}{x^2}, \quad (18)$$

has been made.

The partial-wave cross section $\sigma_l(k)$ and the total cross section $\sigma(k)$ are given by⁴

$$\sigma_l(k) \equiv \frac{4\pi}{k^2} (2l+1) \sin^2(\delta_l) = 4\pi R^2 (2l+1) \frac{\sin^2(\delta_l)}{x^2}, \quad (19)$$

$$\sigma(k) = \sum_{l=0}^{\infty} \sigma_l(k). \quad (20)$$

Using Eq. (15) and trigonometric relations, we find that

$$\sin^2(\delta_l) = \left[1 + \left(\frac{1 + g x j_l(x) n_l(x)}{g x j_l^2(x)} \right)^2 \right]^{-1}. \quad (21)$$

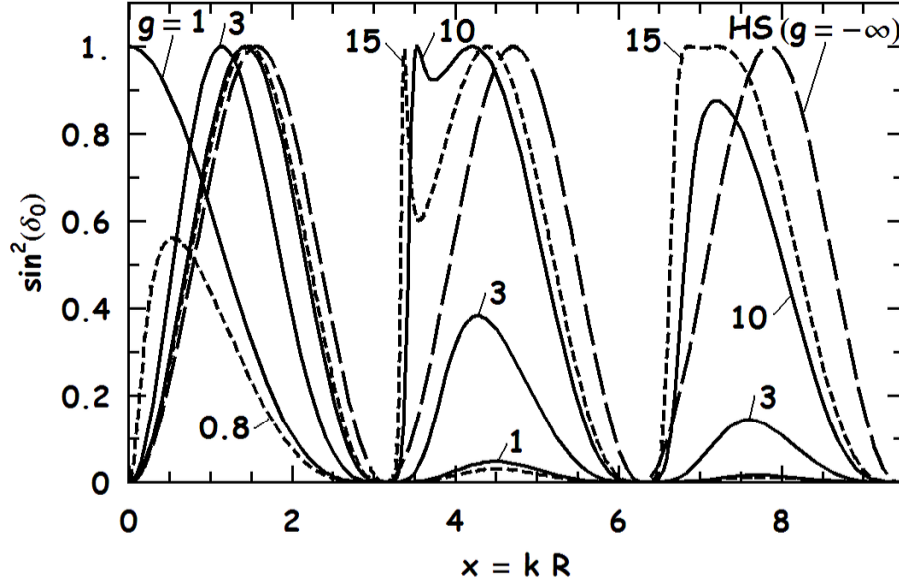


Fig. 2. A comparison of $\sin^2(\delta_0)$ for the delta-shell (Eq. (21)) and hard-sphere(HS) potentials. The abscissa shows the energy variable $x = kR$. Results are for $g = 0.8, 1, 3, 10$ and 15 .

A plot of $\sin^2(\delta_0)$ for various values of g is shown in Fig. 2 for the delta-shell and the hard-sphere potentials. The hard-sphere result is the limiting case of Eq. (15) when $g \rightarrow -\infty$, whence $\tan(\delta_l) = \frac{j_l(x)}{n_l(x)}$ and therefore

$$\sin^2(\delta_l) = \left[1 + \left(\frac{n_l(x)}{j_l(x)} \right)^2 \right]^{-1}. \quad (22)$$

In the case of the delta-shell potential, sharp resonances occur as the wave function can propagate inside the shell as well as bounce off of it. Resonances weaken with increasing energy as a more energetic particle is less influenced by the delta-shell potential. For contrast, results for the hard-sphere potential (long-dashed lines) are also shown.

In order to highlight the relative strengths of the various partial waves, the quantity $(2l+1)\delta_l$ as function of $x = kR$ is shown in Fig. 3 for values of $l = 0, 1, \dots, 6$ for several values of g .

Fig. 4 shows the partial wave cross sections σ_l for $g \approx 2l+1$ for which resonant features are clearly seen; the resonances become narrow with increasing l .

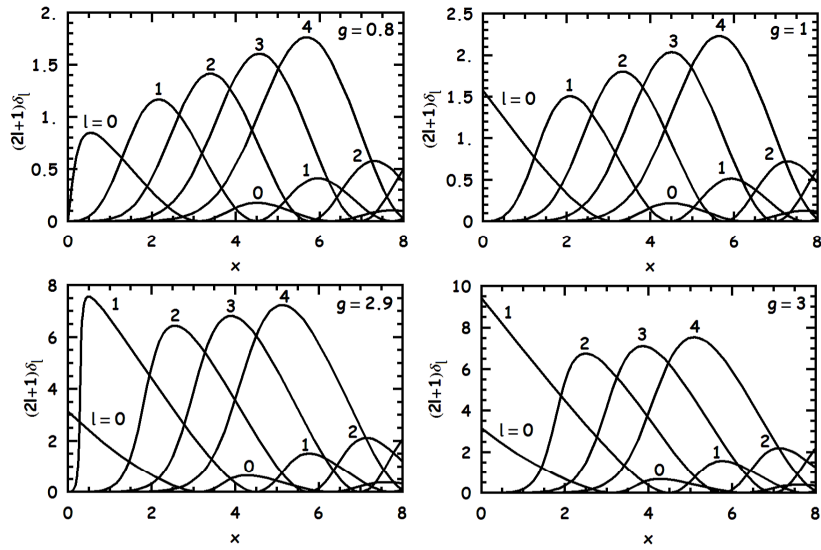


Fig. 3. The quantity $(2l+1)\delta_l$ as function of $x = kR$ for the indicated values of the orbital angular momentum quantum number l . Values of g are shown in the inset.

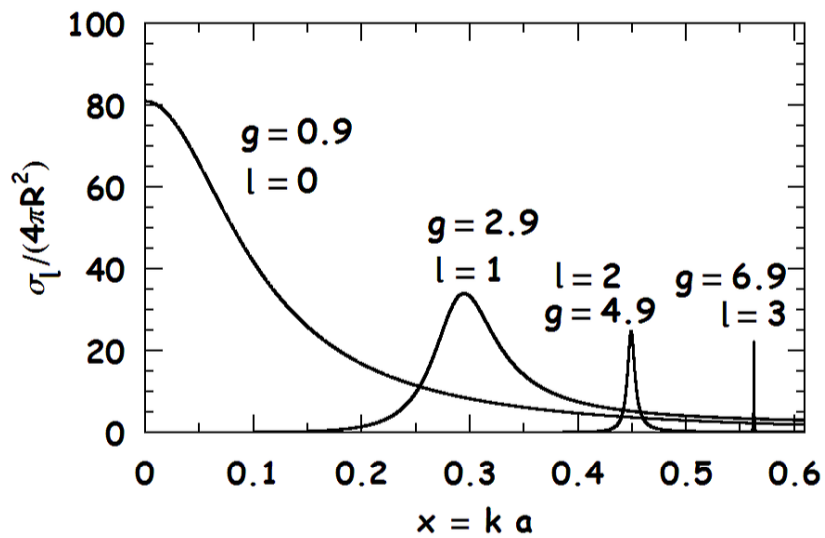


Fig. 4. Partial wave cross sections for $g \approx 2l + 1$ for which resonant features occur.

4. The density of states and the phase shifts

If particles are confined to a large spherical box with radius $L \rightarrow \infty$, the wave function vanishes at the walls of the box¹⁶. Imposing this condition on Eq. (13), one has

$$\begin{aligned} kL - \frac{l\pi}{2} + \delta_l(k) &= \pi m \quad (\text{interacting system}), \\ kL - \frac{l\pi}{2} &= \pi m \quad (\text{noninteracting system}), \end{aligned} \quad (23)$$

where m is an integer.

The number of levels Δm per range Δk of wave number is given by

$$\begin{aligned} \Delta m &= \frac{L}{\pi} \Delta k + \frac{1}{\pi} \frac{\Delta \delta_l(k)}{\Delta k} \Delta k \\ \Delta m^{(0)} &= \frac{L}{\pi} \Delta k^{(0)}, \end{aligned} \quad (24)$$

where the superscript (0) refers to the non-interacting system. The corresponding density of states is $d_l(k) = (2l+1) \frac{\Delta m}{\Delta k}$ and $d_l^{(0)}(k) = (2l+1) \frac{\Delta m^{(0)}}{\Delta k^{(0)}}$. Setting $\Delta k \rightarrow 0$ (box of infinite size, $L \rightarrow \infty$), the momentum derivative of the phase shifts can be expressed as

$$d_l(k) - d_l^{(0)}(k) = \frac{2l+1}{\pi} \frac{\partial \delta_l(k)}{\partial k}. \quad (25)$$

The derivative of the phase shift can also be expressed as

$$\frac{\partial \delta_l(x)}{\partial x} = \frac{1}{1 + \tan^2(\delta_l)} \frac{\partial \tan(\delta_l)}{\partial x}, \quad (26)$$

where $x = kR$. For the delta-shell potential

$$\frac{\partial \delta_l(x)}{\partial x} = \frac{g j_l(x) ((2l+1-g) j_l(x) - 2x j_{l+1}(x))}{g^2 x^2 j_l^4(x) + (g x j_l(x) n_l(x) + 1)^2}, \quad (27)$$

where $\tan(\delta_l)$ from Eq. (15) has been used. By setting $g \rightarrow -\infty$ in Eq. (27), we recover the result for the case of hard spheres:

$$\frac{\partial \delta_l(x)}{\partial x} = -\frac{1}{x^2} \frac{1}{j_l^2(x) + n_l^2(x)}. \quad (28)$$

To establish the low-energy behavior, we expand the phase shifts in a power series of x around zero momentum:

$$\frac{\partial \delta_l(x)}{\partial x} \approx \begin{cases} \frac{x^{2l}}{[(2l-1)!!]^2} \frac{g}{[(2l+1)-g]} & \text{for } g \neq 2l+1, \\ -\frac{2}{3} & \text{for } g=1; \quad l=0, \\ -\frac{x^{2l-2}}{2} \frac{(2l-1)^2 (2l+3)(2l+1)}{[(2l+1)!!]^2} & \text{for } g=2l+1; \quad l>0, \end{cases} \quad (29)$$

or

$$\tan(\delta_l) \approx \begin{cases} \frac{x^{2l+1}}{[(2l+1)!!]^2} \frac{g(2l+1)}{[(2l+1)-g]} & \text{for } g \neq 2l+1, \\ -\frac{x^{2l-1}}{2} \frac{(2l-1)(2l+1)(2l+3)}{[(2l+1)!!]^2} & \text{for } g=2l+1. \end{cases} \quad (30)$$

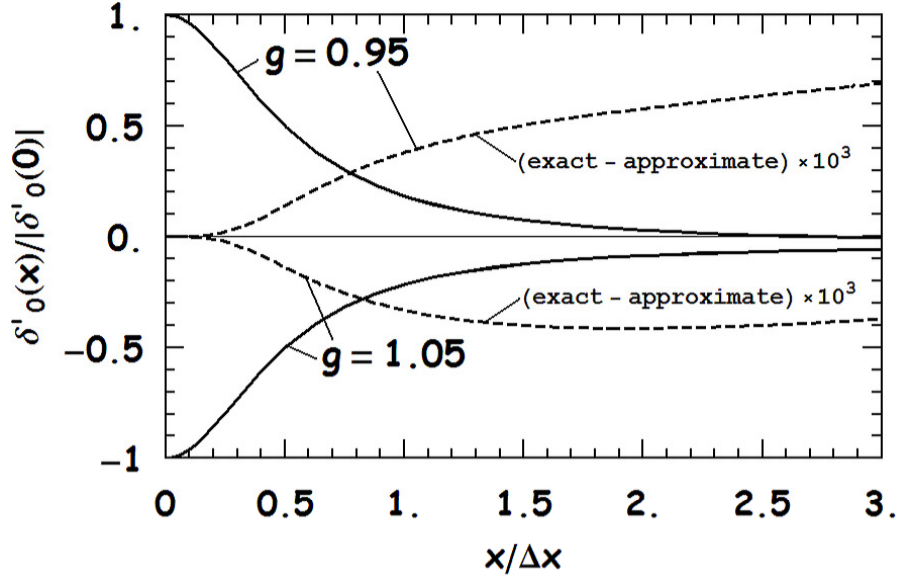


Fig. 5. An illustration of the S-wave phase shift derivative for low momenta near a resonance.

We see here that when g approaches $2l + 1$, the usual k^{2l+1} behavior for the phase shift does not work. Let us investigate the resonance behavior closely. We start with the S-wave first. If we expand the numerator and the denominator of Eq. (27) in a power series of x , we obtain

$$\delta'_{0-res}(x) \equiv \frac{3(g-1)g - (g-3)gx^2}{-3(g-1)^2 + (g-4)gx^2}. \quad (31)$$

We can infer the peak value from this equation to be

$$\delta'_{0-res}(0) \equiv \frac{g}{1-g}, \quad (32)$$

and the width at half the peak

$$\Delta x \equiv \frac{2\sqrt{3(1-g)^2}}{\sqrt{6-g(4-g)}}. \quad (33)$$

From the above relations and from Fig. 5 and Fig. 6, it is clear that as $g \rightarrow 1$ the function becomes more like a Dirac- δ function ($\delta'_{0-res}(0) \rightarrow \infty$ and $\Delta x \rightarrow 0$, but $\delta'_{0-res}(0)\Delta x$ is a finite number), so with the normalization given by the integral over Eq. (31), we have

$$\delta'_{0-res}(g \approx 1) \approx \text{sign}(1-g)\pi \frac{3^{3/2}}{(4-g)^{3/2}\sqrt{g}}\delta(x) - \frac{(3-g)}{(4-g)}, \quad (34)$$

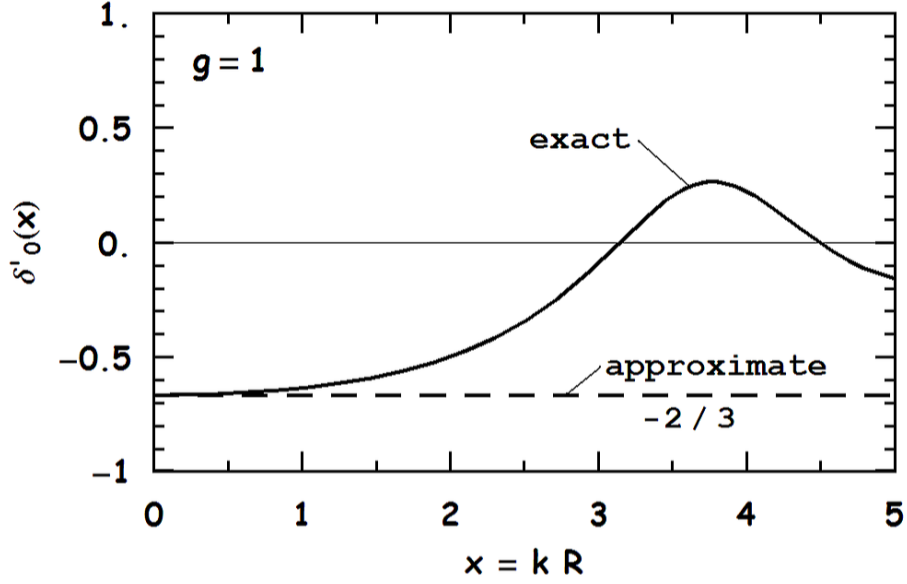


Fig. 6. An illustration of the S-wave phase shift derivative for low momenta at a resonance.

where $\text{sign}(0)\delta(x) \equiv 0$ and $1 = \int_{-\infty}^{\infty} \delta(x)dx = 2 \int_0^{\infty} \delta(x)dx$ due to symmetry.

Now we consider the P-wave for which $l = 1$. As we see from Fig. 7, when $g \approx 3$ the position x_1 of a sharp resonance for which $\sin^2(\delta_1) = 1$ from Eq. (21) is small and can be found from

$$\frac{1 + g x j_1(x) n_1(x)}{g x j_1^2(x)} = 0. \quad (35)$$

By expanding in a Taylor series, the result is

$$x_1^2(g \approx 3) \approx \left(\frac{3-g}{g-1} \right) \frac{5}{3}. \quad (36)$$

Expanding the numerator and the denominator of Eq. (27) in a power series of $\epsilon = x - x_1$ from Eq. (36), we obtain

$$\delta'_{1-res}(x) \equiv -\frac{360(5(g-3) - 51\epsilon^2)}{625(g-3)^2 + 5184\epsilon^2}, \quad (37)$$

with the peak value and the width given by

$$\delta'_{1-res}(x_1) \equiv \frac{72}{25(3-g)}, \quad (38)$$

$$\Delta x_1 \equiv \frac{25(3-g)}{72}. \quad (39)$$

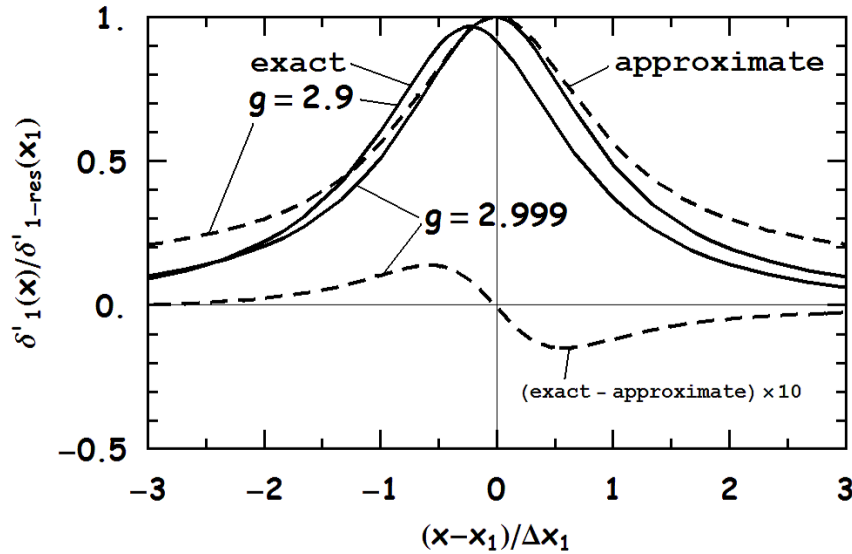


Fig. 7. An illustration of the P-wave phase shift derivative near a resonance.

Again the resonance structure can be approximated by a Dirac- δ function similar to Eq. (34):

$$\delta'_{1-\text{res}}(g \approx 3) \approx H(3-g) \pi \left(1 - \frac{2125}{1728}(3-g) \right) \delta \left(x - \sqrt{\frac{5(3-g)}{2g}} \right) + \frac{85}{24}, \quad (40)$$

where $H(\epsilon)$ is the unit step function: $H(\epsilon) = 1$ for $\epsilon > 0$ and 0 otherwise.

5. Energies of bound states

If the energy is negative ($E < 0$ implies that the wave number k is pure imaginary), the system is bound. The radial wave function in this case is found by requiring Eq. (8) to satisfy the conditions in Eq. (10), Eq. (11) and Eq. (12). The result is

$$\psi_l(r < R) = N_\psi j_l(kr)h_l(kR), \quad (41)$$

$$\psi_l(r > R) = N_\psi j_l(kR)h_l(kr), \quad (42)$$

where $h_l = j_l + i n_l$ is the spherical Hankel function and N_ψ is the normalization factor. Bound-state energies are given by poles of the scattering amplitude in the complex energy plane. Applying the boundary condition in Eq. (9) yields an

equation for the bound state energies⁴

$$i x j_l(x) h_l(x) = \frac{1}{g}, \quad (43)$$

where $x = kR$. In obtaining the above relation, the equality in Eq. (18) has been used. As x is pure imaginary, it is convenient to introduce a real valued variable through $x = iy$. The right hand side of Eq. (43) then becomes a real function $f_l(y)$, which satisfies

$$f_l(y) \equiv -y j_l(iy) h_l(iy). \quad (44)$$

For $l = 0$, one has

$$j_0(iy) = \frac{\sinh(y)}{y}, \quad h_0(iy) = -\frac{e^{-y}}{y}. \quad (45)$$

For $l > 0$, the recurrence formula

$$b_{l+1}(iy) = i \left(-\frac{l}{y} b_l(iy) + \frac{db_l(iy)}{dy} \right), \quad (46)$$

is useful, where b is either j or h . Eq. (46) enables expressions of f_l for successive values of l to be generated:

$$\begin{aligned} f_0(y) &= \sinh(y) \frac{e^{-y}}{y}, \\ f_1(y) &= \left(\cosh(y) - \frac{\sinh(y)}{y} \right) \left(1 + \frac{1}{y} \right) \frac{e^{-y}}{y}, \\ f_2(y) &= \left(\left(\frac{3}{y^2} + 1 \right) \sinh(y) - \frac{3}{y} \cosh(y) \right) \left(1 + \frac{3}{y} + \frac{3}{y^2} \right) \frac{e^{-y}}{y}. \end{aligned} \quad (47)$$

Eq. (43) is of the form

$$f_l(y) = \frac{1}{g}. \quad (48)$$

Written as in Eq. (48), the bound state energies are easily determined by a graphical procedure. Figure 8 shows the main characteristic of the function f_l ; it gradually decreases as y increases. The value of f_l at $y = 0$ and the asymptotic form for $y \rightarrow \infty$ are found by appropriate expansions of the Bessel and Hankel functions⁴:

$$f_l(0) = \frac{1}{2l+1}, \quad (49)$$

$$f_l(y \rightarrow \infty) \rightarrow \frac{1}{2y}. \quad (50)$$

The intersection of $f_l(y)$ with the constant line $\frac{1}{g}$ determines the bound state energy for a given value of l . The magnitude of g sets the total number of bound states. Explicitly,

$g < 1$: no bound states at all,

$g \geq 1$: there are several bound states from $l = 0$ up to $l_{max} = \lfloor \frac{g-1}{2} \rfloor$.

The notation $[q]$ means the integer part of q .

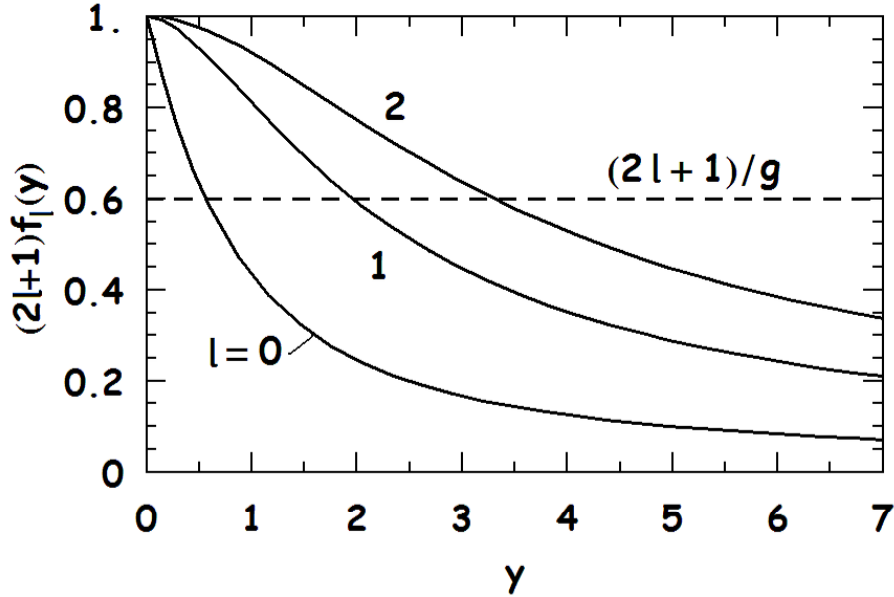


Fig. 8. An illustration of the determination of bound states using Eq. (48).

The binding solutions y_l for low values of $l = 0, 1, \dots$ are plotted in Fig. 9 as a function of the strength parameter g . The bound state energies are given by $-\frac{\hbar^2 y_l^2}{2\mu R^2}$. If $g \approx 2l + 1$, the energies are close to a resonance value. When the energy is small, the solution in Eq. (48) can be well approximated by a power series in y ; the result is

$$y_l^2(g \approx 2l + 1) \approx \begin{cases} \left(\frac{3g - \sqrt{3(8-5g)g}}{4g} \right)^2 \approx \left(\frac{g-1}{g} \right)^2 & \text{for } l = 0, \\ \left(\frac{g-(2l+1)}{g} \right) \frac{(2l-1)(2l+3)}{2} & \text{for } l > 0. \end{cases} \quad (51)$$

Also, for the case $g \gg 2l + 1$, we have from Eq. (50)

$$y_l(g \gg 2l + 1) \approx \frac{g}{2}. \quad (52)$$

6. The scattering length, effective range and the delta-shell model of the deuteron

The properties of the deuteron, the simplest nucleus consisting of a neutron and a proton, are well measured in experiments. Some basic properties include the scattering length a_{sl} , the effective range r_0 and the shape parameter P which are defined through an expansion of $k \cot(\delta_0)$ as¹⁷

$$k \cot(\delta_0) = -\frac{1}{a_{sl}} + r_0 \frac{k^2}{2} - P r_0^3 k^4 + O(k^6). \quad (53)$$

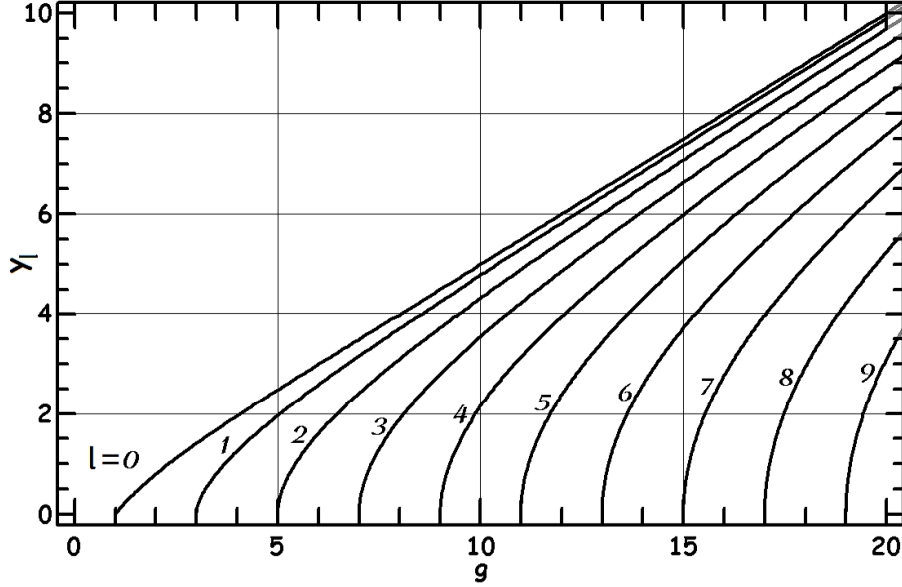


Fig. 9. Solutions $y_l(g)$ of the equation $f_l(y) = \frac{1}{g}$ for different partial waves l versus the strength parameter g .

For $l > 0$ partial waves, Newton¹⁸ generalizes the above to read as

$$k^{2l+1} \cot(\delta_l) = -\frac{1}{a_{sl}^{(l)}} + r_0^{(l)} \frac{k^2}{2} + O(k^4). \quad (54)$$

Expanding Eq. (15) for the delta-shell in a similar manner yields

$$k \cot(\delta_0) = \frac{1-g}{Rg} + R \left(1 + \frac{1}{g}\right) \frac{k^2}{3} + R^3 \frac{(3+g)}{g} \frac{k^4}{45} + o(k^6), \quad (55)$$

from which we infer:

$$\text{scattering length: } \frac{a_{sl}}{R} = \frac{g}{g-1}, \quad (56)$$

$$\text{effective range: } \frac{r_0}{R} = \frac{2}{3} \left(1 + \frac{1}{g}\right), \quad (57)$$

$$\text{shape parameter: } P = -\frac{3}{40} \frac{g^2(3+g)}{(1+g)^3}. \quad (58)$$

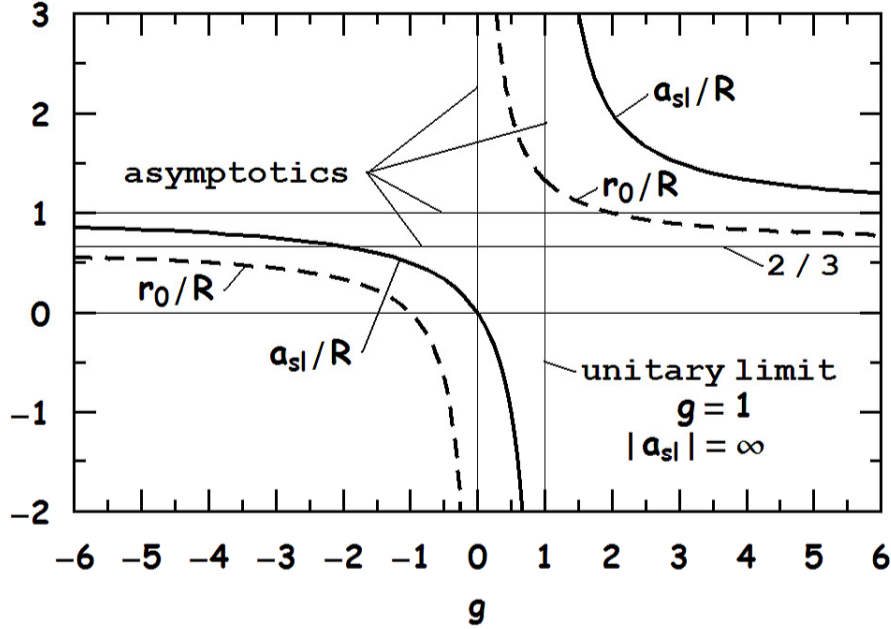


Fig. 10. S-wave ($l = 0$) scattering length and effective range as functions of the strength parameter g .

Generalizing for $l \geq 0$, the l^{th} -wave scattering length parameter $a_{sl}^{(l)}$ and l^{th} -wave range parameter $r_0^{(l)}$ are

$$\frac{a_{sl}^{(l)}}{R^{2l+1}} = \frac{(2l+1)}{((2l+1)!!)^2} \left(\frac{g}{g - (2l+1)} \right), \quad (59)$$

$$\frac{r_0^{(l)}}{R^{1-2l}} = \frac{2((2l+1)!!)^2}{(2l+3)(2l-1)} \left(\frac{2l-1}{g} - 1 \right). \quad (60)$$

These results reflect the leading order behaviors of the partial wave cross sections and have multiple dimensions of length. Fig. 10 shows the scattering length and effective range as functions of the strength parameter g . It is worthwhile to note that one can make the scattering length in Eq. (59) very large by choosing the value of g very close to $2l + 1$.

In the triplet configuration, the deuteron is dominated by the S-state and has a scattering length¹⁹ of 5.42 fm. One can adjust the parameters R and g to get the binding energy to the measured value¹⁹ of 2.2246 MeV. This fitting results in the model parameters $R = 1.564$ fm and $g = 1.406$ or $\Lambda = 0.899$ fm⁻¹. With these numbers, expressions (57) and (58) give the effective range $r_0 = 1.79$ fm which is very close to the experimental value¹⁹ 1.76 fm, but the shape parameter $P = -0.047$ differs substantially from the experimental value¹⁹ of -0.007 . Not

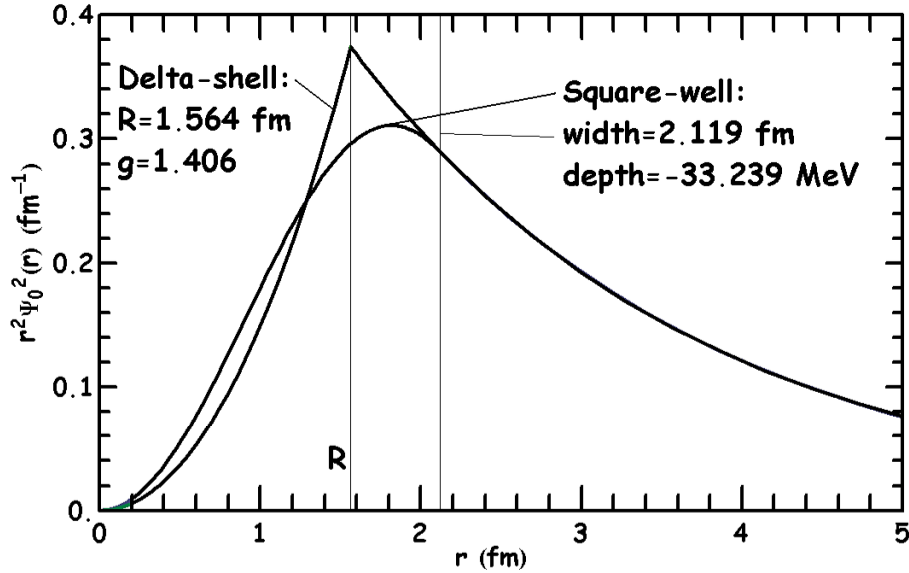


Fig. 11. The deuteron probability density distributions for the delta-shell and square well models.

unexpectedly, the delta shell potential, being spherically symmetric and simplistic, differs from the real potential probed at higher energies²⁰. The bound-state wave function can be used to calculate the root mean square radius of the deuteron:

$$r_{rms} \equiv \frac{1}{2} \sqrt{\frac{\int d^3r r^2 |\psi(r)|^2}{\int d^3r |\psi(r)|^2}}. \quad (61)$$

The result is 1.95 fm, which is close to the experimental value¹⁹ 1.97 fm. The probability densities for the delta-shell and square-well models of the deuteron are shown in Fig. 11. They have very similar distributions in the outer region as expected from low-energy scattering in which the core of the potential is obscured¹⁷.

7. Differential equation for S-wave scattering length and effective range

Here, we derive a set of differential equations for the numerical calculation of the S-wave scattering length and effective range following the method outlined by Flügge²¹. We first cast the potential as

$$V(r) = V_0 \phi(\xi), \quad (62)$$

where V_0 has dimensions of energy and $\phi(\xi)$ is a dimensionless function of $\xi = \frac{r}{R}$, with R being a characteristic length scale of the potential. The S-wave radial

Schrödinger equation then reads

$$u''(\xi) + (g\phi(\xi) + x^2)u(\xi) = 0, \quad (63)$$

where $g = -\frac{2\mu V_0}{\hbar^2}R^2$, $k^2 = \frac{2\mu E}{\hbar^2}$ and $x = kR$. Let us expand the solution as a series in x :

$$u(\xi) = u_0(\xi) + u_1(\xi)x + u_2(\xi)x^2 + \dots \quad (64)$$

Substitution of Eq. (64) into Eq. (63) yields

$$\begin{cases} u_0''(\xi) + g\phi(\xi)u_0(\xi) = 0, \\ u_1''(\xi) + g\phi(\xi)u_1(\xi) = 0, \\ u_2''(\xi) + g\phi(\xi)u_2(\xi) + u_0(\xi) = 0. \end{cases} \quad (65)$$

The condition that the wave function is well behaved at the origin requires

$$u(0) = 0; \quad (66)$$

hence, from Eq. (64), it follows that

$$u_i(0) = 0, \quad (67)$$

where $i = 0, 1, 2, \dots$. Using the freedom of a particular normalization, we can choose

$$u_0'(0) = 1. \quad (68)$$

Expansion of the asymptotic solution as $x\xi = kr \rightarrow \infty$ as a series in ξ gives

$$\begin{aligned} u(x\xi \rightarrow \infty) &\rightarrow A \sin(\delta_0 + x\xi) = \\ &A \sin(\delta_0) \left(1 + x \cot(\delta_0) \xi - \frac{x^2}{2} \xi^2 - x \cot(\delta_0) \frac{x^2 \xi^3}{6} + \dots \right) = \\ &C \left(1 - \frac{\xi}{\alpha} \right) + C \left(\frac{\varrho}{2} \xi - \frac{\xi^2}{2} + \frac{\xi^3}{6\alpha} \right) x^2 + \dots, \end{aligned} \quad (69)$$

and from Eq. (54) we have

$$x \cot(\delta_0) = -\frac{1}{\alpha} + \frac{\varrho}{2}x^2 + \dots, \quad (70)$$

where $\alpha = \frac{a_{sl}}{R}$, $\varrho = \frac{r_0}{R}$ and $C = A \sin(\delta_0)$ is a normalization constant. Equation (65) and Eq. (69) imply

$$\begin{aligned} u_0(x\xi \rightarrow \infty) &\rightarrow C \left(1 - \frac{\xi}{\alpha} \right), \\ u_1(x\xi \rightarrow \infty) &\rightarrow 0, \\ u_2(x\xi \rightarrow \infty) &\rightarrow C \left(\frac{\varrho}{2} \xi - \frac{\xi^2}{2} + \frac{\xi^3}{6\alpha} \right). \end{aligned} \quad (71)$$

Therefore

$$\alpha(\xi) \equiv \xi - \frac{u_0(\xi)}{u_0'(\xi)} \xrightarrow{\xi \rightarrow \infty} \alpha, \quad (72)$$

$$\varrho(\xi) \equiv \xi - \frac{u_{20}(\xi)}{u'_{20}(\xi)} \xrightarrow{\xi \rightarrow \infty} \varrho, \quad (73)$$

where $u_{20}(\xi) \equiv u'_2(\xi) + u_0(\xi)\frac{\xi}{2}$. These formulas are useful for the numerical evaluation of the scattering length and the effective range through integration of the set in Eq. (65) with the initial conditions (67) and (68). Furthermore, in the case of the scattering length we can derive an alternative equation by combining Eq. (72), Eq. (65) and Eq. (68):

$$\begin{cases} \alpha(0) = 0, \\ \alpha'(\xi) + (\xi - \alpha(\xi))^2 g \phi(\xi) = 0. \end{cases} \quad (74)$$

This can be integrated numerically for any spherically symmetric potential (for example, the Yukawa potential $\phi(\xi) = e^{-\xi}/\xi$), but in the case of the delta-shell ($\phi(\xi) = \delta(\xi - 1)$ and $V_0 = -\frac{v}{R}$) an analytical solution can be obtained. Our task here is to apply the method above to alternatively derive the scattering length for a delta-shell potential. To begin with, the delta-shell function can be represented as

$$\delta(\xi - 1) \rightarrow \begin{cases} n & |\xi - 1| < \frac{1}{2n}, \\ 0 & |\xi - 1| \geq \frac{1}{2n}, \end{cases} \quad (75)$$

with the limit $n \rightarrow \infty$, taken at the end. With this representation the solution of Eq. (74) for $\xi > 1$ is

$$\alpha(\xi > 1 + \frac{1}{2n}) = \frac{(4n + g(4n^2 - 1)) \sin(\sqrt{g/n}) - 4\sqrt{gn} \cos(\sqrt{g/n})}{2gn(2n - 1) \sin(\sqrt{g/n}) - 4n\sqrt{gn} \cos(\sqrt{g/n})}, \quad (76)$$

where we have used the continuity conditions

$$\alpha \left(1 - \frac{1}{2n} \right) \Big|_{-0} = \alpha \left(1 - \frac{1}{2n} \right) \Big|_{+0}, \quad (77)$$

$$\alpha \left(1 + \frac{1}{2n} \right) \Big|_{-0} = \alpha \left(1 + \frac{1}{2n} \right) \Big|_{+0}, \quad (78)$$

Finally, taking the limit as $n \rightarrow \infty$ we have

$$\frac{a_{sl}}{R} = \lim_{n \rightarrow \infty} \alpha(\xi > 1 + \frac{1}{2n}) = \frac{g}{g - 1} \quad (79)$$

assuming $g \neq 1$. This coincides with the result in Eq. (56).

8. Momentum-space wave-function and form-factor for the S-wave

The S-state wave-function with the bound state energy $E = -\frac{\hbar^2 \kappa^2}{2\mu}$ has the form

$$\Psi_0(r < R) = N_0 e^{-\kappa R} \frac{\sinh(\kappa r)}{r}, \quad (80)$$

$$\Psi_0(r > R) = N_0 \sinh(\kappa R) \frac{e^{-\kappa r}}{r}, \quad (81)$$

where the normalization factor

$$N_0 = 2 \frac{e^{\kappa R}}{\sqrt{4\pi}} \sqrt{\frac{\kappa}{e^{2\kappa R} - 2\kappa R - 1}}. \quad (82)$$

Using Eq. (61), the *rms* radius turns out to be

$$r_{rms} = \frac{R}{2} \sqrt{1 + \frac{1}{2\kappa^2 R^2} + \frac{4\kappa R}{3(e^{2\kappa R} - 2\kappa R - 1)}}. \quad (83)$$

The wave-function in momentum space is given by

$$\Psi_0(k) = \frac{1}{(2\pi)^{\frac{3}{2}}} \int d^3 r e^{i\vec{k}\vec{r}} \Psi_0(r). \quad (84)$$

Performing the angular integration yields

$$\Psi_0(k) = \frac{2}{k\sqrt{2\pi}} \int_0^\infty dr r \sin(kr) \Psi_0(r). \quad (85)$$

Utilizing Eq. (80) and Eq. (81), we obtain

$$\Psi_0(k) = \frac{\kappa e^{\kappa R} \sin(kR)}{\pi k(k^2 + \kappa^2)} \sqrt{\frac{2\kappa}{e^{2\kappa R} - 2\kappa R - 1}}, \quad (86)$$

The s-state elastic form-factor

$$f_0(q) = \int d^3 r e^{i\vec{q}\vec{r}} |\Psi_0(r)|^2 = \frac{4\pi}{q} \int_0^\infty dr r \sin(qr) |\Psi_0(r)|^2, \quad (87)$$

where q is the momentum transfer in the scattering process, can be calculated numerically (as for example by the Filon method²²). Fig. 12 shows the momentum space wave-function and the form factor for the delta-shell model of the deuteron. Note that the relation between the slope of the form-factor for $q \rightarrow 0$ and the *rms* radius

$$r_{rms} = \frac{1}{2} \sqrt{-3 \frac{\partial^2 f_0}{\partial q^2} \Big|_{q=0}} \quad (88)$$

can be used as a check of the numerical procedure used to calculate Eq. (87).

9. The Feynman-Hellmann theorem applied to the delta-shell model

The Feynman-Hellmann^{7,8} theorem allows us to study the dependence of the bound state energy E on the parameters v and R of the delta-shell potential. The theorem asserts that

$$\frac{\partial E}{\partial \lambda} = \left\langle \frac{\partial H}{\partial \lambda} \right\rangle_{\Psi_{lm}}, \quad (89)$$

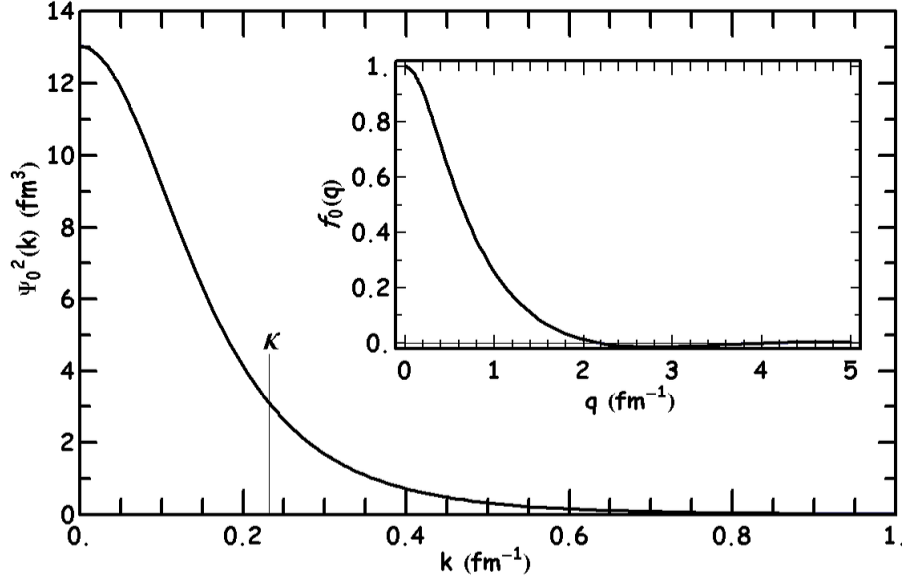


Fig. 12. The delta-shell model momentum space wave-function and form-factor for the deuteron as a function of momentum k and momentum transfer q . The second derivative of the curve at $q = 0$ gives $r_{rms} = 1.95$ fm.

where the angular brackets denote an expectation value in the basis of wavefunctions Ψ , and λ is any parameter in the Hamiltonian H .

In contrast to the commonly studied cases of $V(r) \propto r^q (q > -2)$, the singular behavior of the delta-shell interaction $V(r) = -v \delta(r-R)$ requires special treatment.

Choosing R as the parameter,

$$\begin{aligned} \frac{\partial E}{\partial R} &= \left\langle \frac{\partial V(r)}{\partial R} \right\rangle_{\Psi_{lm}} = -v \left\langle \frac{\partial}{\partial R} \delta(r-R) \right\rangle_{\Psi_{lm}=\psi(r)Y_m^l(\Omega)} = v \left\langle \frac{\partial}{\partial r} \delta(r-R) \right\rangle_{\psi(r)} \\ &= v\kappa \left\langle \frac{\partial}{\partial \rho} \delta(\rho-y) \right\rangle_{u(\rho=\kappa r)} \equiv v\kappa \langle \delta'(\rho-y) \rangle, \end{aligned} \quad (90)$$

where

$$\langle F(r) \rangle_{\psi} \equiv \int_0^{\infty} \psi F(r) \psi r^2 dr, \quad (91)$$

and

$$\langle F(\rho) \rangle = \langle F(\rho) \rangle_u \equiv \int_0^{\infty} u F(\rho) u d\rho. \quad (92)$$

To facilitate easy manipulations, a Gaussian representation of the delta function is helpful:

$$\delta_n(r - R) = \frac{1}{2\sqrt{\pi n}} e^{-(r-R)^2/n} \xrightarrow{n \rightarrow \infty} \delta(r - R), \quad (93)$$

using which one can easily check the validity of Eq. (90).

To start with, consider $l = 0$ (s-wave) for which the Schrödinger Eq. (5) becomes

$$u''_{0n}(\rho) = \left(1 - \frac{\Lambda}{\kappa} \delta_n(\rho - y)\right) u_{0n}(\rho), \quad (94)$$

where $u_{0n}(\rho)$ are continuous. Note first the identity

$$\int_0^\infty u'_{0n} u''_{0n} d\rho = \int_0^\infty d \left(\frac{[u'_{0n}]^2}{2} \right) = -\frac{[u'_{0n}(0)]^2}{2}. \quad (95)$$

Alternatively, multiplying Eq. (94) by u'_{0n} and integrating both sides of Eq. (94) we obtain

$$\begin{aligned} \int_0^\infty u'_{0n} u''_{0n} d\rho &= \int_0^\infty \left(1 - \frac{\Lambda}{\kappa} \delta_n(\rho - y)\right) d \left(\frac{[u_{0n}]^2}{2} \right) \\ &= -\frac{[u_{0n}(0)]^2}{2} + \frac{\Lambda}{2\kappa} \int_0^\infty u_{0n} \delta'_n(\rho - y) u_{0n} d\rho = \frac{\Lambda}{2\kappa} \langle \delta'_n(\rho - y) \rangle_{0n}, \end{aligned} \quad (96)$$

where the condition in Eq. (11) has been used. In the limit $n \rightarrow \infty$, Eq. (95) and Eq. (96) imply that

$$\langle \delta'(\rho - x) \rangle_0 = -\kappa \frac{[u'_0(0)]^2}{\Lambda}. \quad (97)$$

For the case of $l > 0$, the Schrödinger Eq. (5) takes the form

$$u''_{ln}(\rho) = \left(\frac{l(l+1)}{\rho^2} + 1 - \frac{\Lambda}{\kappa} \delta_n(\rho - y) \right) u_{ln}(\rho). \quad (98)$$

In this case, Eq. (96) becomes

$$\begin{aligned} \int_0^\infty u'_{ln} u''_{ln} d\rho &= \int_0^\infty \left(\frac{l(l+1)}{\rho^2} + 1 - \frac{\Lambda}{\kappa} \delta_n(\rho - y) \right) d \left(\frac{[u_{ln}]^2}{2} \right) \\ &= -l(l+1) \frac{[u_{ln}(0)]^2}{2\rho^2} + l(l+1) \int_0^\infty u_{ln} \frac{1}{\rho^3} u_{ln} d\rho + \frac{\Lambda}{2\kappa} \langle \delta'_n(\rho - y) \rangle_{ln} \\ &= l(l+1) \langle \rho^{-3} \rangle_{ln} + \frac{\Lambda}{2\kappa} \langle \delta'_n(\rho - y) \rangle_{ln}, \end{aligned} \quad (99)$$

where $\langle \rho^{-3} \rangle$ is the third inverse moment. The first term in the second line vanishes because $u_{ln}(\rho \rightarrow 0) \propto \rho^{l+1}$ (this is the regular solution given by Eq. (98) in the limit $\rho \rightarrow 0$). Thus for $l > 0$, the left hand side of Eq. (99), using Eq. (95), becomes zero as $u'_{ln}(\rho \rightarrow 0) \propto \rho^l$. Taking the limit $n \rightarrow \infty$, we obtain

$$\langle \delta'(\rho - y) \rangle_l = -2\kappa \frac{l(l+1)}{\Lambda} \langle \rho^{-3} \rangle_l. \quad (100)$$

Eq. (97) and Eq. (100) together with Eq. (90) yield

$$\frac{\partial E}{\partial R} = 2E \cdot \begin{cases} \frac{[u'_0(0)]^2}{2} & l = 0, \\ l(l+1) \langle \rho^{-3} \rangle_l & l_{max} \geq l > 0, \end{cases} \quad (101)$$

where $l_{max} = \lceil \frac{g-1}{2} \rceil$ is the largest angular momentum allowed in order for a bound state to form when the parameter g is fixed (see 5).

Choosing v as the parameter, the theorem in Eq. (89) gives

$$\frac{\partial E}{\partial v} = \left\langle \frac{\partial V(r)}{\partial v} \right\rangle_{\Psi_{lm} = \Psi_l(r) Y_m^l(\Omega)} = - \langle \delta(r-R) \rangle_{\Psi_l(r)} = -R^2 \Psi_l^2(R). \quad (102)$$

The expressions derived using the Feynman-Hellmann theorem will be utilized to advantage in subsequent sections.

10. Wave function normalization for bound states

The Feynman-Hellmann theorem Eq. (89) can be used to normalize the $l \neq 0$ partial waves. If the parameter g is held fixed while varying the parameter R , then the radial wave function of the bound state takes the form

$$\Psi_l(r) = \frac{N_l(y)}{R^{3/2}} \cdot \begin{cases} h_l(iy) j_l(iy \frac{r}{R}) & \text{for } r < R, \\ j_l(iy) h_l(iy \frac{r}{R}) & \text{for } r > R, \end{cases} \quad (103)$$

where y is the solution of Eq. (48); note that now y is fixed too. In this case, the partial derivative of the wave function Eq. (103) with respect to the parameter R (keeping g fixed) is given by

$$\left(\frac{\partial \Psi_l}{\partial R} \right)_g = -\frac{3}{2R} \Psi_l + \frac{N_l(y)}{R^{3/2}} \cdot \begin{cases} h_l(iy) \left(-\frac{l}{R} j_l(iy \frac{r}{R}) + \frac{iy r}{R^2} j_{l+1}(iy \frac{r}{R}) \right); & r < R \\ j_l(iy) \left(-\frac{l}{R} h_l(iy \frac{r}{R}) + \frac{iy r}{R^2} h_{l+1}(iy \frac{r}{R}) \right); & r > R, \end{cases} \quad (104)$$

where the recurrence formula in Eq. (46) was used. In a compact form

$$\left(\frac{\partial \Psi_l}{\partial R} \right)_g = -\frac{3+2l}{2R} \Psi_l + yr \frac{N_l(y)}{R^{7/2}} \cdot \begin{cases} ih_l(iy) j_{l+1}(iy \frac{r}{R}) & \text{for } r < R \\ ij_l(iy) h_{l+1}(iy \frac{r}{R}) & \text{for } r > R. \end{cases} \quad (105)$$

The next step is to use the equality

$$\begin{aligned} \left(\frac{\partial}{\partial R} \langle \Psi_l | \delta(r-R) | \Psi_l \rangle \right)_g &= \left\langle \left(\frac{\partial \Psi_l}{\partial R} \right)_g \middle| \delta(r-R) | \Psi_l \right\rangle + \langle \Psi_l | \delta(r-R) \left(\frac{\partial \Psi_l}{\partial R} \right)_g \rangle \\ &\quad + \langle \Psi_l | \left(\frac{\partial \delta(r-R)}{\partial R} \right)_g | \Psi_l \rangle, \end{aligned} \quad (106)$$

which follows from the chain rule for derivatives. First, we calculate the left hand side of Eq. (106):

$$\left(\frac{\partial (R^2 \Psi_l^2(r=R))}{\partial R} \right)_g = -R \Psi_l^2(r=R), \quad (107)$$

since $R^2\Psi_l^2(r=R) \propto \frac{1}{R}$ as follows from Eq. (103). For the calculation of the first two terms on the right hand side of Eq. (106), we make use of Eq. (103) and Eq. (104) to obtain

$$\begin{aligned} \langle \Psi_l | \delta(r-R) \left| \left(\frac{\partial \Psi_l}{\partial R} \right)_g \right. \rangle &= -\frac{3+2l}{2} R\Psi_l^2(r=R) + \\ y \frac{N_l^2(y)}{R^2} h_l(iy) j_l(iy) &\cdot \begin{cases} ih_l(iy) j_{l+1}(iy); & r=R-0, \\ ij_l(iy) h_{l+1}(iy) & r=R+0. \end{cases} \end{aligned} \quad (108)$$

Note that the difference between the expressions inside the curly bracket is equal to $\frac{1}{y^2}$ from the relations in Eq. (18) and Eq. (46). The discontinuity at $r=R$ must be treated with some care. The average of the left and right limiting values as $r \rightarrow R \pm 0$ is

$$\begin{aligned} \langle \Psi_l | \delta(r-R) \left| \left(\frac{\partial \Psi_l}{\partial R} \right)_g \right. \rangle &= -\frac{3+2l}{2} R\Psi_l^2(r=R) + \\ y \frac{N_l^2(y)}{R^2} h_l(iy) j_l(iy) &\left(ih_l(iy) j_{l+1}(iy) - \frac{1}{2y^2} \right), \end{aligned} \quad (109)$$

or equivalently,

$$\begin{aligned} \langle \Psi_l | \delta(r-R) \left| \left(\frac{\partial \Psi_l}{\partial R} \right)_g \right. \rangle &= -\frac{3+2l}{2} R\Psi_l^2(r=R) + \\ y \frac{N_l^2(y)}{R^2} h_l(iy) j_l(iy) &\left(ij_l(iy) h_{l+1}(iy) + \frac{1}{2y^2} \right). \end{aligned} \quad (110)$$

Finally, we substitute Eq. (109) and Eq. (107) into Eq. (106) to get

$$\begin{aligned} \langle \Psi_l | \left(\frac{\partial \delta(r-R)}{\partial R} \right)_g | \Psi_l \rangle &= 2(l+1) R\Psi_l^2(r=R) - \\ &\frac{N_l^2(y)}{yR^2} h_l(iy) j_l(iy) (2iy^2 h_l(iy) j_{l+1}(iy) - 1). \end{aligned} \quad (111)$$

Now the Feynman-Hellmann theorem can be applied in the form

$$\left(\frac{\partial E(R)}{\partial R} \right)_g = \left\langle \left(\frac{\partial V(r)}{\partial R} \right)_g \right\rangle = -v(R) \left\langle \left(\frac{\partial \delta(r-R)}{\partial R} \right)_g \right\rangle - \frac{\partial v(R)}{\partial R} \langle \delta(r-R) \rangle, \quad (112)$$

where $v(R) = \frac{\hbar^2 g}{2\mu R}$ from Eq. (16), and $E(R) = -\frac{\hbar^2 y^2}{2\mu R^2}$ by the definition of y . Evaluating the derivatives above and the expectation value of the delta function, we find

$$-2 \frac{y^2}{gR^2} = \left\langle \left(\frac{\partial \delta(r-R)}{\partial R} \right)_g \right\rangle - R\Psi_l^2(r=R), \quad (113)$$

where in the intermediate step we divided the whole expression by v and used the definition of g in Eq. (16). Inserting Eq. (108) into Eq. (113) and using the explicit

form of the wave function in Eq. (103) gives the equation for normalization $N_l^2(y)$ as

$$2\frac{y^2}{g} = (2l+1)N_l^2(y)h_l^2(iy)j_l^2(iy) - \frac{N_l^2(y)}{y}h_l(iy)j_l(iy)(2iy^2h_l(iy)j_{l+1}(iy) - 1), \quad (114)$$

where R cancels out as expected, as $N_l(y)$ is independent of R for g held fixed. Recalling that $-yj_l(iy)h_l(iy) = \frac{1}{g}$ as the equation for the bound states (48), we can solve the above equation for the normalization constant $N_l(y)$ with the result

$$N_l^2(y) = \frac{2y^4}{1 + (2l+1)yj_l(iy)h_l(iy) - 2y^2ij_{l+1}(iy)h_l(iy)}. \quad (115)$$

Eq. (44) allows to rewrite the above result in the shorter form

$$N_l^2(y) = \frac{2gy^4}{g - (2l+1) - 2gy^2ij_{l+1}(iy)h_l(iy)}. \quad (116)$$

A quick way to calculate the normalization constant $N_l(y)$ is to use Eq. (102). The partial derivative of the energy with respect to the parameter v is easily calculated from Eq. (48):

$$\frac{\partial E}{\partial v} = -2\frac{E}{y}\frac{\partial y}{\partial v} = 2\frac{E}{v}\left(\frac{j_l(iy)h_l(iy)}{j_l(iy)h_l(iy) + y\left(\frac{dj_l(iy)}{dy}h_l(iy) + j_l(iy)\frac{dh_l(iy)}{dy}\right)}\right). \quad (117)$$

Application of Eq. (46) and Eq. (103) leads to the same expression as Eq. (115). Also, this result coincides with the expression obtained by a straightforward integration of the square of the wave function Eq. (103) using Lommel's integral²³

$$(\alpha^2 - \beta^2) \int_{x_0}^{x_1} x B_n(\alpha x) B_n(\beta x) dx = x [\beta B_n(\alpha x) B_{n-1}(\beta x) - \alpha B_{n-1}(\alpha x) B_n(\beta x)] \Big|_{x_0}^{x_1}, \quad (118)$$

where B_n is the Bessel function of either the first or the second kind.

11. Virial theorem

The virial theorem relates the expectation value of the kinetic energy $\langle T \rangle$ with the expectation value of the potential energy $\langle V \rangle$ for a system in a bound state. For the well known power law potentials $V_n(r) \propto r^n$, the virial theorem gives

$$\frac{\langle T \rangle}{\langle V_n \rangle} = \frac{n}{2}. \quad (119)$$

In the following, we establish the virial relation for the delta-shell potential. First, from the Hamiltonian $H = T + V$ it follows that

$$E = \langle T \rangle + \langle V \rangle, \quad (120)$$

where $E = -\frac{\hbar^2 y^2}{2\mu R^2}$ is a bound state energy. Next, we have

$$\langle V(r) \rangle = -v \langle \delta(r - R) \rangle_{\Psi_l(r)} = \frac{-v N_l^2(y)}{R g(y)^2 y^2} = \frac{N_l^2(y)}{g(y) y^4} E, \quad (121)$$

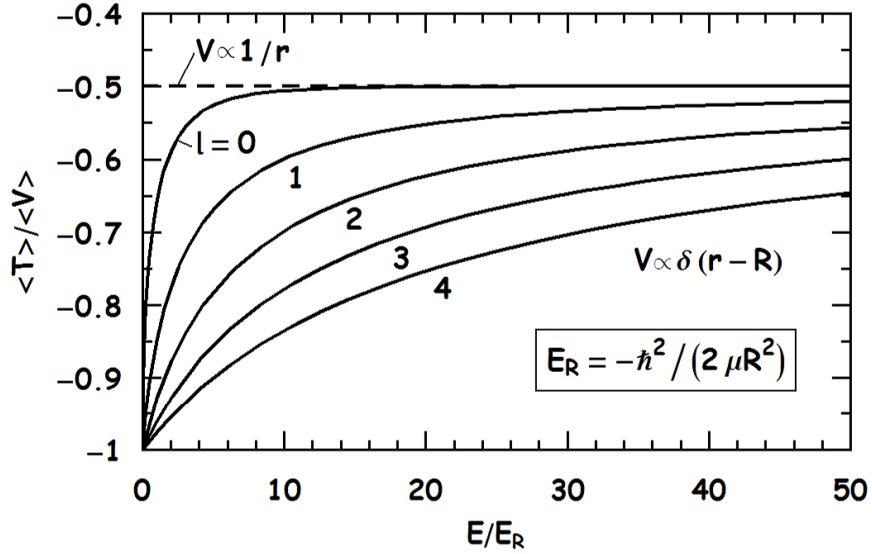


Fig. 13. Ratio of the average kinetic and potential energies (from the virial theorem) for the delta-shell potential. The horizontal dashed line shows the result for $V(r) \propto \frac{1}{r}$.

from Eq. (116), Eq. (48), Eq. (16) and Eq. (103). The kinetic term is found from Eq. (120)

$$\langle T \rangle = E - \langle V \rangle = \left(1 - \frac{N_l^2(y)}{g(y)y^4} \right) E. \quad (122)$$

Hence

$$\frac{\langle T \rangle}{\langle V \rangle} = \left(\frac{g(y)y^4}{N_l^2(y)} - 1 \right), \quad (123)$$

where $g(y) = 1/f_l(y)$ is a bound state energy from Eq. (48) and $f_l(y)$ is defined in Eq. (44). Explicitly

$$\frac{\langle T \rangle}{\langle V \rangle} = -\frac{1}{2} \left(2l + 3 + \frac{1}{y j_l(iy) h_l(iy)} - 2iy \frac{j_{l+1}(iy)}{j_l(iy)} \right). \quad (124)$$

The result is energy and angular momentum dependent as shown in Fig. 13. For deeply bound states ($y \rightarrow \infty$), the result asymptotically behaves as in the case of the Coulomb potential $\frac{1}{r}$ approaching the value of $-1/2$.

12. Relationship between moments: Kramers-Pasternak-like relation

Kramers⁹ and Pasternak¹⁰ independently noted that the various moments $\langle \rho^p \rangle \equiv \int_0^\infty u(\rho) \rho^p u(\rho) d\rho$ of the bound state wave functions of the hydrogen atom (for which the Bohr radius provides the natural length scale) were related according to

$$(p+1)y\langle \rho^p \rangle - (2p+1)\langle \rho^{p-1} \rangle + \frac{p}{4}y((2l+1)^2 - p^2)\langle \rho^{p-2} \rangle = 0, \quad (125)$$

where $p \geq -(2l+1)$.

Here we present Kramers-Pasternak-like relations that connect the various moments of the wave function for the delta-shell potential. It must be noted that, unlike for the hydrogen atom, the wave functions exhibit a kink at the shell size R of the potential, and some care must be taken to enforce the jump conditions.

Let us consider the following expectation value in the basis of wavefunctions $u(\rho)$

$$\begin{aligned} \langle \rho^s \delta'(\rho - y) \rangle &= \int_0^\infty u(\rho) \rho^s \frac{\partial \delta(\rho - y)}{\partial \rho} u(\rho) d\rho = \\ &= \int_0^\infty \frac{\partial}{\partial \rho} (u^2(\rho) \rho^s) \delta(\rho - y) d\rho = \\ 2u(y)u'(y)y^s + s y^{s-1} u^2(y) &= y^s \langle \delta'(\rho - y) \rangle + s y^{s-1} u^2(y), \end{aligned} \quad (126)$$

where s is an integer. Therefore we obtain

$$\langle \rho^s \delta' \rangle = y^{s-1} (s u^2(y) + y \langle \delta' \rangle). \quad (127)$$

Next we define a moment of order q as

$$\langle \rho^q \rangle \equiv \int_0^\infty u(\rho) \rho^q u(\rho) d\rho, \quad (128)$$

with the requirement $q \geq -(2l+2)$ assuring the convergence of the integral (128).

Now we return to the radial Schrödinger equation (98). Integration of Eq. (128) by parts yields the useful formula

$$\int_0^\infty u_n(\rho) \rho^{q+1} u_n'(\rho) d\rho = -\frac{(q+1)}{2} \langle \rho^q \rangle_n. \quad (129)$$

Multiplying Eq. (98) by $u_n(\rho) \rho^{p-1}$ and integrating over ρ , we get

$$\int_0^\infty u_n(\rho) \rho^{p-1} u_n''(\rho) d\rho = l(l+1) \langle \rho^{p-3} \rangle_n + \langle \rho^{p-1} \rangle_n - \frac{g}{y} \langle \rho^{p-1} \delta_n(\rho - y) \rangle_n, \quad (130)$$

where $p > -2l$. On the other hand, we can integrate by parts to get

$$\begin{aligned} \int_0^\infty u_n \rho^{p-1} du_n' &= -(p-1) \int_0^\infty u_n \rho^{p-2} u_n' d\rho - \int_0^\infty (u_n')^2 \rho^{p-1} d\rho \\ &= - \int_0^\infty (u_n')^2 \rho^{p-1} d\rho + \frac{1}{2} (p-1)(p-2) \langle \rho^{p-3} \rangle_n, \end{aligned} \quad (131)$$

30 *Contents*

where we have used Eq. (129) in the last step. Proceeding further with integration by parts

$$\begin{aligned}
& \frac{1}{p} \int_0^\infty (u'_n)^2 d\rho^p = -\frac{2}{p} \int_0^\infty u'_n \rho^p u''_n d\rho \\
&= -\frac{2l(l+1)}{p} \int_0^\infty u_n \rho^{p-2} u'_n d\rho - \frac{2}{p} \int_0^\infty u_n \rho^p u'_n d\rho + \frac{g}{py} \int_0^\infty \rho^p \delta_n(\rho-y) du_n^2 \\
&= l(l+1) \frac{p-2}{p} \langle \rho^{p-3} \rangle_n + \langle \rho^{p-1} \rangle_n - \frac{g}{y} \langle \rho^{p-1} \delta_n(\rho-y) \rangle_n, -\frac{g}{py} \langle \rho^p \delta'_n(\rho-y) \rangle_n.
\end{aligned} \tag{132}$$

Hence

$$\begin{aligned}
\int_0^\infty u_n \rho^{p-1} du'_n &= \frac{1}{2}(p-1)(p-2) \langle \rho^{p-3} \rangle_n \\
&\quad - l(l+1) \frac{p-2}{p} \langle \rho^{p-3} \rangle_n - \langle \rho^{p-1} \rangle_n + \frac{g}{y} \langle \rho^{p-1} \delta_n(\rho-y) \rangle_n + \frac{g}{py} \langle \rho^p \delta'_n(\rho-y) \rangle_n.
\end{aligned} \tag{133}$$

Setting Eq. (133) equal to Eq. (130), we have

$$\begin{aligned}
\langle \rho^p \delta'_n(\rho-y) \rangle_n &= \frac{y(p-1)}{g} \left(2l(l+1) - \frac{p}{2}(p-2) \right) \langle \rho^{p-3} \rangle_n \\
&\quad + \frac{2yp}{g} \langle \rho^{p-1} \rangle_n - 2p \langle \rho^{p-1} \delta_n(\rho-y) \rangle_n.
\end{aligned} \tag{134}$$

In the limit $n \rightarrow \infty$,

$$\langle \rho^p \delta'(\rho-y) \rangle = \frac{y(p-1)}{g} \left(2l(l+1) - \frac{p}{2}(p-2) \right) \langle \rho^{p-3} \rangle + \frac{2yp}{g} \langle \rho^{p-1} \rangle - 2py^{p-1} u^2(y), \tag{135}$$

where $p > -2l$. In particular,

$$\langle \rho \delta'(\rho-y) \rangle = \frac{2y^2}{gR} - 2u^2(y), \tag{136}$$

$$\langle \rho^2 \delta'(\rho-y) \rangle = l(l+1) \frac{2y}{g} \langle \rho^{-1} \rangle + \frac{4y}{g} \langle \rho \rangle - 4yu^2(y), \tag{137}$$

$$\langle \rho^3 \delta'(\rho-y) \rangle = \frac{y^2}{gR} (4l(l+1) - 3) + \frac{6y}{g} \langle \rho^2 \rangle - 6y^2 u^2(y), \tag{138}$$

where the normalization $\langle 1 \rangle = y/R$ is used. Taking Eq. (136), we can rewrite Eq. (127) as

$$\langle \rho^s \delta' \rangle = y^{s-1} \left((s-3) u^2(y) + \frac{2y^2}{gR} \right). \tag{139}$$

Eq. (135) allows us to derive Kramers-Pasternak-like relations for the moments of the delta-shell potential as

$$(s-1)(4l(l+1) - s(s-2))\langle \rho^{s-3} \rangle + 4s\langle \rho^{s-1} \rangle = 2y^{s-2} \left(3g(s-1)u^2(y) + \frac{2y^2}{R} \right), \quad (140)$$

where $s > -2l$. The case $s = 3$ gives

$$u^2(y) = \frac{2l(l+1) - y^2 - 3/2}{3gR} + \frac{\langle \rho^2 \rangle}{gy}, \quad (141)$$

and therefore the final expression is

$$(s-1)(4l(l+1) - s(s-2))R\langle \rho^{s-3} \rangle + 4sR\langle \rho^{s-1} \rangle - 6(s-1)y^{s-3}R\langle \rho^2 \rangle = 2y^{s-2}((s-1)(2l(l+1) - y^2 - 3/2) + 2y^2). \quad (142)$$

The above expression, which is the Kramers-Pasternak-like relation for the delta-shell potential, is the main result of this section.

Also we recall from Eq. (97) and Eq. (100) the relation

$$\langle \delta'(\rho - y) \rangle = -\frac{y}{g} \cdot \begin{cases} [u'_0(0)]^2 & l = 0, \\ 2l(l+1)\langle \rho^{-3} \rangle & l_{max} \geq l > 0. \end{cases} \quad (143)$$

If we take partial derivatives of both sides of Eq. (44) with respect to the parameter R , we can calculate the expression for $\langle \rho^{-3} \rangle_l$ explicitly. The result is

$$\langle \rho^{-3} \rangle_l = \frac{1}{Rl(l+1)} \left(\frac{N_l^2(y)}{2gy^4} - 1 \right), \quad (144)$$

where $l_{max} \geq l > 0$.

Substitution of these relations in Eq. (127) provides one of the moment relations. In the case of $l = 0$, we have

$$\langle \rho \rangle_0 = \frac{y^2}{R} + \frac{y^2}{4}[u'_0(0)]^2 = \frac{y^2}{R} + \frac{R^2}{4}\Psi_0^2(0) = \frac{y^2}{R} \left(\frac{e^{2y} - y - 1}{e^{2y} - 2y - 1} \right). \quad (145)$$

For $l > 0$,

$$2\langle \rho \rangle_l + l(l+1)\langle \rho^{-1} \rangle_l - y^2l(l+1)\langle \rho^{-3} \rangle_l = \frac{2y^2}{R}. \quad (146)$$

We note that since the mean value $\langle \dots \rangle \propto R^{-1}$ and $\Psi^2 \propto R^{-3}$ (see Eq. (103)), the above relations scale with the parameter R and can be calculated knowing only y and l .

Statistical physics of a dilute non-relativistic delta-shell gas

In a dilute gas at sufficiently high temperature, the equilibrium thermal properties such as energy, pressure, specific heat and entropy are adequately described by the familiar ideal gas laws for non-interacting particles. Under similar physical conditions of dilute density and high temperature, potential interactions between the particles in the system bring about corrections to the ideal gas behaviors for all of the state variables. In this section, we calculate the first quantum corrections due to the presence of interactions, specifically through the delta-shell potential, highlighting at the same time the differences that arise from Fermi and Bose statistics. As far as we are aware, such corrections for the delta-shell gas have not been considered before.

13. The first quantum correction to the ideal-gas law

To start with, we outline the formalism following the text book by Huang¹¹. For a system of N identical particles, the partition function Q_N has the form

$$Q_N(V, T) = \text{Tr} e^{-\beta \hat{H}} = \int d^{3N} r \sum_{\alpha} \Psi_{\alpha}^*(1, \dots, N) e^{-\beta \mathcal{H}} \Psi_{\alpha}(1, \dots, N), \quad (147)$$

where Ψ_{α} is a complete set of orthonormal wave functions, \vec{r}_j is the coordinate of particle $j = 1, \dots, N$, $\beta = \frac{1}{k_B T}$ (k_B is the Boltzmann constant), V and T stand for the volume and temperature of the gas, respectively.

If the separation $|\vec{r}_i - \vec{r}_j|$ between any pair of particles is larger than both the thermal de-Broglie wavelength $\lambda = \frac{h}{\sqrt{2\pi m k_B T}}$ and the range of interaction r_0 , then the cluster expansion can be applied. Explicitly, the partition function is given by

$$Q_N(V, T) = \sum_{\{m_n\}} \prod_{n=1}^N \frac{1}{m_n!} \left(\frac{V}{\lambda^3} b_n(V, T) \right)^{m_n}, \quad (148)$$

where the set $\{m_n\}$ satisfies $\sum_{n=1}^N n m_n = N$ and $b_n(V, T)$ is the n^{th} cluster integral

$$b_n(V, T) \equiv \frac{1}{n! \lambda^{3n-3} V} \int d^3 r_1 \dots d^3 r_n U_l(1, \dots, n). \quad (149)$$

If we define the Slater sum

$$W_M(1, \dots, M) \equiv M! \lambda^{3M} \sum_{\alpha} \Psi_{\alpha}^*(1, \dots, M) e^{-\beta \mathcal{H}} \Psi_{\alpha}(1, \dots, M), \quad (150)$$

then a sequence of cluster functions $U_n(1, \dots, n)$ can be generated:

$$\begin{aligned} W_1(1) &= U_1(1) \\ W_2(1, 2) &= U_1(1)U_1(2) + U_2(1, 2) \\ W_3(1, 2, 3) &= U_1(1)U_1(2)U_1(3) + U_1(1)U_2(2, 3) + U_1(2)U_2(3, 1) \\ &\quad + U_1(3)U_2(1, 2) + U_3(1, 2, 3) \\ &\dots \end{aligned} \quad (151)$$

Introducing the fugacity $z = e^{\beta\mu}$, where μ is the chemical potential, the grand canonical partition function $\mathcal{L}(z, V, T) = \sum_{N=0}^{\infty} z^N Q_N(V, T)$ in the cluster expansion has the compact form

$$\log(\mathcal{L}(z, V, T)) = \frac{V}{\lambda^3} \sum_{n=1}^{\infty} b_n z^n, \quad (152)$$

and is used to obtain the equation of state for the gas:

$$\frac{PV}{k_B T} = \log(\mathcal{L}(z, V, T)), \quad (153)$$

$$\langle N \rangle = z \frac{\partial}{\partial z} \log(\mathcal{L}(z, V, T)). \quad (154)$$

The equation of state in parametric form is expressed in terms of the cluster integrals

$$\frac{P}{k_B T} = \frac{1}{\lambda^3} \sum_{n=1}^{\infty} b_n z^n, \quad (155)$$

$$\frac{1}{v} = \frac{1}{\lambda^3} \sum_{n=1}^{\infty} n b_n z^n, \quad (156)$$

where $v = V/\langle N \rangle$ is the volume per particle. Now, one sets the volume to infinity, $V \rightarrow \infty$, to define a new quantity

$$\bar{b}_n(T) = \lim_{V \rightarrow \infty} b_n(T, V), \quad (157)$$

whence Eq. (155) and Eq. (156) are unchanged, but $b_n(T, V)$ is replaced by $\bar{b}_n(T)$. The virial expansion of the equation of state takes the form

$$\frac{Pv}{k_B T} = \sum_{n=1}^{\infty} a_n(T) \left(\frac{\lambda^3}{v} \right)^{n-1}, \quad (158)$$

where a_n are the virial coefficients. As seen from Eq. (155) and Eq. (156), the virial coefficients can be expressed in terms of the cluster integrals \bar{b}_n as

$$\begin{aligned} a_1 &= \bar{b}_1 = 1 && \rightarrow \text{ideal-gas law} \\ a_2 &= -\bar{b}_2 && \rightarrow \text{the first quantum correction} \\ a_3 &= 4\bar{b}_2^2 - 2\bar{b}_3 && \rightarrow \text{the second quantum correction} \\ a_4 &= -20\bar{b}_2^3 + 18\bar{b}_2\bar{b}_3 - 3\bar{b}_4 \\ &\dots \end{aligned} \quad (159)$$

The first correction to the ideal-gas equation of state is given by the second virial coefficient which entails the calculation of the cluster-two integral b_2 . Recall that for noninteracting ideal quantum gases the cluster integrals are¹¹

$$\bar{b}_n^{(0)} = \begin{cases} n^{-\frac{5}{2}} & \text{for an ideal Bose gas,} \\ (-1)^{n+1} n^{-\frac{5}{2}} & \text{for an ideal Fermi gas.} \end{cases} \quad (160)$$

14. Cluster-two integral and the first correction

For two interacting particles with the center of mass coordinate \vec{R} and separation \vec{r} , the cluster-two integral can be calculated as¹¹

$$\begin{aligned}\bar{b}_2 - \bar{b}_2^{(0)} &= \frac{1}{2\lambda^3 V} \int d^3 R d^3 r [W_2(1, 2) - W_2^{(0)}(1, 2)] \\ &= 2\sqrt{2} \int d^3 r \sum_n [|\psi_n(\vec{r})|^2 e^{-\beta E_n} - |\psi_n^{(0)}(\vec{r})|^2 e^{-\beta E_n^{(0)}}] \\ &= 2\sqrt{2} \sum_n (e^{-\beta E_n} - e^{-\beta E_n^{(0)}}),\end{aligned}\quad (161)$$

where the unit normalization of the two-body wave function

$$\int d^3 r |\psi_n(\vec{r})|^2 = \int d^3 r |\psi_n^{(0)}(\vec{r})|^2 = 1 \quad (162)$$

is used.

In general, the energy spectrum consists of discrete (for bound) and continuum (for scattering) states. Let $d(k)dk$ be the number of states with the wave number lying between k and dk . Equation (161) takes the form

$$\bar{b}_2 - \bar{b}_2^{(0)} = 2^{3/2} \left[\sum_{Bound} e^{-\beta E_{Bound}} + \int_0^\infty dk \left(d(k) - d^{(0)}(k) \right) e^{-\beta \frac{\hbar^2 k^2}{2\mu}} \right] \quad (163)$$

as first shown by Beth and Uhlenbeck²⁴. The expression for the density of states was found before in Eq. (25) and can be used here to obtain the working expression for the second virial coefficient (159):

$$a_2 = -\bar{b}_2^{(0)} - 2^{3/2} \sum_l' (2l+1) \left[e^{-\beta E_l} - \frac{I_l(T)}{\pi} \right], \quad (164)$$

where $2l+1$ is the multiplicity of the energy level E_l and the prime on the summation sign indicates the use of even l for Bosons and odd l for Fermions.

For the delta-shell potential, one must be careful when $g = 2l + 1$ for which $E_{Bound(l)} = 0$. As these zero-energy bound states are not normalizable, they are excluded from the discrete sum, but are accounted for by the continuous part of the energy spectrum at $k = 0$. It is also related to a proper definition of the phase shift as is done in formulating Levinson's theorem²⁵, which connects the zero-energy phase shift $\delta_l(0)$ with the number of discrete bound states¹⁸.

Some comments about the physics elucidated by the theorem are instructive. Consider zero-energy scattering by a potential, and, at first, ignore subtleties associated with the zero-energy bound states. (The subtleties arise for the zero angular momentum $l = 0$ state only). Denote the phase shift for a particle incident at an energy E with an angular momentum $l\hbar$ by $\delta_l(E)$. It is given an absolute meaning, that is, with no ambiguity with regard to multiples of π , by setting $\delta_l(E \rightarrow \infty) \rightarrow 0$. The theorem states that

$$\delta_l(E = 0) = \pi N_l, \quad (165)$$

where N_l is the number of bound states with angular momentum $l\hbar$.

In the case of the delta-shell potential, the theorem gives

$$\delta_0(0) = \pi \cdot \begin{cases} 0 & \text{for } g < 1, \\ 1/2 & \text{for } g = 1, \\ 1 & \text{for } g > 1, \end{cases} \quad (166)$$

and

$$\delta_{l>0}(0) = \pi \cdot \begin{cases} 0 & \text{for } g < 2l + 1, \\ 1 & \text{for } g \geq 2l + 1. \end{cases} \quad (167)$$

The temperature dependent partial wave integral $I_l(T)$ is given by

$$I_l(T) \equiv \int_0^\infty dx \left[-\frac{\partial \delta_l(x)}{\partial x} \right] e^{-\gamma(T)x^2}, \quad (168)$$

where $\gamma(T) = \frac{1}{2\pi} \left(\frac{\lambda(T)}{R} \right)^2$. For the virial approximation to hold, $\lambda > R$ and $\frac{\partial \delta_l}{\partial x} \propto x^{2l}$. Far from the resonances which occur for $g = 2l + 1$, these considerations imply

$$I_l \propto \left(\frac{R}{\lambda} \right)^{2l+1}. \quad (169)$$

Therefore, the smaller the partial wave, the larger the contribution to the first correction to the ideal gas equation of state. Figure 14 shows the partial wave integral $I_l(T \simeq \tilde{T})$, where \tilde{T} is defined by $\lambda(\tilde{T}) = R$ (whence $k_B \tilde{T} = \frac{1}{2\pi} \frac{(hc)^2}{R^2 mc^2}$), as a function of the parameter g . For $l > 0$, the function $I_l(T \simeq \tilde{T})$ exhibits a discontinuous jump at the resonance point $g = 2l + 1$. Let us closely examine these discontinuities for the cases of S - and P -waves. Splitting the integral, we have

$$\begin{aligned} I_0(g \approx 1) &\approx - \int_{3\Delta x}^\infty dx \delta'_0(x) e^{-\gamma(T)x^2} - \int_0^{3\Delta x} dx \delta'_{0-res}(x) e^{-\gamma(T)x^2} \approx \\ &I_0(g = 1) + \text{sign}(g - 1) \left(\frac{\pi}{2} - \sqrt{\pi\gamma(T)} |g - 1| \right), \end{aligned} \quad (170)$$

and

$$\begin{aligned} I_1(g \approx 3) &\approx - \int_{x_1+3\Delta x_1}^\infty dx \delta'_1(x) e^{-\gamma(T)x^2} - \int_0^{x_1+3\Delta x_1} dx \delta'_{1-res}(x) e^{-\gamma(T)x^2} \approx \\ &I_1(g = 3) - U(3 - g) \pi \left(1 - \frac{2125}{1728} (3 - g) \right) e^{-\gamma(T) \frac{5(3-g)}{2g}}, \end{aligned} \quad (171)$$

where Δx , Δx_1 and x_1 all $\rightarrow 0$ and we have used Eq. (31) and Eq. (40). The magnitude of the jump is π (only for $l = 0$, there are two jumps of $\pi/2$ each), which is temperature independent. This jump feature is due to the fact that the derivative of the phase shift $\frac{\partial \delta_l(x)}{\partial x}$ tends to become delta-function-like in the proximity of the resonance values of g with a normalization factor of π . For $l > 0$, the delta-function-like part is off-set from the origin and appears only if the limit is approached by g from the left hand side. So the value of the function at the exact resonance

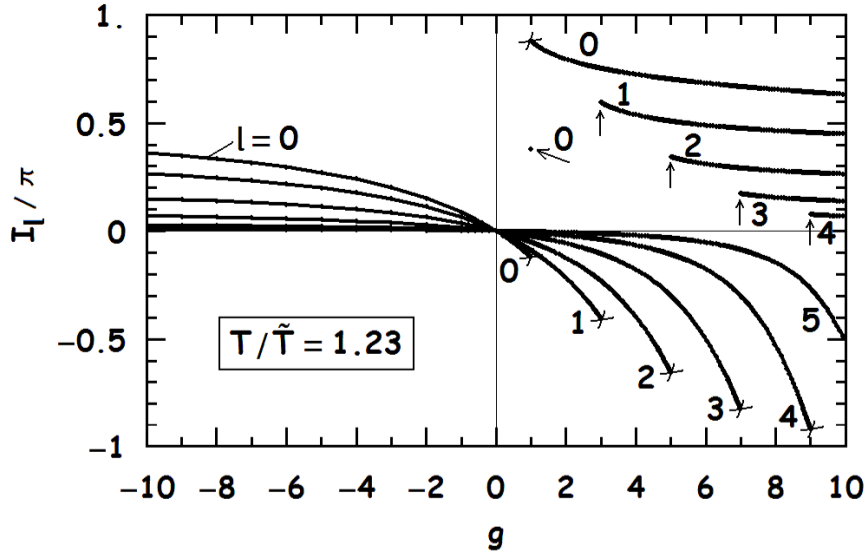


Fig. 14. The partial wave integral $I_l(T \simeq \tilde{T})$, where \tilde{T} is defined by $\lambda(\tilde{T}) = R$, as a function of the parameter g for $l = 0, 1, \dots, 5$. For $l > 0$, and at resonance points where $g = 2l + 1$, the function jumps discontinuously through a value of π . For $l = 0$, there are two discontinuous jumps each of magnitude $\frac{\pi}{2}$. Crosses indicate the limiting values which the function never takes.

point belongs to the right hand side piece of $I_l(T)$. If the temperature is taken to be much lower than \tilde{T} , the integrals tend to zero except in the proximity of the resonance points. Here, the “ π ”-jump persists, but the region in which the function significantly differs from zero narrows.

For $l = 0$, there are two discontinuous jumps of magnitude $\frac{\pi}{2}$ each. In this case, the delta-function-like peak stays centered around the origin (that gives a factor of $\frac{1}{2}$) and flips sign depending on the manner in which (left or right) the limit ($g \rightarrow 1$) is taken. However, there is no delta function at the exact resonance value. These arguments explain the discontinuous pattern for $I_0(T)$.

The above features can also be understood by interpreting the derivative of the phase shift as the density of levels. The system receives a non-vanishing contribution from zero energy levels for the resonance configuration as seen from the low energy expansions of Eq. (29). This is also the case for almost-bound (loosely bound) states near the resonance values of g .

15. Region of validity for the second virial coefficient

The two main physical conditions in our model gas are low density ($nR^3 < 1$) and temperature such that $\lambda(T) > R$. These conditions set the limits for the range of

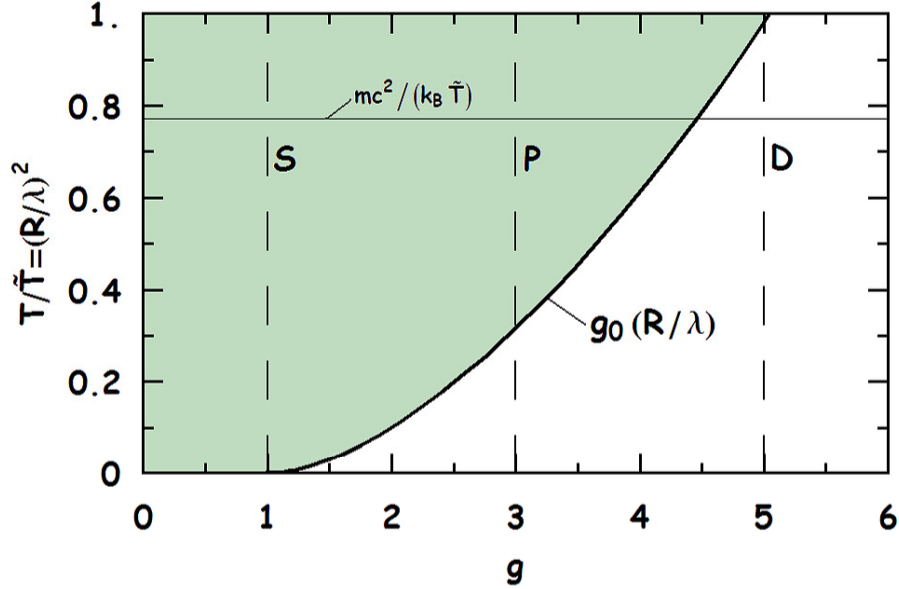


Fig. 15. The safe region in the parameter space of T and g for the second virial coefficient. The left boundary line is given by $g_0\left(\frac{R}{\lambda}\right) \equiv \frac{1}{f_0(y=\sqrt{2\pi}\left(\frac{R}{\lambda}\right))}$. At the vertical dashed lines indicated by letters of the corresponding angular momentum values, one has resonance conditions $g = 2l + 1$. The horizontal dashed line sets the upper boundary from the non-relativity condition for the gas.

the potential parameter, namely the strength g , for the second virial approximation to be valid. As shown in Fig. 15, for the upper temperature boundary $\left(\frac{R}{\lambda}\right)^2 \leq 1$ or if the mass of the particles is sufficiently small, then $\left(\frac{R}{\lambda}\right)^2 \ll \frac{mc^2}{k_B \tilde{T}}$ (the temperature scale $k_B \tilde{T} = 2\pi(\hbar c)^2/(R^2 mc^2)$) for the gas to be non-relativistic. For the second virial coefficient, two-body bound states contribute through the term $e^{-\beta E_{Bound}}$. To keep that contribution low, we have to stay in the region in which $g \leq g_0\left(\frac{R}{\lambda}\right)$; that is on the left of the curve $g_0\left(\frac{R}{\lambda}\right) \equiv \frac{1}{f_0(y=\sqrt{2\pi}\left(\frac{R}{\lambda}\right))}$, where the thermal energy equals the energy of the first bound state. Altogether, one has to stay in the grey region indicated not to exceed the relativity limit. The vertical dashed lines labeled by letters of the corresponding angular momentum values show the resonance values $g = 2l + 1$. The regions around these values require special care in the evaluation of integrals $I_l(T)$, $I_l^{(2)}(T)$ and $I_l^{(4)}(T)$ (see Eq. (230) & Eq. (231)).

16. The second virial coefficient in terms of the scattering length and the range parameter

In this section, we derive an expression for the second virial coefficient in terms of the scattering length and the range parameter. Using the expansion in Eq. (53),

we can obtain a series in powers of the momentum for the function in the square brackets in the kernel of the integral in Eq. (168). From Eq. (53),

$$\begin{aligned} \frac{\partial \delta_l(x)}{\partial x} &= \frac{1}{1 + \tan^2(\delta_l)} \frac{\partial \tan(\delta_l)}{\partial x} = \\ &= -(2l+1) \frac{a_{sl}^{(l)}}{R^{2l+1}} x^{2l} + \delta_{0,l} \left(\frac{a_{sl}^{(l)}}{R} \right)^3 x^{2l+2} - \frac{(2l+3)}{2} \frac{(a_{sl}^{(l)})^2 r_0^{(l)}}{R^{2l+3}} x^{2l+2} \\ &+ O(x^{2l+4}), \end{aligned} \quad (172)$$

where $\delta_{0,l}$ is the Kronecker delta. Now the integral I_l in Eq. (168) can be calculated term by term giving

$$I_l(T) = (2l+1)!! \frac{\pi^{l+1}}{\sqrt{2}} \frac{a_{sl}^{(l)}}{\lambda^{2l+1}} - \delta_{0,l} \frac{\pi^2}{\sqrt{2}} \left(\frac{a_{sl}^{(l)}}{\lambda} \right)^3 + \frac{(2l+3)!!}{2} \frac{\pi^{l+2}}{\sqrt{2}} \frac{(a_{sl}^{(l)})^2 r_0^{(l)}}{\lambda^{2l+3}} + O(\lambda^{-2l-5}). \quad (173)$$

This result captures the manner in which the scattering length and the effective range influence the second virial coefficient. Note that the temperature dependence resides in the De-Broglie wavelength λ . Applied to the delta-shell potential

$$\begin{aligned} I_l(T) &= \frac{1}{(2l-1)!!} \frac{\pi^{l+1}}{\sqrt{2}} \frac{g}{(g-(2l+1))} \left(\frac{R}{\lambda} \right)^{2l+1} + \delta_{0,l} \frac{\pi^2}{\sqrt{2}} \frac{g^3}{(1-g)^3} \left(\frac{R}{\lambda} \right)^3 \\ &- \frac{(2l+1)}{2(2l-1)(2l-1)!!} \frac{\pi^{l+2}}{\sqrt{2}} \frac{g(g-(2l-1))}{(g-(2l+1))} \left(\frac{R}{\lambda} \right)^{2l+3} + O\left(\left(\frac{R}{\lambda} \right)^{2l+5} \right), \end{aligned} \quad (174)$$

following Eq. (56) and (57). In order for the above series to be a good approximation, the temperature must be such that $\lambda \gg R$ and the strength parameter g must not be near the resonance values $2l+1$.

In the case of an infinite scattering length, $a_{sl}^{(l)} \rightarrow \infty$ (or $g = 2l+1$), that is, in the unitary limit, one can adopt the same steps as above, but without the term involving the scattering length. The result is

$$I_0(T) = \frac{\pi}{2\sqrt{2}} \frac{r_0}{\lambda} + O(\lambda^{-3}), \quad (175)$$

and

$$I_{l>0}(T) = -(2l-1)!! \frac{\sqrt{2}\pi^l}{r_0^{(l)} \lambda^{2l-1}} + O(\lambda^{-2l-1}). \quad (176)$$

For the delta-shell potential,

$$I_0(T) = \frac{\pi}{3\sqrt{2}} \frac{R}{\lambda} + O\left(\left(\frac{R}{\lambda} \right)^3 \right), \quad (177)$$

and

$$I_{l>0}(T) = \frac{(2l+3)(2l-1)}{(2l+1)!!} \frac{\pi^l}{\sqrt{2}} \left(\frac{R}{\lambda}\right)^{2l-1} + O\left(\left(\frac{R}{\lambda}\right)^{2l+1}\right). \quad (178)$$

In the last case the range of the potential R becomes the relevant length scale.

It is worthwhile to note that when the scattering length $a_s^{(l)} \rightarrow \infty$, it ceases to be of relevance in the final results for physical quantities which now depend on the remaining finite quantities such as the delta-shell radius R , the effective range r_0 and the de-Broglie wavelength λ .

17. Gas of nonzero spin particles

If particles have nonzero spin, then in addition to even or odd partial wave (spatially symmetric and antisymmetric wave functions) contributions from Bose or Fermi statistics, the appropriate symmetry separation of states must be made¹⁶. The results for spin s then read as

$$a_2^{(s)} = \frac{s+1}{2s+1} a_{Bose}^{(0)} + \frac{s}{2s+1} a_{Fermi}^{(0)} \quad \text{for integer } s, \quad (179)$$

$$a_2^{(s)} = \frac{s+1}{2s+1} a_{Fermi}^{(0)} + \frac{s}{2s+1} a_{Bose}^{(0)} \quad \text{for half-integer } s.$$

In order to illustrate the role played by spin, we consider the cases of spin-zero, spin-half and spin-one particles in what follows.

Figure 16 shows the second virial coefficient for the case of spin-zero particles as a function of temperature for various values of the interaction parameter g . For comparison, results for hard spheres (HS) are also shown in this figure.

For the repulsive potential ($g < 0$), the second virial coefficient is positive and increases with temperature. When the interaction becomes weak ($g \approx 0$), the coefficient tends to zero. For the attractive potential ($g > 0$), a_2 turns negative.

The curve which corresponds to resonance ($g = 1$) in the S-wave channel stands out. It is negative for $T > \tilde{T}$ and positive for $T < \tilde{T}$. However the curve is negative when $g \approx 1$, near but not exactly at resonance.

The curve which corresponds to the P-wave ($g = 3$) is absent due to odd l being forbidden in the scattering of a pair of particles with spin zero. In the cases of spin-half and spin-one particles, results for which are shown in Fig. 17 and Fig. 18, all l 's contribute. For non-zero spin, effects of the P-wave resonance ($g = 3$) stand out and that of the S-wave resonance ($g = 1$) changes its value.

In Fig. 19, Fig. 20 and Fig. 21, corresponding to different spin values ($s = 0, 1/2$, and 1, respectively), the second virial coefficient is shown as a function of the strength parameter g for one value of temperature $T/\tilde{T} = 0.72$. Positive values of a_2^s for repulsive case ($g < 0$), negative values of a_2^s for attractive case ($g > 0$) and prominent resonance points are shown in these figures.

Negative (positive) values of the second virial coefficient decrease (increase) the pressure of the system with respect to that of the ideal gas. For $T/\tilde{T} \rightarrow 0$, the coefficient tends to the corresponding ideal quantum gas values in Eq. (160).

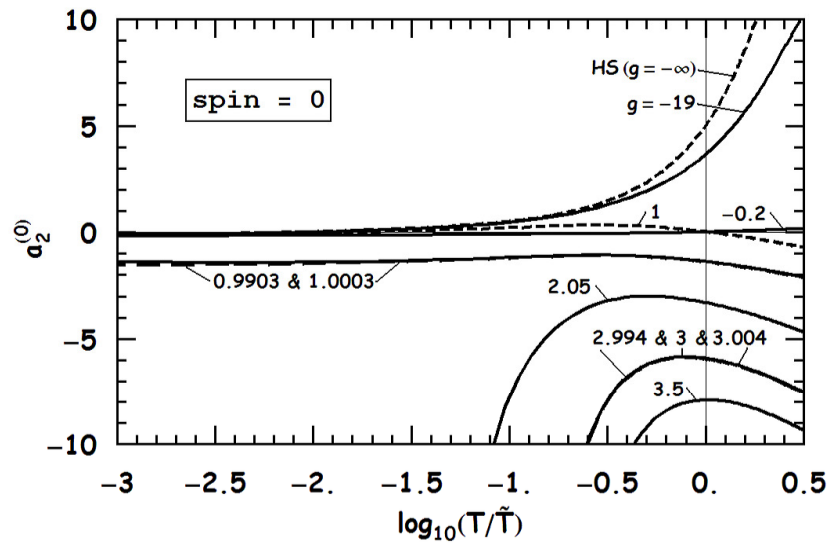


Fig. 16. Second virial coefficient as a function of temperature for various values of g for spin-zero particles. Special cases are shown by dashed lines. See text for explanation.

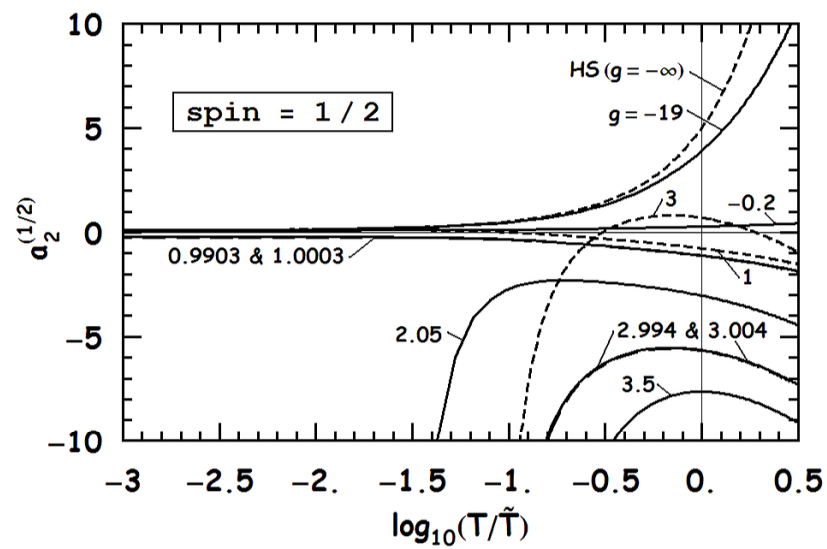


Fig. 17. Second virial coefficient as a function of temperature for various values of g , for spin-half particles. Special cases are shown by dashed lines. See text for explanation.

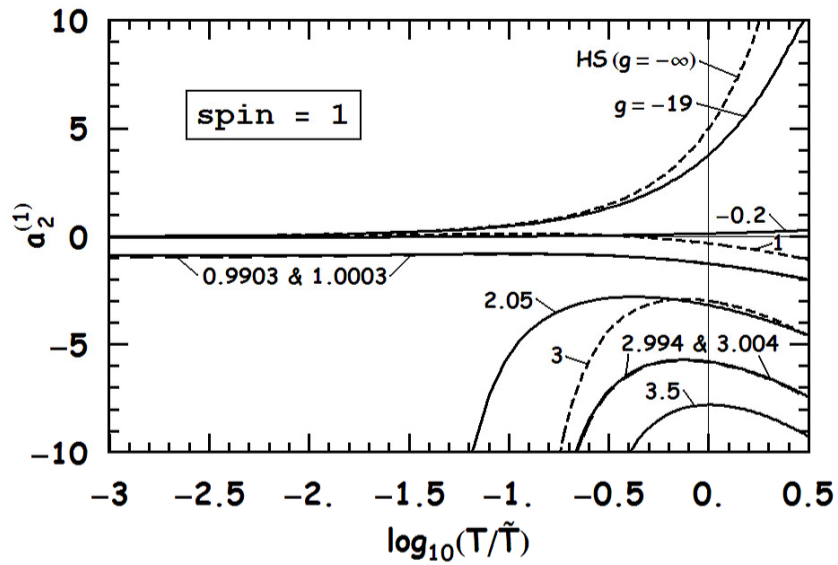


Fig. 18. Second virial coefficient as a function of temperature for various values of g , for spin-one particles. Special cases are shown by dashed lines. See text for explanation.

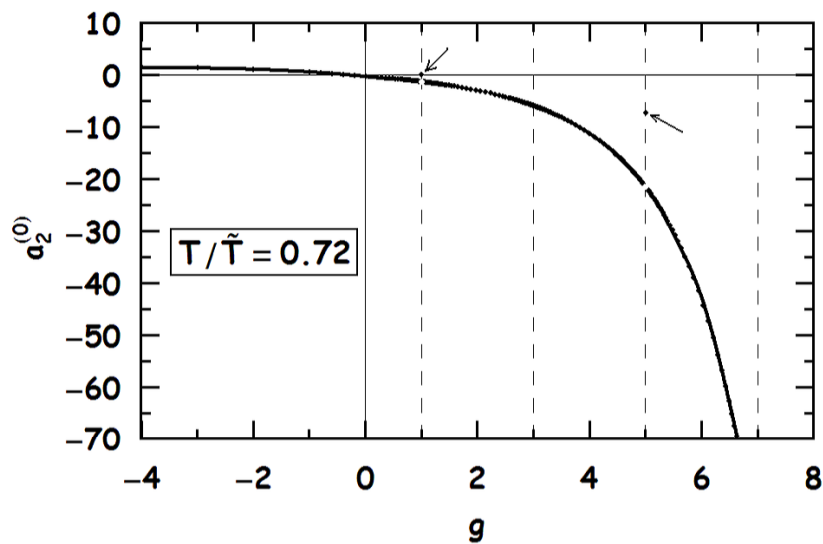


Fig. 19. Second virial coefficient as a function of g for temperature $T/\tilde{T} = 0.72$, for spin-zero particles. Resonance values are indicated by arrows.

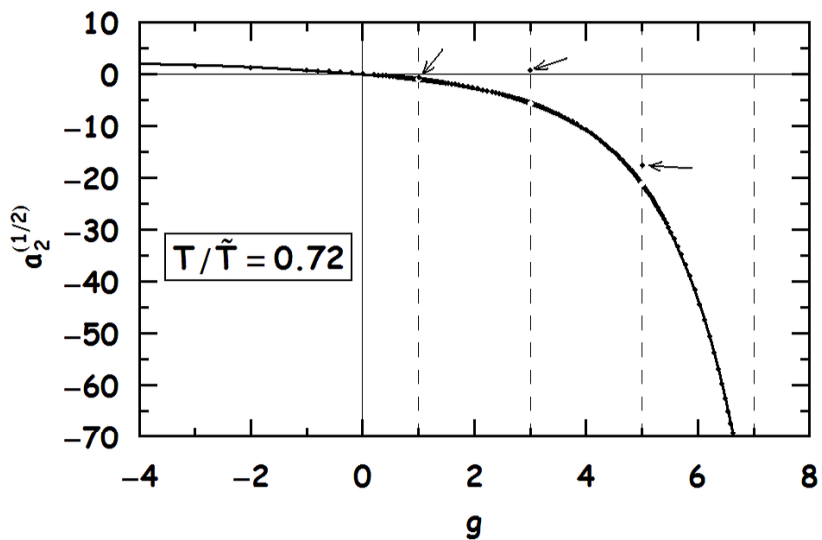


Fig. 20. Second virial coefficient as a function of g for temperature $T/\tilde{T} = 0.72$, for spin-half particles. Resonance values are indicated by arrows.

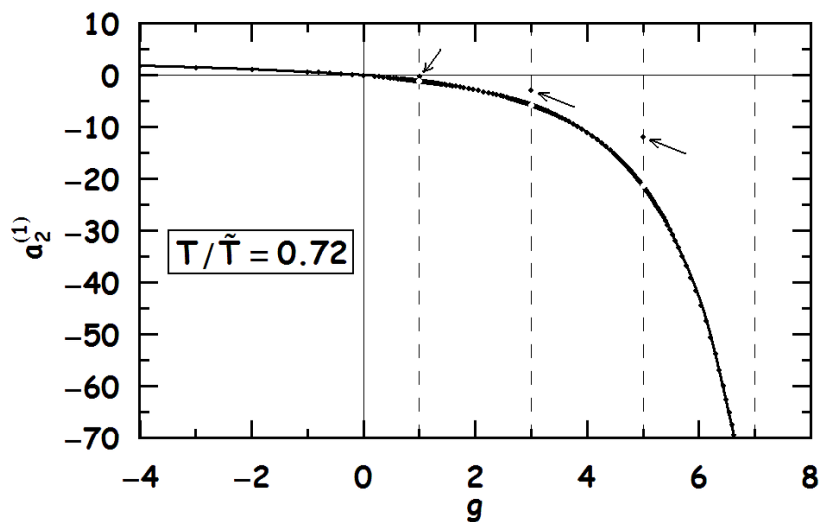


Fig. 21. Second virial coefficient as a function of g for temperature $T/\tilde{T} = 0.72$, for spin-one particles. Resonance values are indicated by arrows.

18. Thermodynamical properties in terms of the second virial coefficient

We begin with the cluster expansion of the grand partition function in Eq. (152) up to the second order term:

$$\log(\mathcal{L}(z, V, T)) = \frac{V}{\lambda^3} (z + b_2(T)z^2 + O(z^3)) = \frac{V}{\lambda^3} \left(e^{\frac{\mu_c}{k_B T}} + b_2(T)e^{\frac{2\mu_c}{k_B T}} + O(e^{\frac{3\mu_c}{k_B T}}) \right), \quad (180)$$

where $z = e^{\frac{\mu_c}{k_B T}}$ is the fugacity. The pressure is then²⁶

$$\begin{aligned} p &= k_B T \left(\frac{\partial \log(\mathcal{L}(\mu_c, V, T))}{\partial V} \right)_{T, \mu_c} = k_B T \left(\frac{\partial \log(\mathcal{L}(z, V, T))}{\partial V} \right)_{T, z} = \\ &= \frac{k_B T}{\lambda^3} (z + b_2(T)z^2 + O(z^3)). \end{aligned} \quad (181)$$

The number density

$$n = \frac{T}{V} \left(\frac{\partial \log(\mathcal{L}(\mu_c, V, T))}{\partial \mu_c} \right)_{V, T} = \frac{1}{\lambda^3} \left(e^{\frac{\mu_c}{k_B T}} + 2b_2(T)e^{\frac{2\mu_c}{k_B T}} + O(e^{\frac{3\mu_c}{k_B T}}) \right), \quad (182)$$

or in equivalent form

$$n\lambda^3 = z + 2b_2(T)z^2 + O(z^3). \quad (183)$$

Note that $n\lambda^3$ serves as the small parameter for expansion in this method. Inverting Eq. (183) for fugacity, we obtain

$$z = n\lambda^3 - 2b_2(T)(n\lambda^3)^2 + O((n\lambda^3)^3). \quad (184)$$

Inserting this z in Eq. (181), we have the virial equation of state

$$p = nk_B T (1 - b_2(T)(n\lambda^3) + O((n\lambda^3)^2)), \quad (185)$$

and as $b_2(T) \rightarrow -a_2(T)$ from Eq. (159),

$$p = nk_B T (1 + a_2(T)(n\lambda^3) + O((n\lambda^3)^2)). \quad (186)$$

The entropy is given by²⁶

$$S = k_B \left(\frac{\partial}{\partial T} T \log(\mathcal{L}(\mu_c, V, T)) \right)_{V, \mu_c}. \quad (187)$$

After inserting Eq. (180) and doing some algebra, we obtain the entropy density due to interactions as

$$s - \left(\frac{5}{2}nk_B - nk_B \log(n\lambda^3) \right) = nk_B \left(\frac{1}{2}a_2(T) - T \frac{da_2(T)}{dT} \right) (n\lambda^3) + O((n\lambda^3)^2), \quad (188)$$

where the term in parentheses on the left hand side gives the ideal gas contribution.

In dimensionless form

$$\delta s \equiv \frac{s - s_0}{\tilde{s}} = \left(\frac{1}{2}a_2(T) - T \frac{da_2(T)}{dT} \right) \left(\frac{\lambda}{R} \right)^3 + O \left(\left(\frac{\lambda}{R} \right)^6 (nR^3) \right), \quad (189)$$

where the ideal gas entropy density

$$s_0 = \frac{5}{2}nk_B - nk_B \log(n\lambda^3), \quad (190)$$

and the scaling value

$$\tilde{s} \equiv nk_B(nR^3). \quad (191)$$

The quantity nR^3 can be thought of as a measure of diluteness, as we assume $nR^3 < 1$.

Spin-zero particles: The dimensionless entropy density shift δs for spin zero particles is shown in Fig. 22 as a function of temperature for various values of the parameter g . The overall shift is negative, becoming small as the temperature increases. The S-wave resonance stands out and also acquires positive values, but odd l partial waves do not contribute.

Figure 23 shows the same shift as a function of the strength parameter for various values of temperature. The entropy density shift increases with the strength of the interaction and has some positive values at resonances which are separated from the curves.

Spin-half particles: Results for spin half particles are shown in Fig. 24 and Fig. 25. In this case all partial waves contribute. The entropy density shift can become positive at lower temperatures and also receives contributions from the P-wave resonance ($g = 3$) which are positive for higher temperatures. Positive shifts occur for the weakly interacting system (small g).

Spin-one particles: Results for particles with spin unity, shown in Fig. 26 and Fig. 27, are qualitatively the same as for spin zero particles, but with the addition of the special case of the P-wave resonance ($g = 3$).

For Eq. (189) to be a correction, the requirement

$$\delta s \ll \frac{s_0}{\tilde{s}} \quad (192)$$

must be met. We can define the dimensionless entropy density shift boundary function

$$\Delta s(n, T) \equiv \frac{s_0}{\tilde{s}} = \frac{\frac{5}{2} - \log(nR^3) + \frac{3}{2} \log\left(\frac{R}{\lambda}\right)^2}{nR^3}, \quad (193)$$

which is important to know once the density n is specified.

The thermodynamic identity

$$u = -p + Ts + \mu n, \quad (194)$$

used in conjunction with Eq. (186) and Eq. (188) gives the kinetic energy density

$$u - \frac{3}{2}nk_B T = nk_B T \left(\frac{3}{2}a_2(T) - T \frac{da_2(T)}{dT} \right) (n\lambda^3) + O((n\lambda^3)^2), \quad (195)$$

Shifts due to interactions can be gauged by the dimensionless quantity

$$\delta u \equiv \frac{u - u_0}{\tilde{u}} = \left(\frac{3}{2}a_2(T) - T \frac{da_2(T)}{dT} \right) \left(\frac{\lambda}{R} \right)^3 + O\left(\left(\frac{\lambda}{R} \right)^6 (nR^3) \right). \quad (196)$$

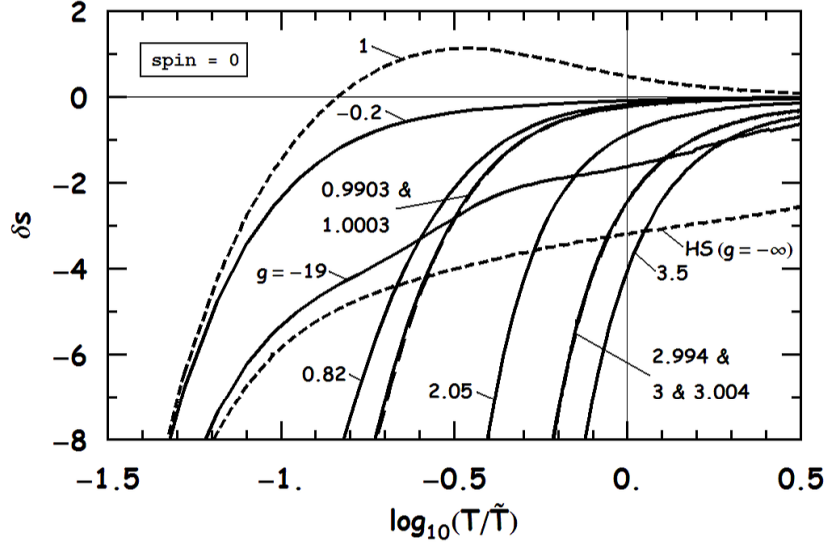


Fig. 22. Dimensionless entropy density shift for spin zero particles as a function of temperature for various values of the parameter g . Special cases are shown by dashed lines.

For an ideal gas

$$u_0 = \frac{3}{2}nk_B T, \quad (197)$$

with the energy density scale

$$\tilde{u} \equiv nk_B T (nR^3) = T\tilde{s}. \quad (198)$$

Similar to Eq. (193), we can define a dimensionless energy density shift boundary function

$$\Delta u(n) \equiv \frac{u_0}{\tilde{u}} = \frac{3}{2} \frac{1}{nR^3}. \quad (199)$$

The total energy density includes the mass term which dominates as $\epsilon \simeq mc^2 n$

$$\epsilon - \left(\frac{3}{2}nk_B T + mc^2 n \right) = nk_B T \left(\frac{3}{2}a_2(T) - T \frac{da_2(T)}{dT} \right) (n\lambda^3) + O((n\lambda^3)^2), \quad (200)$$

or

$$\delta\epsilon \equiv \frac{\epsilon - \epsilon_0}{\tilde{u}} = \left(\frac{3}{2}a_2(T) - T \frac{da_2(T)}{dT} \right) \left(\frac{\lambda}{R} \right)^3 + O\left(\left(\frac{\lambda}{R} \right)^6 (nR^3) \right), \quad (201)$$

$$\epsilon_0 = \frac{3}{2}nk_B T + mc^2 n. \quad (202)$$

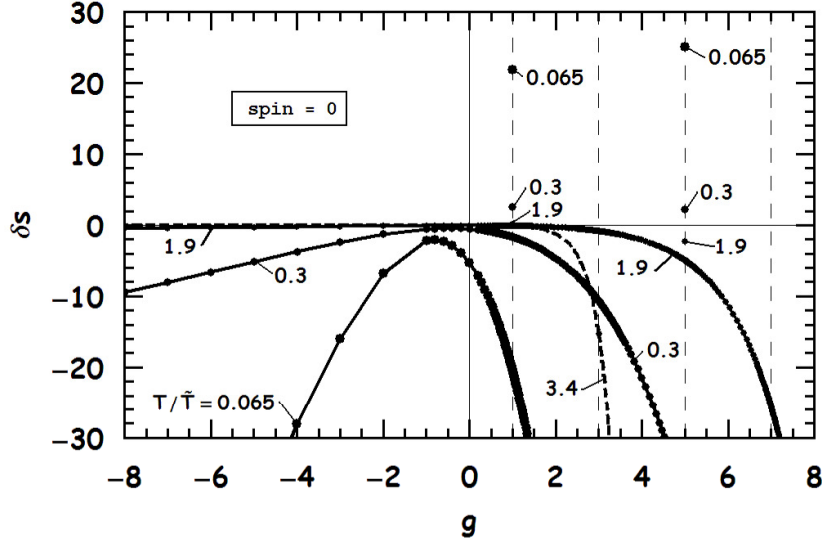


Fig. 23. Dimensionless entropy density shift for spin zero particles as a function of the parameter g for various temperatures. Resonance values of g are shown by vertical dashed lines.

Therefore the enthalpy, $h = \epsilon + p$, will be

$$h - \left(\frac{5}{2} n k_B T + m c^2 n \right) = n k_B T \left(\frac{5}{2} a_2(T) - T \frac{d a_2(T)}{d T} \right) (n \lambda^3) + O((n \lambda^3)^2), \quad (203)$$

or

$$\delta h \equiv \frac{h - h_0}{\tilde{u}} = \left(\frac{5}{2} a_2(T) - T \frac{d a_2(T)}{d T} \right) \left(\frac{\lambda}{R} \right)^3 + O\left(\left(\frac{\lambda}{R} \right)^6 (n R^3) \right), \quad (204)$$

$$h_0 = \frac{5}{2} n k_B T + m c^2 n, \quad (205)$$

whence

$$\Delta \epsilon(n, T) \equiv \frac{\epsilon_0}{\tilde{u}} = \frac{3}{2} \frac{1}{n R^3} + \frac{m c^2}{k \tilde{T}} \left(\frac{\lambda}{R} \right)^2, \quad (206)$$

and

$$\Delta h(n, T) \equiv \frac{h_0}{\tilde{u}} = \frac{5}{2} \frac{1}{n R^3} + \frac{m c^2}{k \tilde{T}} \left(\frac{\lambda}{R} \right)^2. \quad (207)$$

The specific heat per particle at constant volume is given by the integral¹⁶

$$c_v - \frac{3}{2} k_B = -T \int_0^n \frac{\partial^2 p(\tilde{n}, T)}{\partial T^2} \frac{d \tilde{n}}{\tilde{n}^2}, \quad (208)$$

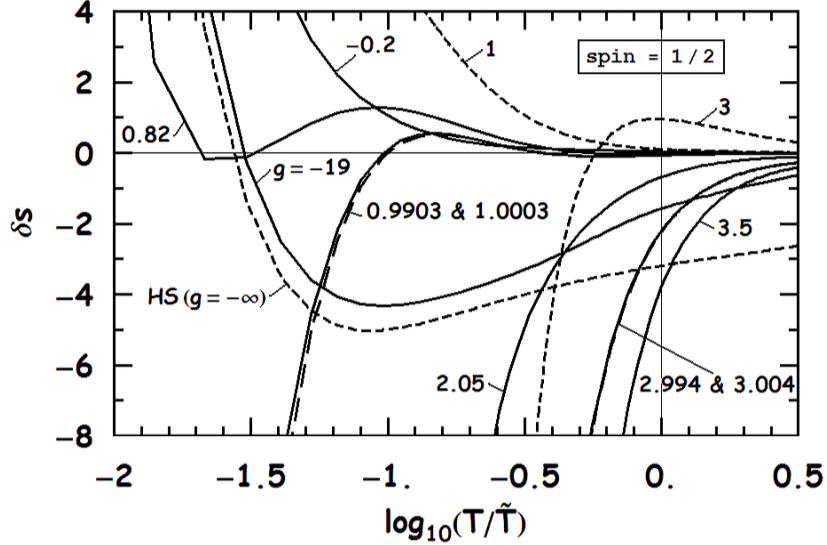


Fig. 24. Dimensionless entropy density shift for spin half particles as a function of temperature for various values of the parameter g . Special cases are shown by dashed lines.

where using the virial Eq. (186), we obtain

$$c_v - \frac{3}{2}k_B = -k_B \left(\frac{3}{4}a_2(T) - T \frac{da_2(T)}{dT} + T^2 \frac{d^2a_2(T)}{dT^2} \right) (n\lambda^3) + O((n\lambda^3)^2). \quad (209)$$

Again, shifts due to interactions can be seen through the dimensionless quantity

$$\delta c_v \equiv \frac{c_v - c_{v0}}{\tilde{c}} = \left(\frac{3}{4}a_2(T) - T \frac{da_2(T)}{dT} + T^2 \frac{d^2a_2(T)}{dT^2} \right) \left(\frac{\lambda}{R} \right)^3 + O \left(\left(\frac{\lambda}{R} \right)^6 (nR^3) \right), \quad (210)$$

with

$$c_{v0} = \frac{3}{2}k_B, \quad (211)$$

$$\tilde{c} \equiv k_B(nR^3), \quad (212)$$

whence

$$\Delta c_v(n) \equiv \frac{c_{v0}}{\tilde{c}} = \frac{3}{2} \frac{1}{nR^3}. \quad (213)$$

Fig. 28, Fig. 29 and Fig. 30 show the shifts in specific heat per particle. They have maximum values close to zero near $g = 1$ and separated points for values at exact resonances.

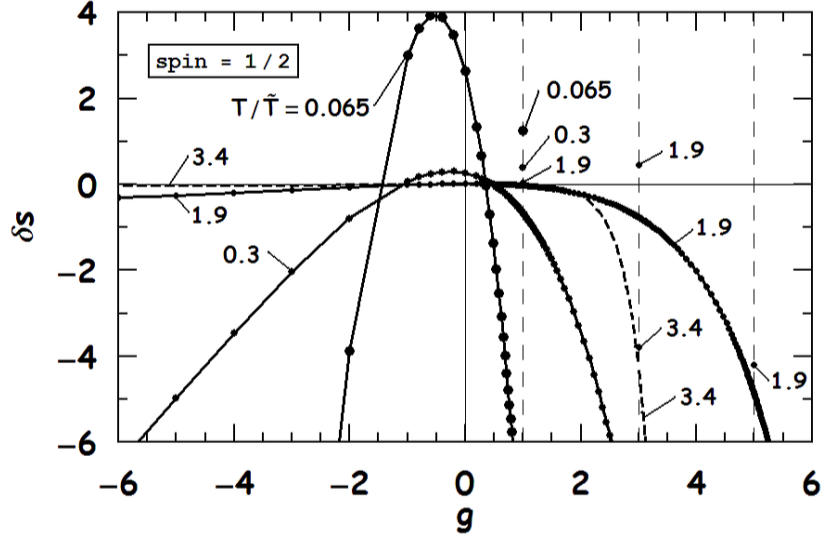


Fig. 25. Dimensionless entropy density shift for spin half particles as a function of the parameter g for various temperatures. Resonance values of g are shown by vertical dashed lines.

The specific heat per particle at constant pressure is given by the ratio¹⁶

$$c_p - c_v = \frac{T \left(\frac{\partial p(n, T)}{\partial T} \right)^2}{\left(\frac{\partial p(n, T)}{\partial n} \right) n^2}, \quad (214)$$

where using the virial Eq. (186) again, we obtain

$$c_p - \frac{5}{2}k_B = -k_B \left(\frac{15}{4}a_2(T) - 3T \frac{da_2(T)}{dT} + T^2 \frac{d^2a_2(T)}{dT^2} \right) (n\lambda^3) + O((n\lambda^3)^2). \quad (215)$$

or

$$\delta c_p \equiv \frac{c_p - c_{p0}}{\bar{c}} = \left(\frac{15}{4}a_2(T) - 3T \frac{da_2(T)}{dT} + T^2 \frac{d^2a_2(T)}{dT^2} \right) \left(\frac{\lambda}{R} \right)^3 + O \left(\left(\frac{\lambda}{R} \right)^6 (nR^3) \right), \quad (216)$$

and

$$c_{p0} = \frac{5}{2}k_B. \quad (217)$$

The dimensionless boundary function for c_p is

$$\Delta c_p(n) \equiv \frac{c_p - c_{p0}}{\bar{c}} = \frac{5}{2} \frac{1}{nR^3}. \quad (218)$$

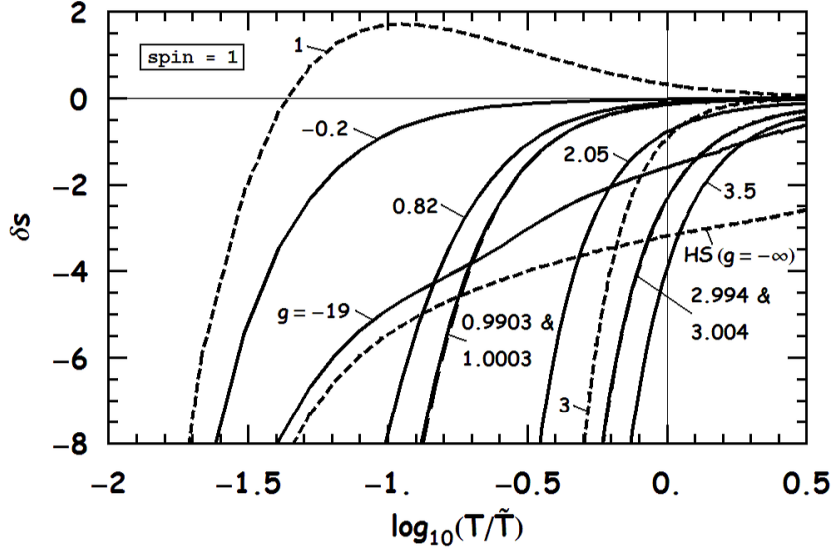


Fig. 26. Dimensionless entropy density shift for spin-one particles as a function of temperature for various values of the parameter g . Special cases are shown by dashed lines.

Hence, the adiabatic constant $\gamma_a = \frac{c_p}{c_v}$ has the form

$$\gamma_a - \frac{5}{3} = - \left(\frac{15}{9} a_2(T) - \frac{8}{9} T \frac{da_2(T)}{dT} - \frac{4}{9} T^2 \frac{d^2 a_2(T)}{dT^2} \right) (n\lambda^3) + O((n\lambda^3)^2). \quad (219)$$

The adiabatic sound speed is given by the expression²⁷

$$\left(\frac{c_0}{c} \right)^2 = \frac{\gamma_a n}{h} \left(\frac{\partial p(n, T)}{\partial n} \right), \quad (220)$$

where c is the speed of light in vacuum. In the non-relativistic case, for which $h \simeq mc^2 n$,

$$c_0^2 = \frac{\gamma_a}{m} \left(\frac{\partial p(n, T)}{\partial n} \right), \quad (221)$$

whence

$$c_0^2 - \frac{5}{3} \frac{k_B T}{m} = \frac{k_B T}{m} \left(\frac{5}{3} a_2(T) + \frac{8}{9} T \frac{da_2(T)}{dT} + \frac{4}{9} T^2 \frac{d^2 a_2(T)}{dT^2} \right) (n\lambda^3) + O((n\lambda^3)^2). \quad (222)$$

Making it dimensionless, we obtain

$$\delta c_0^2 \equiv \frac{c_0^2 - c_i^2}{c_0^2} = \left(\frac{5}{3} a_2(T) + \frac{8}{9} T \frac{da_2(T)}{dT} + \frac{4}{9} T^2 \frac{d^2 a_2(T)}{dT^2} \right) \left(\frac{\lambda}{R} \right)^3 + O \left(\left(\frac{\lambda}{R} \right)^6 (nR^3) \right), \quad (223)$$

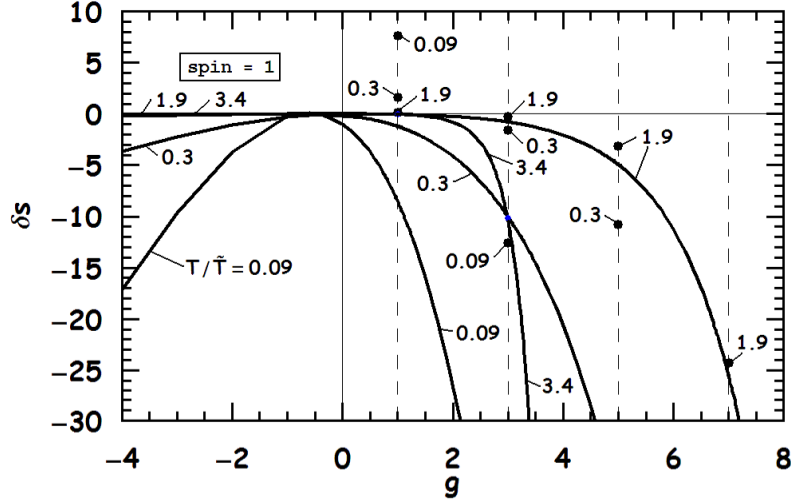


Fig. 27. Dimensionless entropy density shift for spin-one particles as a function of the parameter g for various temperatures. Resonance values of g are shown by vertical dashed lines.

$$c_i^2 = \frac{5}{3} \frac{k_B T}{m}, \quad (224)$$

$$\tilde{c}_0^2 = \frac{k_B T}{m} (nR^3). \quad (225)$$

The boundary is provided by

$$\Delta c_0^2(n) \equiv \frac{c_i^2}{\tilde{c}_0^2} = \frac{5}{3} \frac{1}{nR^3}. \quad (226)$$

Let us emphasize that the corrections above are only valid for the range of temperatures and densities for which

$$\Delta F \gg \delta F, \quad (227)$$

where F is any of the thermodynamical property calculated in this section. Therefore, we define the density function $n_F(T)$ which is found from the equation

$$|\Delta F(n_F(T), T)| = |\delta F(T)|, \quad (228)$$

and the requirement $n \ll n_F(T)$ reflects the fact that the system at fixed temperature T must be dilute enough for the virial approximation for F to be valid. The critical quantum density

$$n_Q(T) \equiv \frac{1}{\lambda^3(T)}, \quad (229)$$

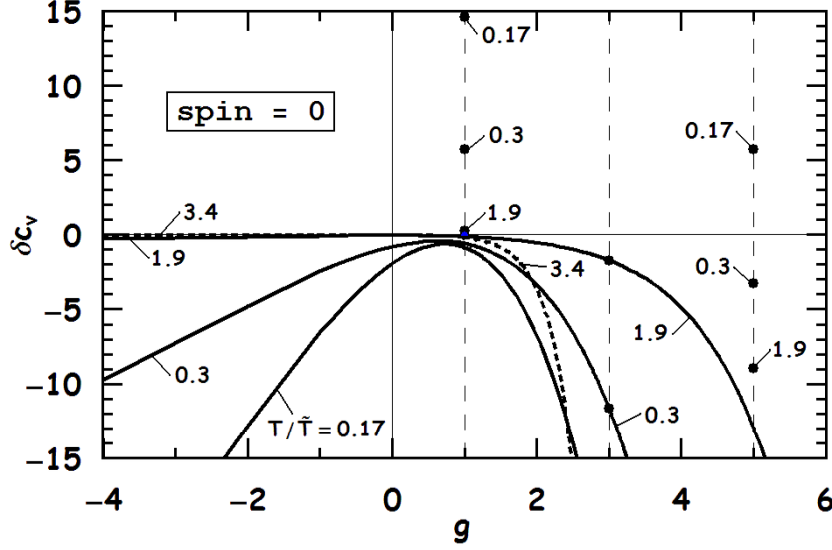


Fig. 28. Dimensionless density boundary of entropy for spin zero particles as a function of the parameter g for various temperatures. Resonance values of g are shown by vertical dashed lines.

also signals the degenerate quantum regime as the system becomes dense.

The dimensionless boundary density $n_s R^3$ for the entropy is shown in Fig. 31, Fig. 33 and Fig. 35 as a function of temperature for various values of g . For the system to be dilute, the density must fall below these boundary values of density.

The same dimensionless boundary density, in Fig. 32, Fig. 34 and Fig. 36, is shown as a function of the strength parameter g for various temperatures.

The boundary density for the specific heat is shown in Fig. 37, Fig. 38 and Fig. 39 as a function of the strength parameter g for various temperatures. Values at resonances stand out as pointed out by the solid dots.

The first and second derivatives of the second virial coefficient are found by calculating the following integrals

$$I_l^{(2)}(T) \equiv \frac{T}{\gamma} \frac{dI_l(T)}{dT} = \int_0^\infty dx \left[-\frac{\partial \delta_l(x)}{\partial x} \right] x^2 e^{-\gamma(T) x^2}, \quad (230)$$

and

$$I_l^{(4)}(T) \equiv \frac{T}{\gamma} \frac{dI_l^{(2)}(T)}{dT} = \int_0^\infty dx \left[-\frac{\partial \delta_l(x)}{\partial x} \right] x^4 e^{-\gamma(T) x^2}. \quad (231)$$

Hence

$$T \frac{da_2(T)}{dT} = -2^{\frac{3}{2}} \left(\sum'_{Bound} g E_{Bound} \beta E_{Bound} e^{-\beta E_{Bound}} - \frac{\gamma}{\pi} \sum'_l (2l+1) I_l^{(2)}(T) \right), \quad (232)$$

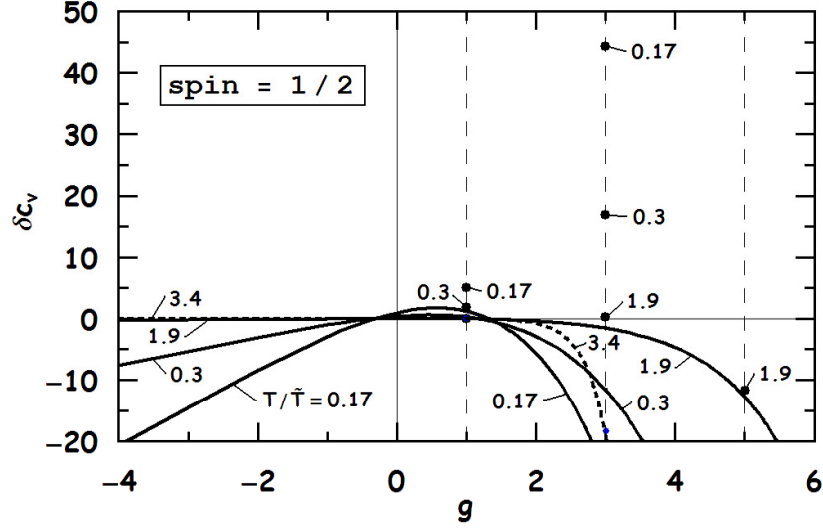


Fig. 29. Dimensionless density boundary of entropy for spin half particles as a function of the parameter g for various temperatures. Resonance values of g are shown by vertical dashed lines.

and

$$\begin{aligned}
 T^2 \frac{d^2 a_2(T)}{dT^2} = & -2^{\frac{3}{2}} \left[\sum'_{Bound} g_E \beta E_{Bound} (\beta E_{Bound} - 2) e^{-\beta E_{Bound}} \right. \\
 & \left. + \frac{\gamma}{\pi} \sum'_l (2l+1) \left(2I_l^{(2)}(T) - \gamma I_l^{(4)}(T) \right) \right], \quad (233)
 \end{aligned}$$

where $g_E = 2l + 1$ is the multiplicity of the bound state.

To conclude this section, we note that the second virial coefficient corrections to the thermodynamic state variables for a dilute gas of particles interacting through a delta-shell potential exhibit distinct features when the interaction is tuned to the unitary limit and when resonances occur for different partial waves.

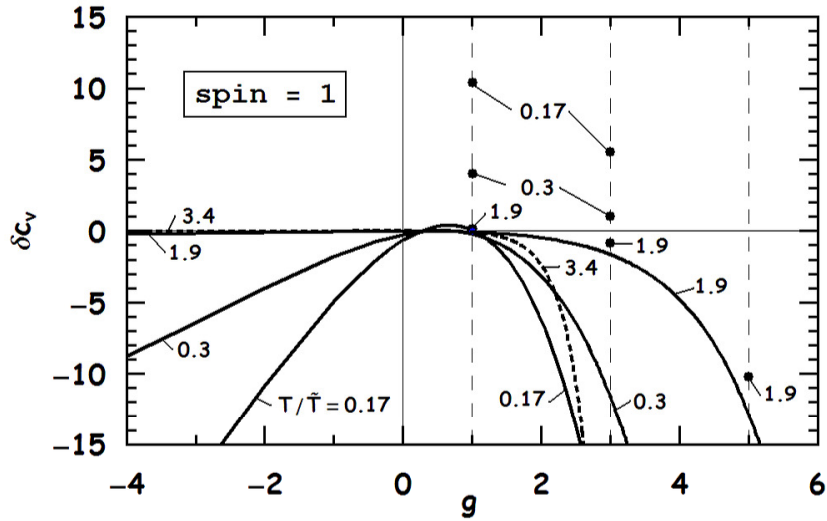


Fig. 30. Dimensionless density boundary of entropy for spin-one particles as a function of the parameter g for various temperatures. Resonance values of g are shown by vertical dashed lines.

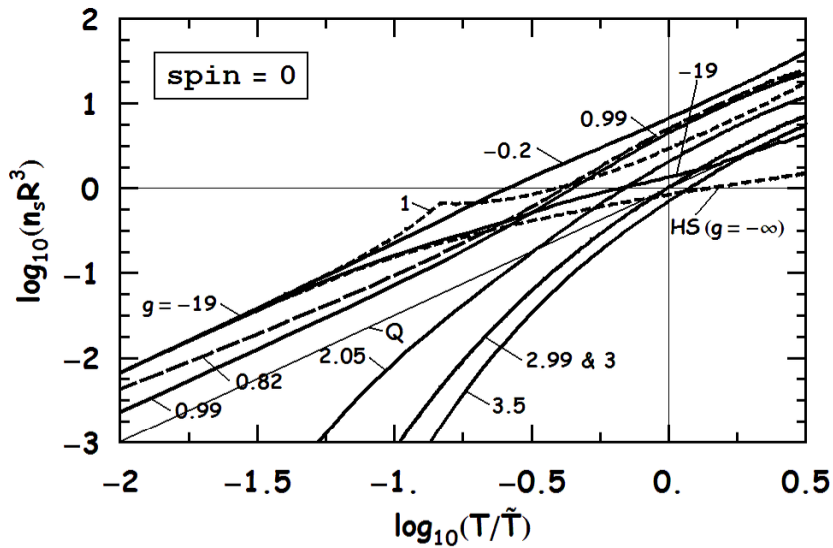


Fig. 31. Dimensionless density boundary of entropy for spin zero particles as a function of temperature for various values of the parameter g . Special cases are shown by dashed lines and the critical quantum density is labeled by 'Q'.

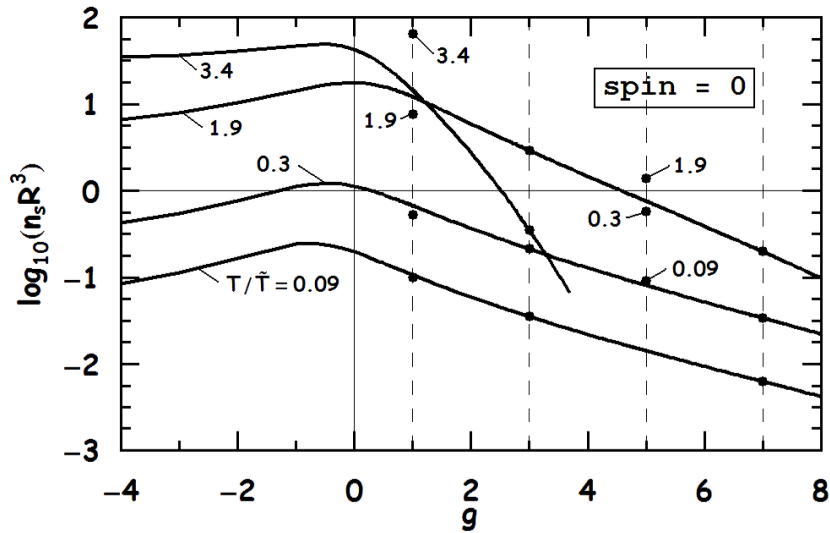


Fig. 32. Dimensionless density boundary of entropy for spin zero particles as a function of the parameter g for various temperatures. Resonance values of g are shown by vertical dashed lines.

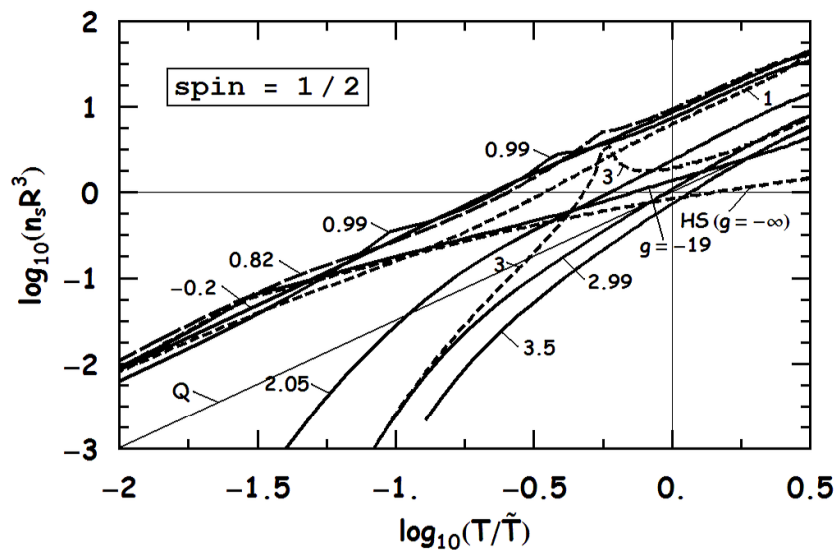


Fig. 33. Dimensionless density boundary of entropy for spin half particles as a function of temperature for various values of the parameter g . Special cases are shown by dashed lines and critical quantum density is labeled by 'Q'.

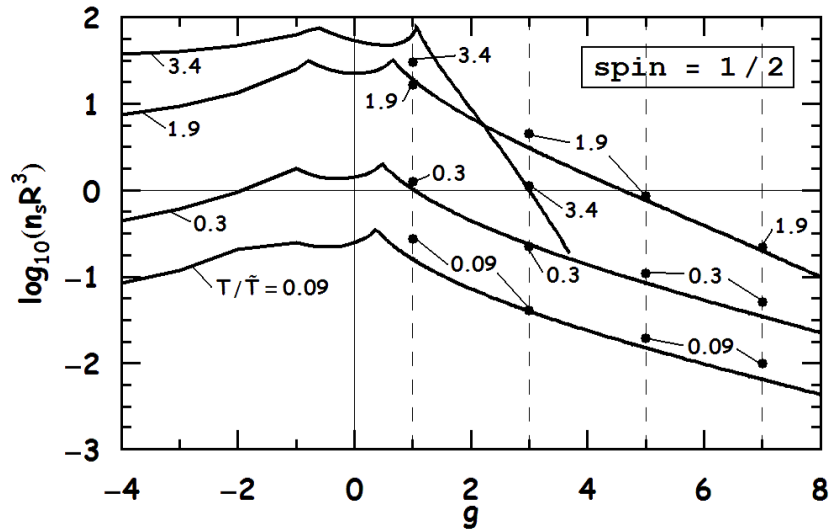


Fig. 34. Dimensionless density boundary of entropy for spin half particles as a function of the parameter g for various temperatures. Resonance values of g are shown by vertical dashed lines.

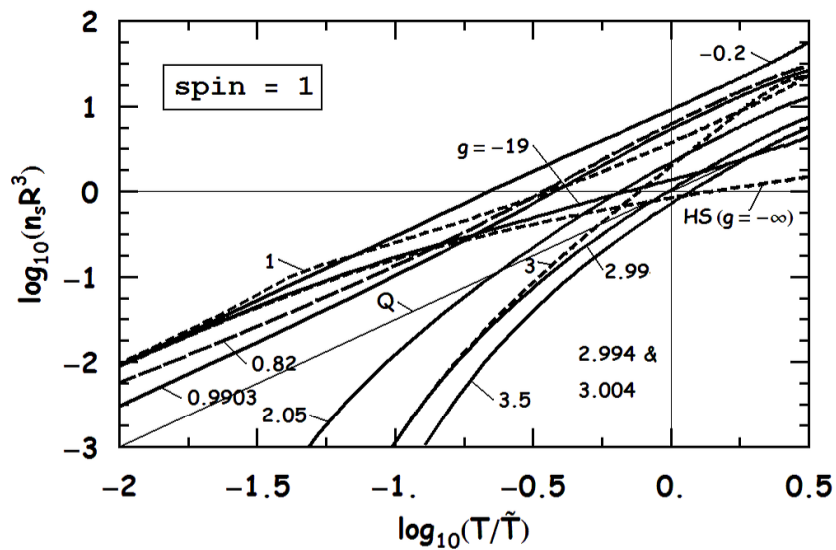


Fig. 35. Dimensionless density boundary of entropy for spin-one particles as a function of temperature for various values of the parameter g . Special cases are shown by dashed lines and critical quantum density is labeled by 'Q'.

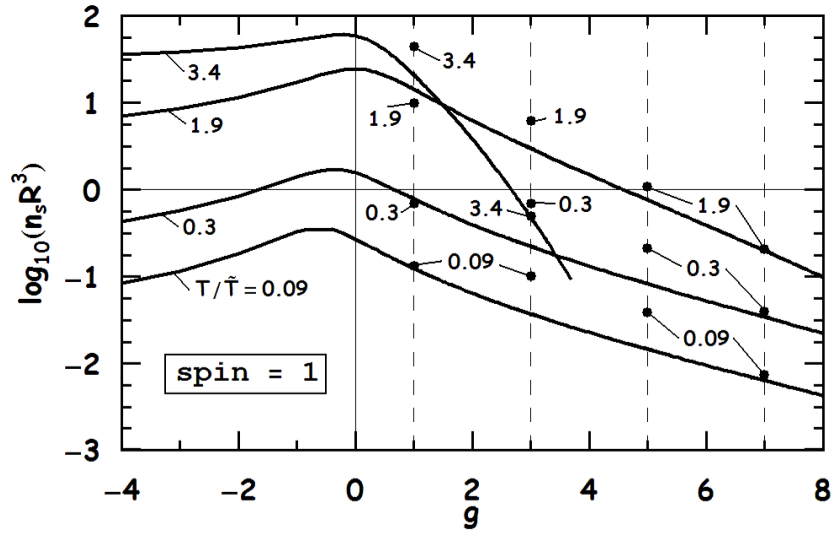


Fig. 36. Dimensionless density boundary of entropy for spin-one particles as a function of the parameter g for various temperatures. Resonance values of g are shown by vertical dashed lines.

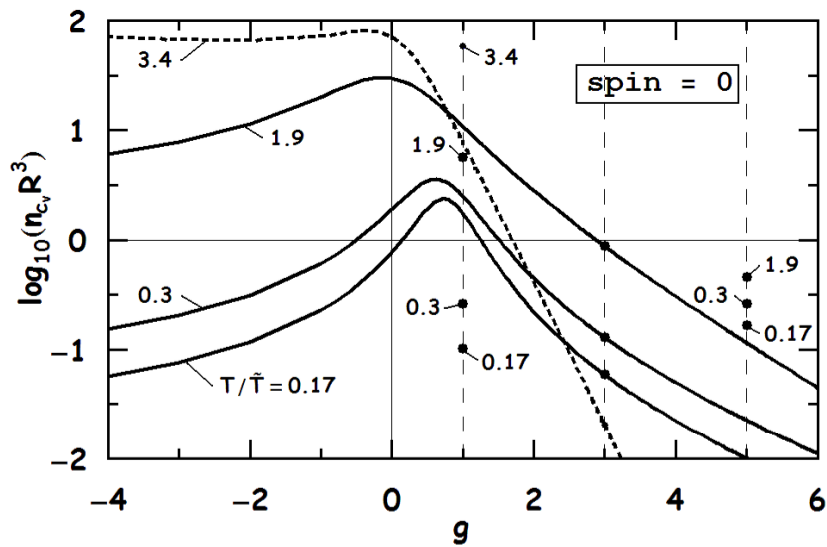


Fig. 37. Dimensionless density boundary of entropy for spin zero particles as a function of the parameter g for various temperatures. Resonance values of g are shown by vertical dashed lines.

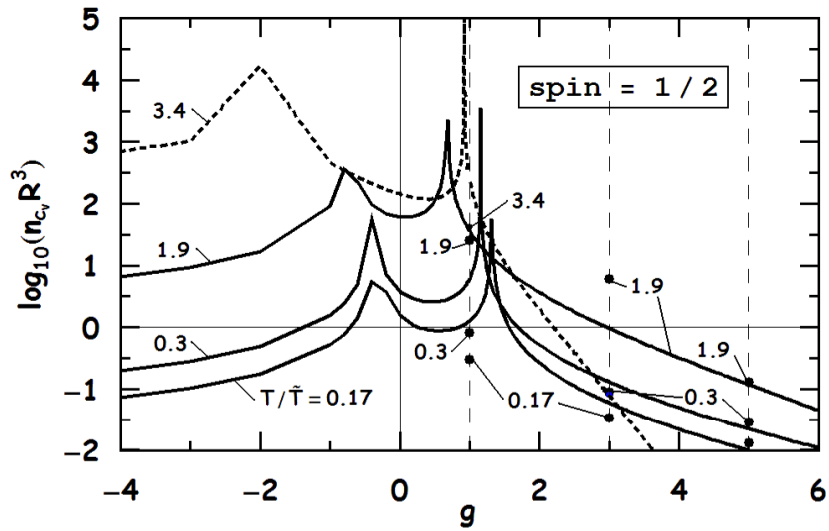


Fig. 38. Dimensionless density boundary of entropy for spin half particles as a function of the parameter g for various temperatures. Resonance values of g are shown by vertical dashed lines.

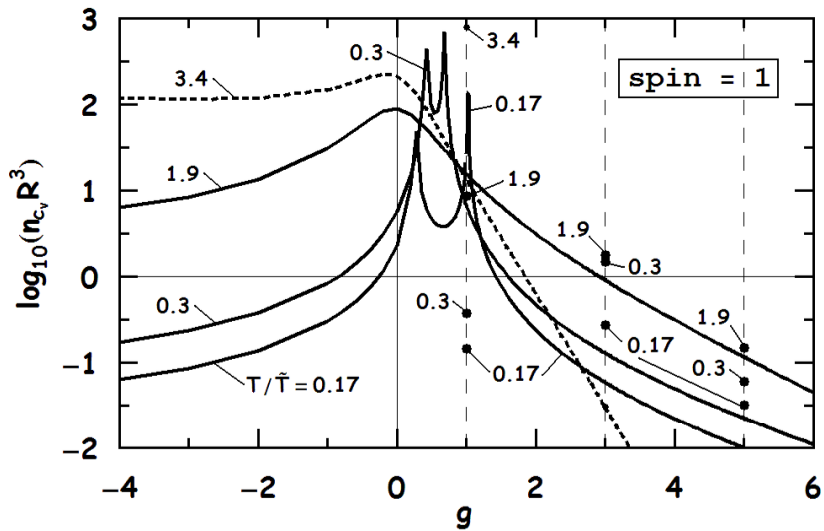


Fig. 39. Dimensionless density boundary of entropy for spin-one particles as a function of the parameter g for various temperatures. Resonance values of g are shown by vertical dashed lines.

Transport properties of a dilute non-relativistic delta-shell gas

19. Transport coefficients

If a system is disturbed from equilibrium, net flows of mass, energy and momentum are generated. In the first approximation, these flows are described by coefficients of diffusion, thermal conductivity and viscosity. A detailed description of the theory based on an approximate solution of the Boltzmann equation is given in Chapman¹² and Hirschfelder¹⁶. The formalism described in these references is adopted here to calculate results for the delta-shell potential.

The transport cross-section of order n is given by the integral¹²

$$\phi^{(n)} = 2\pi \int_{-1}^{+1} d \cos \theta (1 - \cos^n \theta) \frac{d\sigma(k, \theta)}{d\Omega} \Big|_{c.m.}, \quad (234)$$

where the scattering angle θ and the collisional differential cross-section $\frac{d\sigma(k, \theta)}{d\Omega} \Big|_{c.m.}$ are calculated in the center of mass reference frame of the two colliding particles. For indistinguishable particles, an expansion of the amplitude in partial waves $\sum_l' (2l+1)(e^{i2\delta_l} - 1)P_l(\cos \theta)$ and the orthogonality of the Legendre polynomials P_l simplifies the above integral to the infinite sums

$$q_{Fermi, Bose}^{(1)} \equiv \frac{\phi^{(1)}}{4\pi R^2} = \frac{2}{x^2} \sum_l' (2l+1) \sin^2(\delta_l), \quad (235)$$

$$q_{Fermi, Bose}^{(2)} \equiv \frac{\phi^{(2)}}{4\pi R^2} = \frac{2}{x^2} \sum_l' \frac{(l+1)(l+2)}{(2l+3)} \sin^2(\delta_{l+2} - \delta_l), \quad (236)$$

where the prime on the summation sign indicates the use of even l for Bosons and odd l for Fermions. In Eqs. (236), the low energy hard-sphere cross section $4\pi R^2$ has been used to render the transport cross sections dimensionless. If the particles possess spin s , then the properly symmetrized forms are:

$$\begin{aligned} q_{(s)}^{(n)} &= \frac{s+1}{2s+1} q_{Bose}^{(n)} + \frac{s}{2s+1} q_{Fermi}^{(n)}, \text{ for integer } s, \\ q_{(s)}^{(n)} &= \frac{s+1}{2s+1} q_{Fermi}^{(n)} + \frac{s}{2s+1} q_{Bose}^{(n)}, \text{ for half-integer } s. \end{aligned}$$

The transport coefficients are given in terms of the transport integrals

$$\omega_\alpha^{(n,t)}(T) \equiv \int_0^\infty d\gamma e^{-\alpha\gamma^2} \gamma^{2t+3} q^{(n)}(x), \quad (237)$$

where α is a pure number and $\gamma = \frac{\hbar k}{\sqrt{2\mu k_B T}} = \frac{x}{\sqrt{2\pi}} \left(\frac{\lambda(T)}{R} \right)$ (the quantity γ can also be thought of as the ratio of relative velocity to the average thermal velocity) with the thermal de-Broglie wavelength $\lambda = (2\pi\hbar^2/m k_B T)^{1/2}$. We also note the useful relation

$$\omega_\alpha^{(n,t)}(T) = \frac{1}{\alpha^{t+2}} \omega_1^{(n,t)}(T/\alpha). \quad (238)$$

For numerical calculations it is useful to rewrite the expressions using the definitions

$$\Omega_{\alpha,l}^{(1,t)}(T) \equiv \int_0^\infty d\gamma e^{-\alpha\gamma^2} \gamma^{2t+3} \sin^2(\delta_l(\gamma)), \quad (239)$$

$$\Omega_{\alpha,l}^{(2,t)}(T) \equiv \int_0^\infty d\gamma e^{-\alpha\gamma^2} \gamma^{2t+3} \sin^2(\delta_{l+2}(\gamma) - \delta_l(\gamma)). \quad (240)$$

Then, for integer s ,

$$\omega_{\alpha,s}^{(1,t)}(T) = \frac{(\lambda/R)^2}{\pi} \left[\frac{s+1}{2s+1} \sum_{\text{even } l} (2l+1) \Omega_{\alpha,l}^{(1,t)}(T) \right. \quad (241)$$

$$\left. + \frac{s}{2s+1} \sum_{\text{odd } l} (2l+1) \Omega_{\alpha,l}^{(1,t)}(T) \right], \quad (242)$$

$$\omega_{\alpha,s}^{(2,t)}(T) = \frac{(\lambda/R)^2}{\pi} \left[\frac{s+1}{2s+1} \sum_{\text{even } l} \frac{(l+1)(l+2)}{(2l+3)} \Omega_{\alpha,l}^{(2,t)}(T) \right. \quad (243)$$

$$\left. + \frac{s}{2s+1} \sum_{\text{odd } l} \frac{(l+1)(l+2)}{(2l+3)} \Omega_{\alpha,l}^{(2,t)}(T) \right], \quad (244)$$

and, for half-integer s ,

$$\omega_{\alpha,s}^{(1,t)}(T) = \frac{(\lambda/R)^2}{\pi} \left[\frac{s}{2s+1} \sum_{\text{even } l} (2l+1) \Omega_{\alpha,l}^{(1,t)}(T) \right. \quad (245)$$

$$\left. + \frac{s+1}{2s+1} \sum_{\text{odd } l} (2l+1) \Omega_{\alpha,l}^{(1,t)}(T) \right], \quad (246)$$

$$\omega_{\alpha,s}^{(2,t)}(T) = \frac{(\lambda/R)^2}{\pi} \left[\frac{s}{2s+1} \sum_{\text{even } l} \frac{(l+1)(l+2)}{(2l+3)} \Omega_{\alpha,l}^{(2,t)}(T) \right. \quad (247)$$

$$\left. + \frac{s+1}{2s+1} \sum_{\text{odd } l} \frac{(l+1)(l+2)}{(2l+3)} \Omega_{\alpha,l}^{(2,t)}(T) \right]. \quad (248)$$

In what follows, the coefficients of self diffusion \mathcal{D} , shear viscosity η , and thermal conductivity κ are normalized to the corresponding hard-sphere-like values

$$\tilde{\mathcal{D}} = \frac{3\sqrt{2}}{32} \frac{\hbar}{mnR^3}, \quad \tilde{\eta} = \frac{5\sqrt{2}}{32} \frac{\hbar}{R^3}, \quad \text{and} \quad \tilde{\kappa} = \frac{75}{64\sqrt{2}} \frac{\hbar k_B}{mR^3}. \quad (249)$$

In the first order of deviations from the equilibrium distribution function, the transport coefficients are

$$\frac{[\mathcal{D}]_1}{\tilde{\mathcal{D}}} = \left(\frac{R}{\lambda(T)} \right) \frac{1}{\omega_{1,s}^{(1,1)}(T)},$$

$$\frac{[\eta]_1}{\tilde{\eta}} = \frac{[\kappa]_1}{\tilde{\kappa}} = \left(\frac{R}{\lambda(T)} \right) \frac{1}{\omega_{1,s}^{(2,2)}(T)}, \quad (250)$$

Eq. (250) shows clearly that if $\omega_{1,s}^{(2,2)}$ is T -independent (as for hard-spheres with a constant cross section), the shear viscosity exhibits a $T^{1/2}$ dependence which arises solely from its inverse dependence with $\lambda(T)$. For energy-dependent cross sections, however, the temperature dependence of the viscosity is sensitive also to the temperature dependence of the omega-integral.

Note that in the first-order approximation, the specific heat capacity for a monoatomic gas is expressible as

$$c_{vo} = \frac{2m}{5} \frac{[\kappa]_1}{[\eta]_1} = \frac{3k_B}{2}. \quad (251)$$

The second-order results can be cast as

$$\frac{[\mathcal{C}]_2}{[\mathcal{C}]_1} = (1 + \delta_{\mathcal{C}}(T)) (1 \pm n\lambda^3 \epsilon_{\mathcal{C}}(T)), \quad (252)$$

where \mathcal{C} is \mathcal{D} or η or κ , and the \pm refers to Bose (+) and Fermi (−) statistics. Explicitly,

$$\delta_{\eta} \equiv \frac{3(7\omega_{1,s}^{(2,2)} - 2\omega_{1,s}^{(2,3)})^2}{2 \left(\omega_{1,s}^{(2,2)} (77\omega_{1,s}^{(2,2)} + 6\omega_{1,s}^{(2,4)}) - 6 \left(\omega_{1,s}^{(2,3)} \right)^2 \right)}, \quad (253)$$

$$\delta_{\mathcal{D}} \equiv \frac{(5\omega_{1,s}^{(1,1)} - 2\omega_{1,s}^{(1,2)})^2 / \omega_{1,s}^{(1,1)}}{\left(30\omega_{1,s}^{(1,1)} + 4\omega_{1,s}^{(1,3)} + 8\omega_{1,s}^{(2,2)} \right) - 4 \frac{\left(\omega_{1,s}^{(1,2)} \right)^2}{\omega_{1,s}^{(1,1)}}}, \quad (254)$$

$$\delta_{\kappa} \equiv \frac{(7\omega_{1,s}^{(2,2)} - 2\omega_{1,s}^{(2,3)})^2}{4 \left(\omega_{1,s}^{(2,2)} (7\omega_{1,s}^{(2,2)}(T) + \omega_{1,s}^{(2,4)}) - \left(\omega_{1,s}^{(2,3)} \right)^2 \right)}, \quad (255)$$

and

$$\epsilon_{\kappa} \equiv 2^{-7/2} \left[7 - \frac{128}{3^{3/2}} \frac{\omega_{4/3,s}^{(2,3)} + 6\omega_{4/3,s}^{(2,2)}}{9\omega_{1,s}^{(2,2)}} \right], \quad (256)$$

$$\epsilon_{\eta} \equiv 2^{-7/2} \left[4 - \frac{128}{3^{3/2}} \frac{\omega_{4/3,s}^{(2,2)}}{\omega_{1,s}^{(2,2)}} \right]. \quad (257)$$

It is worthwhile to note that at the first order of deviations from the equilibrium distribution function, all the dimensionless transport coefficients are independent of density, unless density dependent cut-offs are used to delimit the transport cross sections. An explicit density dependence arises only at the second order.

It is useful to define a characteristic temperature

$$\tilde{T} \equiv \frac{2\pi\hbar^2}{k_B m R^2} \quad \text{or} \quad \frac{T}{\tilde{T}} = \left(\frac{R}{\lambda} \right)^2 \quad (258)$$

in terms of which limiting forms of the transport coefficients can be studied.

20. Delta-shell gas and resonances

Figures 40, 41 and 42 show $[\eta]_1$ from Eq. (250) normalized to $\tilde{\eta}$ from Eq. (249). As expected, the shear viscosity grows steadily with temperature. At low temperatures the results acquire the asymptotic trends inferred from Chapter 21. Also at low temperatures the slope of the curves is $1/2$ except for the case of S-wave resonance for which the slope equals $3/2$. For high temperatures the slope tends to the classical value of $1/2$. The spin of the particles affects only the low temperature result. For high temperatures, the results become spin independent. Qualitatively the same features are exhibited by the coefficient of diffusion.

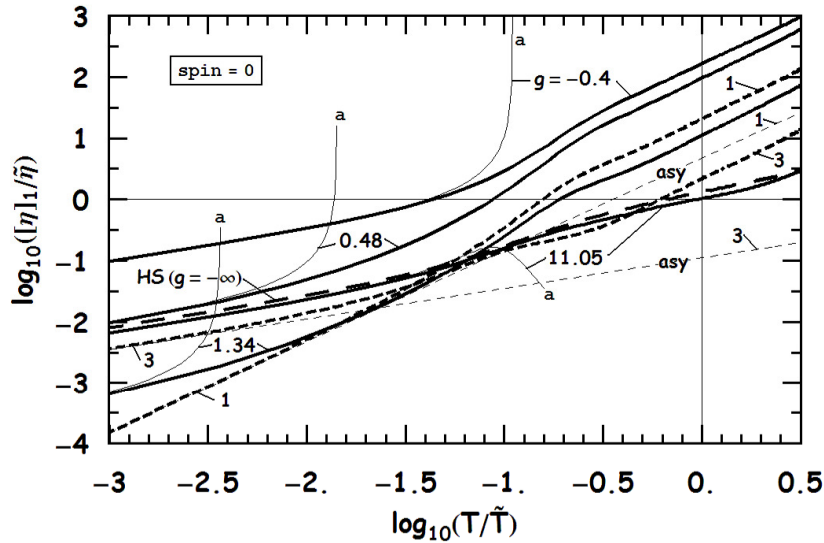


Fig. 40. Normalized (to $\tilde{\eta}$ in Eq. (249)) diffusion coefficient for spin zero particles as a function of normalized (to \tilde{T} in Eq. (258)) temperature for various values of the strength parameter g in Eq. (16). Thin curves show the asymptotic trends (also labeled as 'a' and 'asy') for $T \ll \tilde{T}$. The dashed curves highlight special cases.

Figures 43, 44 and 45 show the normalized viscosity coefficient as a function of $\frac{R}{a_{sl}} = \frac{g-1}{g}$ (inverse scattering length) for $T < \tilde{T}$. Enhanced cross sections at resonances produce significant drops in the viscosity as $g \rightarrow 2l + 1$. In the case of zero spin, odd l partial waves do not contribute, but for non-zero spins all l -wave resonances are present. The widths of the dips in viscosity decrease with increasing values of l . For $T \leq \tilde{T}$, the dips become less prominent and disappear for $T \geq \tilde{T}$. Spin affects only the low temperature values of the transport coefficient.

For the densities and temperatures considered, the contribution from the second approximation is given by δ_C and ϵ_C . The density dependent correction is propor-

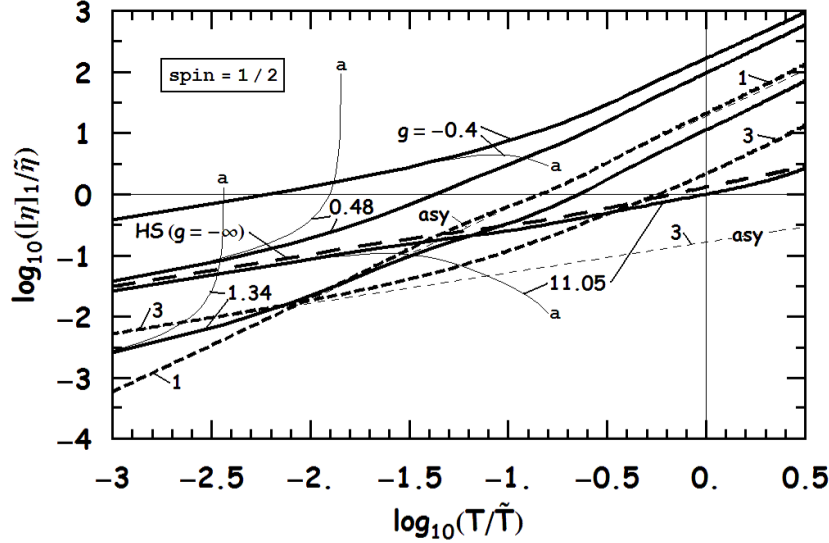


Fig. 41. Normalized (to $\tilde{\eta}$ in Eq. (249)) diffusion coefficient for spin half particles as a function of normalized (to \tilde{T} in Eq. (258)) temperature for various values of the strength parameter g in Eq. (16). Thin curves show the asymptotic trends (also labeled as 'a' and 'asy' for $T \ll \tilde{T}$). The dashed curves highlight special cases.

tional to $\epsilon_C n \lambda^3$ and allows us to define the characteristic density

$$n_{\epsilon_C} R^3 \equiv \frac{(T/\tilde{T})^{3/2}}{\epsilon_C(T)}. \quad (259)$$

As shown in Fig. 46 and Fig. 47, it approximately equals the quantum critical density from Eq. (229), $n_{\epsilon_C} \approx n_Q$.

The density independent part δ_η is shown in Fig. 48 for spin=0 and in Fig. 49 for spin=12/. The second order corrections are below 15% for all cases shown.

In Fig. 50, Fig. 51 and Fig. 52, the ratio of the coefficients of diffusion (times mn to make it dimensionless) and viscosity is shown as function of R/a_{sl} for various values of $T \leq \tilde{T}$. As expected, the largest variations in this ratio occur as $g \rightarrow 2l + 1$, that is, as resonances are approached. For $T \ll \tilde{T}$, the ratio approaches the asymptotic value $6/5$ away from resonances and $4/5$ for the S -wave resonance (a point). With increasing T , resonances become progressively broader with diminishing strengths; for $T \approx \tilde{T}$ resonances disappear. Different spin values affect the ratio only at low temperatures. For comparison, this figure also includes the results for hard spheres (HS).

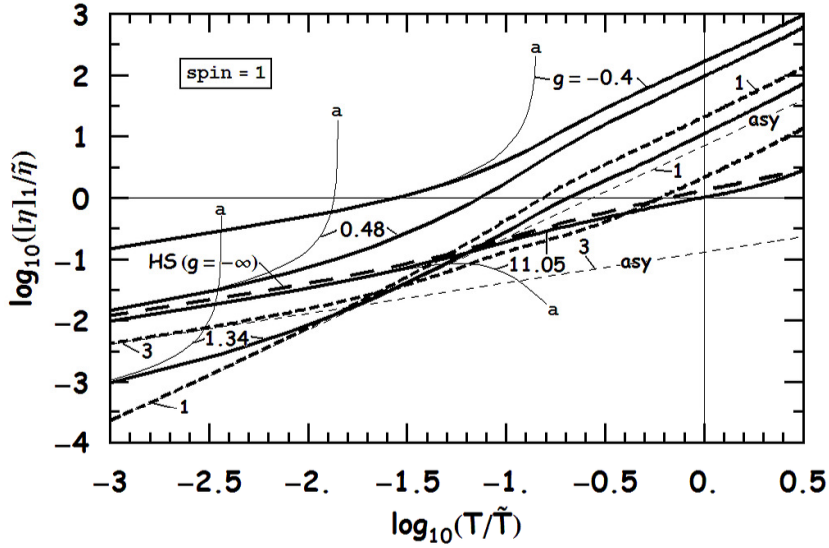


Fig. 42. Normalized (to $\tilde{\eta}$ in Eq. (249)) diffusion coefficient for spin-one particles as a function of normalized (to \tilde{T} in Eq. (258)) temperature for various values of the strength parameter g in Eq. (16). Thin curves show the asymptotic trends (also labeled as 'a' and 'asy') for $T \ll \tilde{T}$. The dashed curves highlight special cases.

21. Asymptotic behavior at low temperatures

At low temperatures, the integrands in Eq. (239) and Eq. (240) can be expanded in a series involving γ . The first order terms can be integrated leading to expressions

$$\begin{aligned} \Omega_{\alpha,0}^{(2,t)}(T \rightarrow 0) &\rightarrow \Omega_{\alpha,0}^{(1,t)}(T \rightarrow 0) \\ &\rightarrow \pi g^2 \alpha^{-(t+3)} \Gamma(t+2) \\ &\times \left[\frac{\alpha}{(g-1)^2} - \frac{2\pi(2+g^2)(2+t)}{3(g-1)^4} (T/\tilde{T}) \right] (T/\tilde{T}), \end{aligned} \quad (260)$$

for $l = 0$ and $g \neq 1$. For $l = 0$ and $g = 1$

$$\begin{aligned} \Omega_{\alpha,0}^{(2,t)}(T \rightarrow 0) &\rightarrow \Omega_{\alpha,0}^{(1,t)}(T \rightarrow 0) \\ &\rightarrow (1/18) \alpha^{-(t+2)} \Gamma(t+1) \\ &\times \left[9\alpha - 8\pi(2+t)(T/\tilde{T}) \right]. \end{aligned} \quad (261)$$

For $l > 0$ and $g \neq 2l+1$

$$\begin{aligned} \Omega_{\alpha,l}^{(2,t)}(T \rightarrow 0) &\rightarrow \Omega_{\alpha,l}^{(1,t)}(T \rightarrow 0) \\ &\rightarrow 4^l \pi^{2l+1} \frac{g^2(2l+1)^2 \alpha^{-(2l+2+t)}}{(2l+1-g)^2 ((2l+1)!!)^4} \\ &\times \Gamma(2l+2+t) (T/\tilde{T})^{2l+1}, \end{aligned} \quad (262)$$

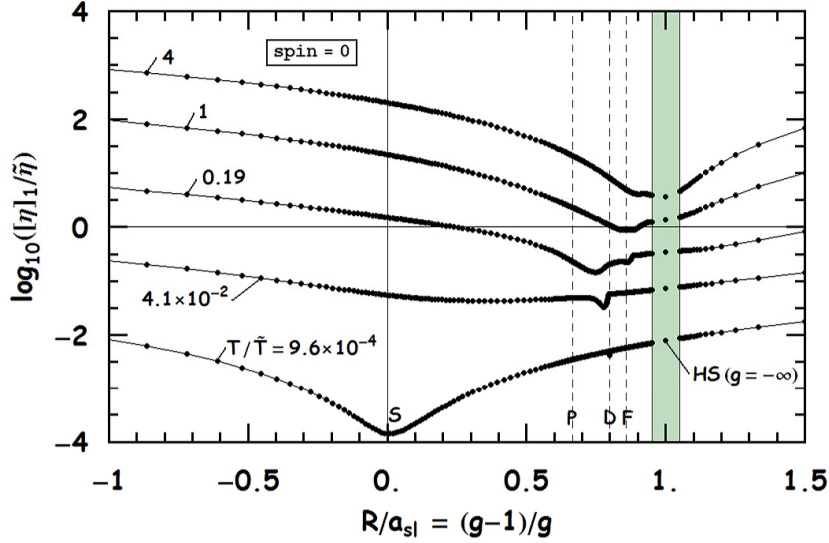


Fig. 43. The normalized viscosity coefficient in Eq. (250) for spin zero particles as a function of the inverse scattering length. Effects due to resonances associated with the partial waves $l = 0, 1, 2, 3$ are indicated by the letters S, P, D, F , respectively. For states of two spin zero particles odd l partial waves are absent and do not produce any feature. In the vertical shaded region, a large number of partial waves are required to obtain convergent results.

Table 1. The asymptotic behavior of diffusion coefficient $[D]_1/\tilde{D}$ at low temperatures.

Case	$s = 0$	$s = 1/2$	$s = 1$	Common multiplier
$g = 1$	2π	8π	3π	$\times (T/\tilde{T})^{3/2}$
$g = 3$	$2/9$	$4/17$	$18/79$	$\times (T/\tilde{T})^{1/2}$
$g \neq 1, 3$	$1/2$	2	$3/4$	$\times \left(\frac{g-1}{g}\right)^2 (T/\tilde{T})^{1/2}$

and, finally, for $l > 0$ and $g = 2l + 1$

$$\begin{aligned}
 \Omega_{\alpha,l}^{(2,t)}(T \rightarrow 0) &\rightarrow \Omega_{\alpha,l}^{(1,t)}(T \rightarrow 0) \\
 &\rightarrow \frac{4^{l-2} \pi^{2l-1} (2l+3)^2 (2l+1)^2 (2l-1)^2 \alpha^{-(2l+t)}}{((2l+1)!!)^4} \\
 &\quad \times \Gamma(2l+t) (T/\tilde{T})^{2l-1}.
 \end{aligned} \tag{263}$$

Above $\Gamma(t)$ stands for Euler's gamma function¹⁵.

It is seen that the cases $g \rightarrow 1, 3$ require special consideration. In these cases, the asymptotic behavior for $T \ll \tilde{T}$ is obtained from a series expansion in $x = kR$ of the transport cross sections $q^{(n)}(x)$ in Eqs. (236), and subsequent integrations of Eq. (237). The limiting forms we found are listed in Table 1 and Table 2. The asymptotic behavior (for $T \ll \tilde{T}$) of the shear viscosity $[\eta]_1$ in Table 2 is similar

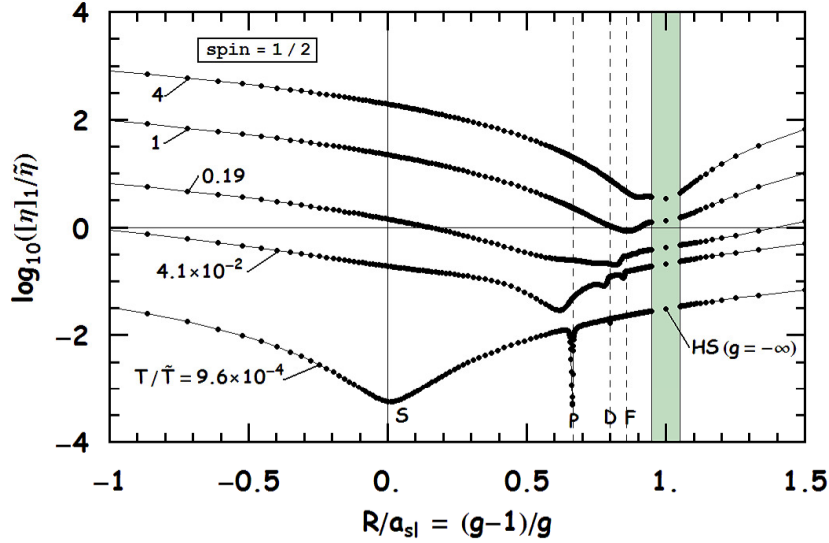


Fig. 44. The normalized viscosity coefficient in Eq. (250) for spin half particles as a function of the inverse scattering length. Effects due to resonances associated with the partial waves $l = 0, 1, 2, 3$ are indicated by the letters S, P, D, F , respectively. In the vertical shaded region, a large number of partial waves are required to obtain convergent results.

Table 2. The asymptotic behavior of shear viscosity coefficient $[\eta]_1/\tilde{\eta}$ at low temperatures.

Case	$s = 0$	$s = 1/2$	$s = 1$	Common multiplier
$g = 1$	$3\pi/2$	6π	$9\pi/4$	$\times (T/\tilde{T})^{3/2}$
$g = 3$	$1/9$	$1/6$	$3/23$	$\times (T/\tilde{T})^{1/2}$
$g \neq 1, 3$	$1/4$	1	$3/8$	$\times \left(\frac{g-1}{g}\right)^2 (T/\tilde{T})^{1/2}$

to that of the diffusion coefficient in Table 1. It is interesting that even at the two-body level, the coefficients of diffusion, thermal conductivity and viscosity acquire a significantly larger temperature dependence as the scattering length $a_{sl} \rightarrow \infty$ ($g \rightarrow 1$).

The coefficient of viscosity (as also mn times the coefficient of diffusion) has the dimension of action (\hbar) per unit volume. The manner in which the effective physical volume \mathcal{V} changes as the strength parameter g is varied is illuminating in our results for $T \ll \tilde{T}$ (see next section) as Table 3 shows. In the unitary limit ($g = 1$), the relevant volume is $\mathcal{V} \propto \lambda^3$. For $g = 3$, $\mathcal{V} \propto \lambda R^2$ (independent of a_{sl}), and for $g \neq 1, 3$, $\mathcal{V} \propto \lambda a_{sl}^2$ (independent of R).

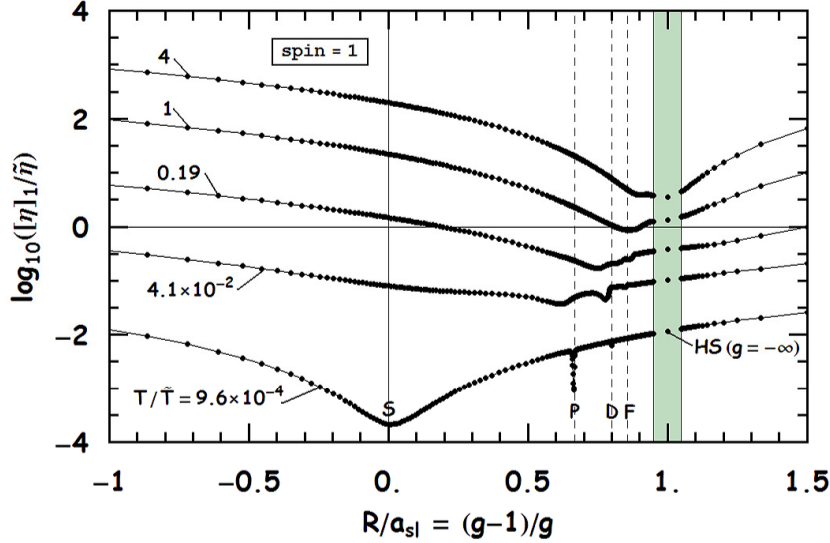


Fig. 45. The normalized viscosity coefficient in Eq. (250) for spin-one particles as a function of the inverse scattering length. Effects due to resonances associated with the partial waves $l = 0, 1, 2, 3$ are indicated by the letters S, P, D, F , respectively. In the vertical shaded region, a large number of partial waves are required to obtain convergent results.

Table 3. First order coefficients of diffusion (times mn), shear viscosity, and their ratios for $T \ll \tilde{T}$ for select strength parameters g and spins s (c. m. is common multiplier). The unitary limit ($g = 1$) result for η was obtained earlier²⁸.

Case	mnD			η			c. m.	mnD/η		
	0	1/2	1	0	1/2	1		0	1/2	1
$g = 1$	$\frac{3\sqrt{2}\pi}{16}$	$\frac{3\sqrt{2}\pi}{4}$	$\frac{9\sqrt{2}\pi}{32}$	$\frac{15\pi}{32\sqrt{2}}$	$\frac{15\pi}{8\sqrt{2}}$	$\frac{45\pi}{64\sqrt{2}}$	$\times \frac{\hbar}{\lambda^3}$	4/5	4/5	4/5
$g = 3$	$\frac{\sqrt{2}}{48}$	$\frac{3\sqrt{2}}{136}$	$\frac{27\sqrt{2}}{1264}$	$\frac{5}{144\sqrt{2}}$	$\frac{5}{96\sqrt{2}}$	$\frac{15}{368\sqrt{2}}$	$\times \frac{\hbar}{\lambda R^2}$	6/5	72/85	414/395
$g \neq 1, 3$	$\frac{3\sqrt{2}}{64}$	$\frac{3\sqrt{2}}{16}$	$\frac{9\sqrt{2}}{128}$	$\frac{5}{64\sqrt{2}}$	$\frac{5}{16\sqrt{2}}$	$\frac{15}{128\sqrt{2}}$	$\times \frac{\hbar}{\lambda a_{sl}^2}$	6/5	6/5	6/5

22. Ratio of shear viscosity to entropy density

A lower limit to the ratio of shear viscosity to entropy density is being sought²⁹ with results even lower than $(4\pi)^{-1}(\hbar/k_B)$ first proposed by Kovtun¹³. Using string theory methods, they show that this ratio is equal to a universal value for a large class of strongly interacting quantum field theories whose dual description involves black holes in anti-de Sitter space.

We therefore will use our simple model to examine $[\eta]_{1,2}/s$ in the light of the results of this work. Also we recall the entropy density

$$s = (5/2 - \ln(n\lambda^3) + \delta s(T)) nR^3 nk_B, \quad (264)$$

which includes the second virial correction from Eq. (189) to the ideal gas entropy

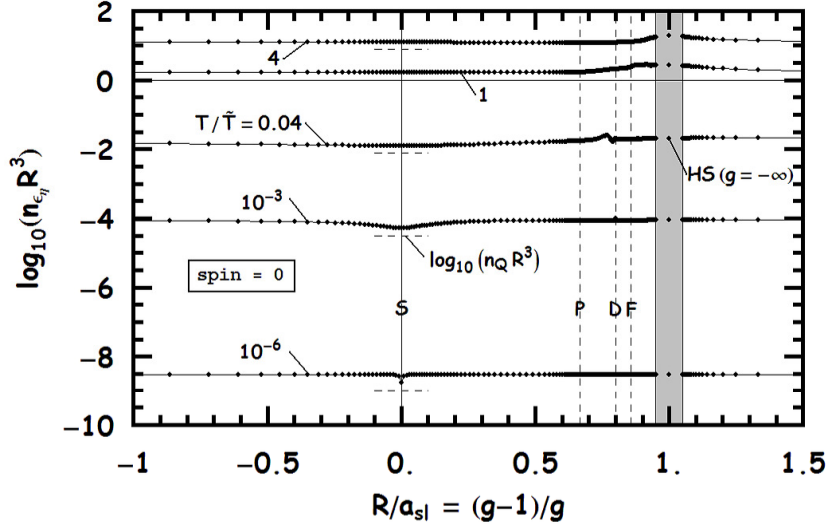


Fig. 46. Characteristic density for spin zero particles as a function of the inverse scattering length. Resonances associated with the partial waves $l = 0, 1, 2, 3$ are indicated by the letters S, P, D, F , respectively. In the vertical shaded region, a large number of partial waves are required to obtain convergent results.

density. The validity is checked through Eq. (228).

The inserts in Fig. 53, Fig. 54 and Fig. 55 show a characteristic minimum of η/s versus T for fixed dilution nR^3 and strength g . Values of $[\eta]_{1,2}/s$ at the minimum are also shown as functions of R/a_{sl} (inverse scattering length) for several nR^3 . The lower (upper) curve for each nR^3 corresponds to the first (second) order calculations of η . The large role of the improved estimates of η on the ratio η/s is noticeable. The case of $nR^3 = 1$ possibly requires an adequate treatment of many-body effects not considered here. We can, however, conclude that in the dilute gas limit η/s for the delta-shell gas remains above $(1/4\pi)\hbar/k_B$.

Our analysis here of the transport coefficients of particles subject to a delta-shell potential has been devoted to the dilute gas (non-degenerate) limit, in which two-particle interactions dominate, but with scattering lengths that can take various values including infinity. Even at the two-body level considered, a rich structure in the temperature dependence and the effective physical volume responsible for the overall behavior of the transport coefficients are evident. The role of resonances in reducing the transport coefficients are amply delineated. The cases of intermediate and extreme degeneracies cases are considered in Refs. ^{28 30 31} and ³² which highlight the additional roles of many-body effects. Their result in the limiting case $T \gg$

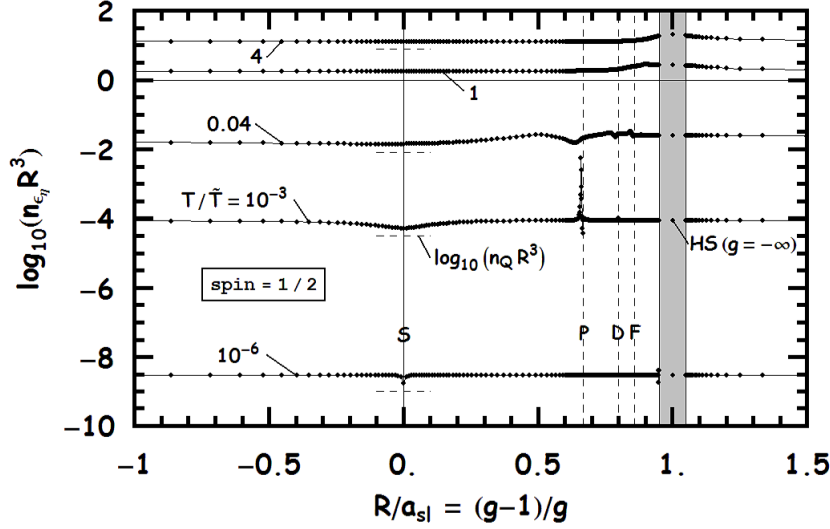


Fig. 47. Characteristic density for spin half particles as a function of the inverse scattering length. Resonances associated with the partial waves $l = 0, 1, 2, 3$ are indicated by the letters S, P, D, F , respectively. In the vertical shaded region, a large number of partial waves are required to obtain convergent results.

$\frac{\hbar^2/a_{sl}^2}{m}$ (and also well above the Fermi temperature) is

$$\eta = \frac{15(mk_B T)^{3/2}}{32\sqrt{\pi}\hbar^2}, \quad (265)$$

and for $T \ll \frac{\hbar^2/a_{sl}^2}{m}$ the result is

$$\eta = \frac{5\sqrt{mk_B T}}{32\sqrt{\pi}a_{sl}^2}, \quad (266)$$

which coincides with the corresponding ($g = 1$ and $g \neq 1, 3$) results in Table 2.

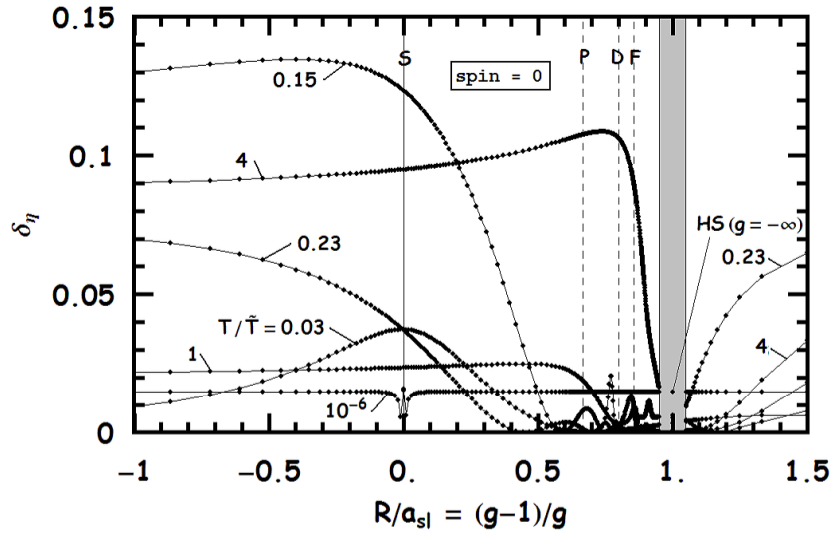


Fig. 48. Second order correction δ_η for spin zero particles as a function of the inverse scattering length. Resonances associated with the partial waves $l = 0, 1, 2, 3$ are indicated by the letters S, P, D, F , respectively. In the vertical shaded region, a large number of partial waves are required to obtain convergent results.

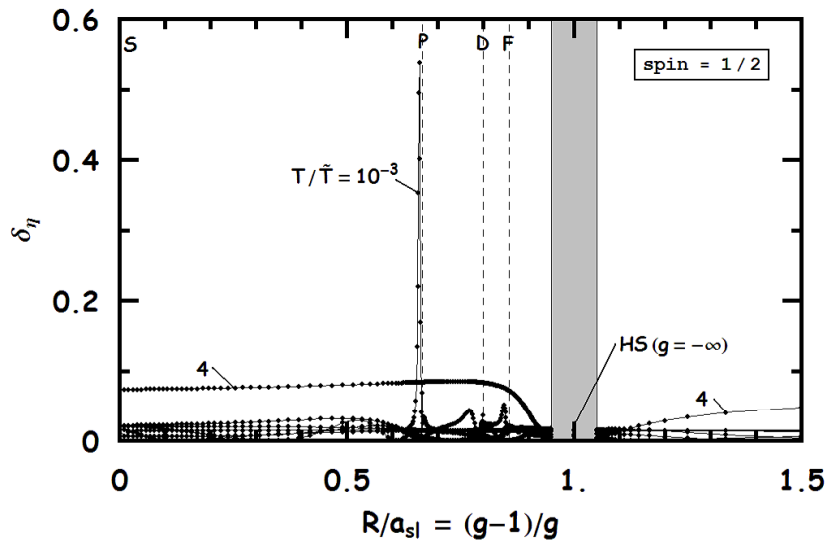


Fig. 49. Second order correction δ_η for spin half particles as a function of the inverse scattering length. Resonances associated with the partial waves $l = 0, 1, 2, 3$ are indicated by the letters S, P, D, F , respectively. In the vertical shaded region, a large number of partial waves are required to obtain convergent results.

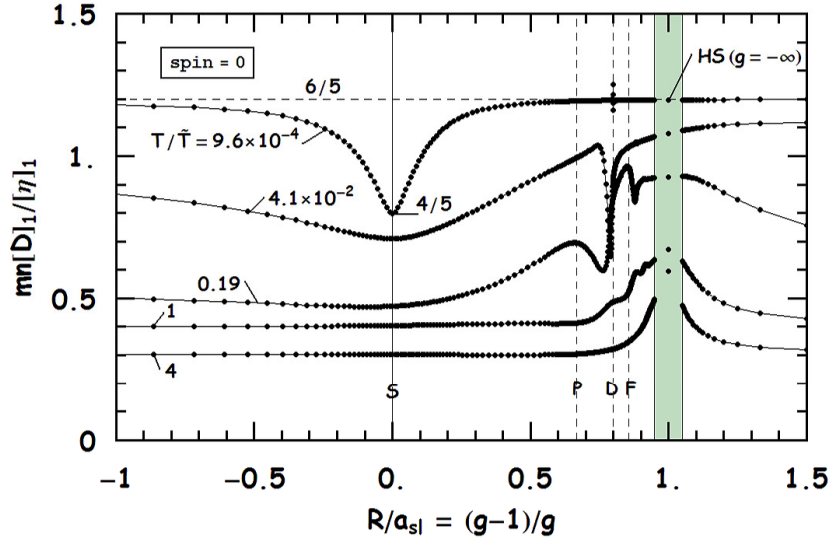


Fig. 50. Ratio of diffusion (times mn) to shear viscosity versus inverse scattering length for spin zero particles. In the vertical shaded region, a large number of partial waves are required to obtain convergent results. The hard-sphere results ($g \rightarrow -\infty$) are shown by solid circles.

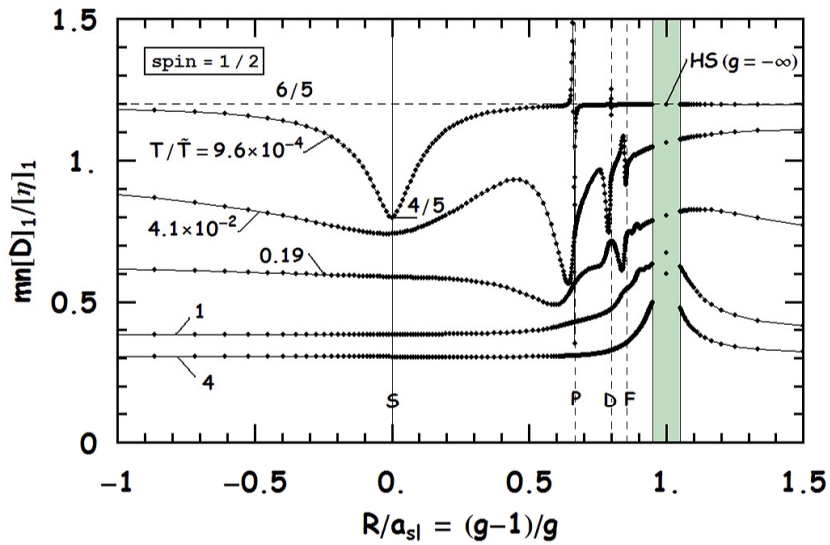


Fig. 51. Ratio of diffusion (times mn) to shear viscosity versus inverse scattering length for spin half particles. In the vertical shaded region, a large number of partial waves are required to obtain convergent results. The hard-sphere results ($g \rightarrow -\infty$) are shown by solid circles.

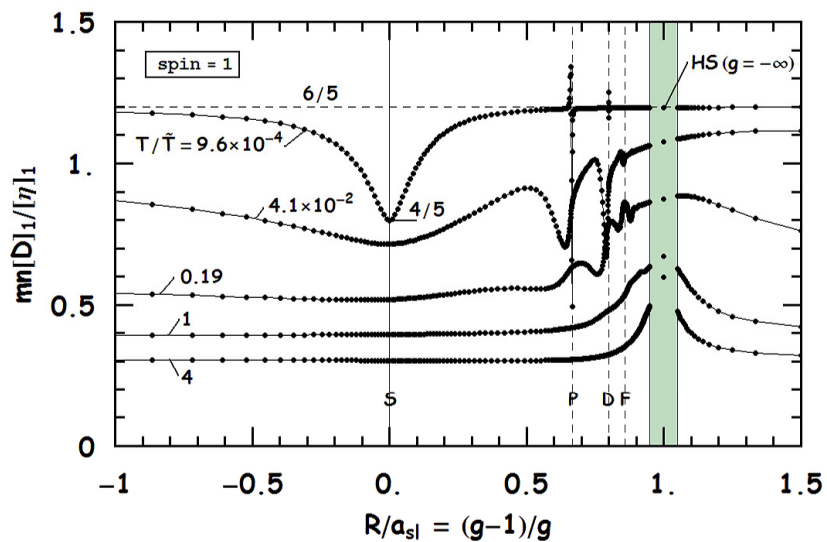


Fig. 52. Ratio of diffusion (times mn) to shear viscosity versus inverse scattering length for spin-one particles. In the vertical shaded region, a large number of partial waves are required to obtain convergent results. The hard-sphere results ($g \rightarrow -\infty$) are shown by solid circles.

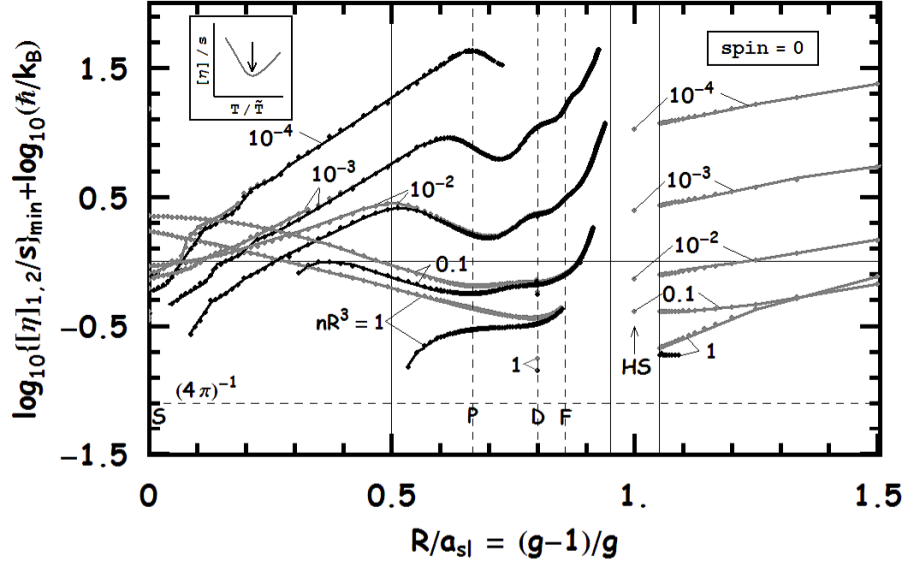


Fig. 53. For each nR^3 , the minimum value in the first (lower curve) and second (upper curve) order calculations of shear viscosity is plotted versus R/a_{sl} for the indicated nR^3 for spin zero particles. In the vertical blank region, a large number partial waves are needed. Vertical lines with letters S , P , D , and F , respectively, indicate resonances associated with the partial waves $l = 0, 1, 2$ and 3 . The symbol HS denotes hard-spheres for which $g \rightarrow -\infty$. The horizontal dashed line shows the conjectured lower bound $1/(4\pi)^{13}$. The inset shows the occurrence of a minimum in the ratio of viscosity to entropy density versus T .

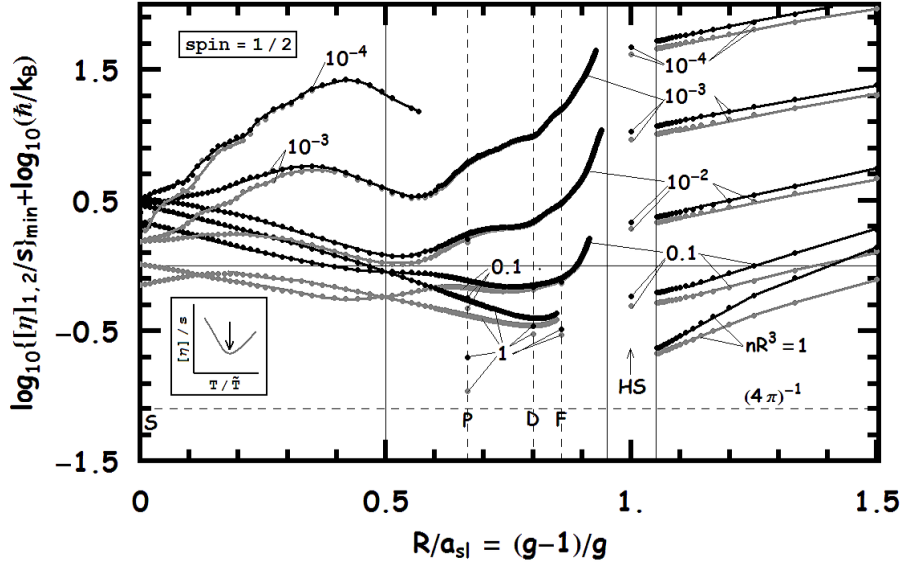


Fig. 54. For each nR^3 , the minimum value in the first (lower curve) and second (upper curve) order calculations of shear viscosity is plotted versus R/a_{sl} for the indicated nR^3 for spin half particles. In the vertical blank region, a large number partial waves are needed. Vertical lines with letters S , P , D , and F , respectively, indicate resonances associated with the partial waves $l = 0, 1, 2$ and 3 . The symbol HS denotes hard-spheres for which $g \rightarrow -\infty$. The horizontal dashed line shows the conjectured lower bound $1/(4\pi)^{13}$. The inset shows the occurrence of a minimum in the ratio of viscosity to entropy density versus T .

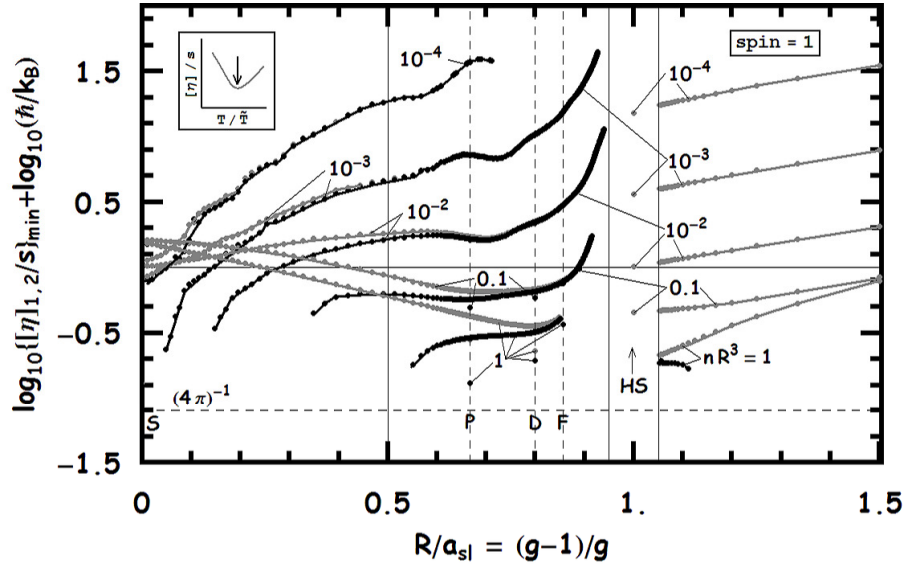


Fig. 55. For each nR^3 , the minimum value in the first (lower curve) and second (upper curve) order calculations of shear viscosity is plotted versus R/a_{sl} for the indicated nR^3 for spin-one particles. In the vertical blank region, a large number partial waves are needed. Vertical lines with letters S , P , D , and F , respectively, indicate resonances associated with the partial waves $l = 0, 1, 2$ and 3 . The symbol HS denotes hard-spheres for which $g \rightarrow -\infty$. The horizontal dashed line shows the conjectured lower bound $1/(4\pi)^{13}$. The inset shows the occurrence of a minimum in the ratio of viscosity to entropy density versus T .

23. Summary and conclusions

In this work, we have extended the seminal work of Gottfried^{4,5} on the two-body quantum mechanics of the delta-shell potential to the many-body context by studying the thermal and transport properties of a dilute gas. We start with the two-body physics of the delta-shell potential $V(r) = -v\delta(r - R)$. The potential has two parameters: strength v and range R . The Schrödinger equation for this potential has analytical solutions and enables the analysis of bound, resonant and scattering states. The physics of interaction depends only on the dimensionless strength parameter $g \propto vR$, where R sets the length scale. Low energy scattering is effectively described by the scattering length and the effective range, which, for this particular case, are $a_{sl}/R = g/(g-1)$ and $r_0/R = (2/3)(1+1/g)$. Therefore, for values of $g \approx 1$ the scattering length a_{sl} becomes large and diverges at $g = 1$ (unitary limit). This provides a simple model to study properties of the system near the unitary limit. Also g controls how many bound states the system has (integer part of $(g + 1)/2$), so that contributions from bound and scattering states can be investigated.

Scattering states are described by the partial wave phase shifts δ_l (l is the angular momentum quantum number). The derivative of the phase shifts with respect to the wave number k , $d\delta_l/dk$, is proportional to the density of states. Additionally, higher- l scattering lengths are derived and diverge at values of $g = 2l + 1$. When the corresponding partial-wave scattering length is large, it produces loosely bound l -states with energy close to zero. It appears as a delta-function-like feature in the $d\delta_l/dk$ vs. k plot and represents a resonance. Near resonance values, $g \approx 1$ for S-wave ($l = 0$) and $g \approx 3$ for P-wave ($l = 1$), approximate analytical expressions for the phase shift derivatives were obtained, and they confirm the $\pi/2$ and π values for zero-energy phase shifts from Levinson's theorem. Using the scattering wave differential equation, the S-wave scattering length for the delta-shell potential is alternatively obtained.

The bound state wave-function normalization was found with the help of the Feynman-Hellmann theorem. The delta-shell model of the deuteron was examined by adjusting parameters to reproduce the binding energy of 2.22 MeV and the scattering length of 5.42 fm (in the triplet configuration, the deuteron is dominated by the S-state). This model gives an effective range $r_0 = 1.79$ fm, which is close to the experimental value of 1.76 fm. The Feynman-Hellmann theorem when applied to the delta-shell potential also allowed us to confirm the virial theorem for bound-states and obtain Kramers-Pasternak-like relations for moments of the bound states.

With the two-body physics inputs in hand, the statistical physics of a dilute delta-shell gas allows to study its thermal and transport properties, especially near resonances. Two-body interactions can be tuned by the parameter g and they contribute to the thermal properties through the second virial coefficient, a_2 . This coefficient is the first correction to the ideal-gas behavior and incorporates scattering and bound states. Near S- and P-resonances, the scattering part of the virial integral can be well approximated by loosely bound discrete states, signaling the

formation of an admixture of long-living dimers. Limits for the virial approximation are discussed and require the density to be small ($nR^3 < 1$, that is, dilute) and the thermal de-Broglie wavelength to be large ($\lambda(T) > R$, that is, low temperature T). Also dimers have to be the minority to avoid significant contribution from three-body interactions and the bound state energy E_b should not be much larger than the temperature (since it contributes in a_2 as $e^{-E_b/(k_B T)}$). Nevertheless, the effective range expansion for the second virial coefficient can be obtained, including the unitary limit and resonances.

A knowledge of the second virial coefficient and its derivatives with respect to temperatures enables us to calculate virial corrections to the ideal-gas thermodynamical properties, such as the entropy density. When varying g , all state variables experience a sudden change in value only at exact resonance $g = 2l + 1$.

The Chapman-Enskog method for solving the Boltzmann equation involves small perturbations of the distribution function from its equilibrium state. For dilute systems only two-body collisions affect the particle's distribution function, thus the collisional integral can be expressed in terms of thermally weighted differential cross-sections. Hence, the transport coefficients are given by transport integrals ($\omega_1^{(1,1)}(T)$ and $\omega_1^{(2,2)}(T)$). Use of classical or quantum cross sections will produce corresponding results for the transport coefficients. The second-order calculations include higher-order transport integrals ($\omega_1^{(1,2)}(T)$, $\omega_1^{(2,3)}(T)$ and etc.) and corrections due to the quantum higher-density effects ($n\lambda^3 \approx 1$ and $\omega_{4/3}^{(2,2)}(T), \dots$).

It is found that when interactions are tuned close to resonance values it results in a reduction of the transport coefficients. That is, a cold ($\lambda(T) > R$) unitary gas and a gas with P-wave zero-energy dimers will have several orders of magnitude lower (dips) shear viscosity $[\eta]_1$ than in other regimes. Also, it is shown that the delta-shell result coincides with that for hard-spheres when g is set to $-\infty$. These dips also show up in the ratio of self-diffusion to shear viscosity. Investigation of the asymptotic behavior of transport coefficients, when $\lambda(T) \gg R$, reveals that the coefficient $\propto T^{3/2}$ in the unitary limit and $\propto T^{1/2}$ otherwise. The asymptotic value of shear viscosity also uncovers the relevant volumes: λ^3 for the unitary limit ($g = 1$), λR^2 for $g = 3$ and $\lambda a_{s_l}^2$ for the rest.

Taking the ratio of the coefficient of shear viscosity and entropy density and plotting it versus temperature allows us to find its minimum value. Calculation of this minimum for various interactions (and therefore scattering lengths) at several densities puts it well above the suggested universal value of $(4\pi)^{-1} \hbar/k_B$ ¹³. Although the system has to be dilute, significant insights into the physical properties of a unitary and resonant gas are gained.

It would be interesting to study three-body physics with delta-shell interactions. But the difficulty is that it requires the introduction of three-body forces and the summation of many terms (three-body clusters) arising from non-commuting operators. Surmounting this difficulty is a task for future work.

Acknowledgments

Through the course of this work, SP's research was supported in part by the U.S. DOE grants DE-FG02-93ER-40756 (Ohio University), DE-FG02-87ER40365 (Indiana University) and de-sc0008808 (NUCLEI SciDAC Collaboration), and by a grant from Conacyt (CB-2009-01, #132400). He also acknowledges a postdoctoral fellowship from DGAPA at the Universidad Nacional Autonoma de Mexico. MP thanks research support from the U.S. DOE grant DE-FG02-93ER-40756.

References

1. T. Schafer and D. Teaney, Rept. Prog. Phys. **72**, 126001 (2009), 0904.3107.
2. J. Kinast, A. Turlapov, and J. E. Thomas, Phys. Rev. Lett. **94**, 170404 (2005).
3. U. W. Heinz, J. S. Moreland, and H. Song, Phys. Rev. **C80**, 061901 (2009), 0908.2617.
4. K. Gottfried, *Quantum Mechanics, Vol. I: Fundamentals* (W. A. Benjamin, Inc., New York, 1966).
5. K. Gottfried and T.-M. Yau, *Quantum Mechanics, Vol. II* (Springer-Verlag, New York, 2004).
6. J. Deng, A. Sipe, and W. von Witsch, Phys. Rev. **C66**, 047001 (2002).
7. R. P. Feynman, Phys. Rev. **56**, 340 (1939).
8. H. Hellmann, *Einführung in die Quantenchemie* (Deuticke, Leipzig, 1937).
9. H. A. Kramers, *Quantum Mechanics* (North-Holland, Amsterdam, 1957).
10. S. Pasternak, Proc. Nat. Acad. Sci. **23**, 91 (1937).
11. K. Huang, *Statistical Mechanics* (John Wiley and Sons, New York, 1987).
12. S. Chapman and T. G. Cowling, *The Mathematical Theory of Non-Uniform Gases* (Cambridge University Press, Cambridge, Eng., 1970).
13. P. K. Kovtun, D. T. Son, and A. O. Starinets, Phys. Rev. Lett. **94**, 111601 (2005).
14. L. Salasnich and F. Toigo (2011), 1107.4552.
15. M. Abramowitz and I. Stegun, *Handbook of Mathematical Functions* (Dover, New York, 1964), 5th ed.
16. J. O. Hirschfelder, C. F. Curtiss, and R. B. Bird, *Molecular Theory of Gases and Liquids* (John Wiley & Sons, New York, 1967).
17. A. G. Sitenko and V. K. Tartakovskii, *Lectures on the Theory of the Nucleus* (Pergamon Press, New York, 1975).
18. R. G. Newton, *Scattering Theory of Waves and Particles* (McGRAW-HILL, New York, 1966).
19. E. Epelbaum, W. Gloeckle, and U.-G. Meissner, Eur. Phys. J. **A19**, 401 (2004), nucl-th/0308010.
20. S. A. Moszkowski, M. W. Kermode, and W. van Dijk, Acta Physica Polonica B **24**, 597 (1993).
21. S. Flugge, *Practical Quantum Mechanics* (Springer, Berlin, 1999).
22. M. Abramowitz and I. A. Stegun, *Handbook of Mathematical Functions* (Dover Publications, New York, 1937).
23. G. Arfken, *Mathematical Methods for Physicists* (Academic Press, St. Louis, Missouri, 2000).
24. E. Beth and G. Uhlenbeck, Physica **4**, 915 (1937).
25. N. Levinson, Adv. Math. **13**, 383 (1974).
26. J. I. Kapusta, *Finite-Temperature Field Theory* (Cambridge University Press, Cambridge, 1989).
27. R. Venugopalan and M. Prakash, Nucl. Phys. **A546**, 718 (1992).

REFERENCES 79

28. P. Massignan, G. M. Bruun, and H. Smith, Phys. Rev. A **71**, 033607 (2005).
29. Y. Kats and P. Petrov, JHEP **01**, 044 (2009), 0712.0743.
30. G. M. Bruun and H. Smith, Phys. Rev. A **72**, 043605 (2005).
31. G. M. Bruun and H. Smith, Phys. Rev. A **75**, 043612 (2007).
32. G. Rupak and T. Schafer, Phys. Rev. **A76**, 053607 (2007), 0707.1520.